Modelling population and disease dynamics in complex ecological systems

Morag Fiona Macpherson

Submitted for the degree of
Doctor of Philosophy

Heriot-Watt University

Department of Mathematics,
School of Mathematical and Computer Sciences.

August 29, 2014

Abstract

Mathematical models are a theoretical tool used to understand ecological processes. In this thesis we create mathematical frameworks to describe and evaluate four ecological systems.

In the first case study we extend a host-pathogen framework to include a maternal effect which increases the disease resistance of offspring when the maternal environment is poor. Maternal effects impacting life-history traits have been shown to increase the propensity for population cycles. Our contrasting results show maternal effects acting on disease resistance stabilise host-pathogen systems.

The second case study examines the impact infection may have on population estimates using Capture-Mark-Recapture (CMR) studies. We show that the estimates using the statistical Program Capture are accurate when capture rates are infection dependent.

The final two case studies use spatial, individual-based, stochastic models to simulate disease spread and the colonisation of the Eurasian red squirrel (*Sciurus vulgaris*) on real-life landscapes. Using novel techniques we highlight the role habitat connectivity has on the dispersal routes which influence the spread of disease and re-population dynamics. Moreover the inclusion of seasonality shows that squirrel population dynamics are driven by the multi-year signal of resources.

Acknowledgements

Firstly I would like to thank my supervisors Andy White, Dugald Duncan and Ross Davidson for all their help and support throughout my PhD. Their combined knowledge has been wonderful to learn from and their generous guidance and patience has been very much appreciated (especially in regards to my writing 'style').

I wish to acknowledge the support of Heriot-Watt University and Scottish Rural University College for funding. I am appreciative of the help from the staff in the mathematics department at Heriot-Watt and the disease systems team at SRUC.

In the last year of my PhD I had the fortunate opportunity to work with Andrew Jarrett (at the Forestry Commission Scotland) and Peter Lurz (at University of Edinburgh). I thoroughly enjoyed meeting with Andrew and the local foresters on Arran, and I am thankful for all their time and help. I am indebted to Peter for taking his time to impart some of his ecological knowledge. I am very grateful for all his very useful advice and enjoyable conversations!

Lastly, I would like to thank my office mates, family and friends for their continued support and encouragement; my PhD would probably have been insurmountable without you all.

Contents

List of Figures

List of Tables

Chapter 1

An introduction to modelling population and disease dynamics in complex ecological systems

The term *Ecology* - which is derived from the Greek words 'oikos' and 'logos' meaning 'household' and 'study' - is commonly defined as the study of the relationship between all organisms and their environment (Odum et al., 1971). Ecological processes range across several magnitudes from cellular to the biosphere, and over the last century many tools have been developed to advance our knowledge of these systems and their interactions. For example, in the field of microbial ecology the recent creation of genomics tools permits the DNA structure of single cells to be examined (Xu, 2006); this has increased the data available which can, for example, be used in disease research (Feero et al., 2011). At the other end of the scale, the word biosphere is used to describe the global layers of interaction between ecological systems encompassing all living organisms. This subject has extensive coverage when issues such as climate change are being evaluated; tools like complex mathematical models can be used to identify the effect climate change may have on the landscape and biodiversity of the Earth (Opdam and Wascher, 2004; Travis, 2003).

Mathematical modelling is widely used across all scales of ecological research, spanning areas such as the kinetics of enzymes and cells (Cornish-Bowden, 2013; Hethcote, 2000), single or multiple species population dynamics (Edelstein-Keshet, 1988; Leibold et al., 2004; Murray, 2002), and the spread of infectious disease in wildlife and human populations (Anderson and May, 1979, 1981; Anderson et al., 1992; Keeling and Rohani, 2008; May and Anderson, 1979). Models can be used as a theoretical tool in a number of ways. For example to understand the ecological processes leading to population dynamics such as extinction or cycles; to examine the impact of infectious disease spread; or to test the effect of management strategies in conservation programs. In this thesis I shall use various mathematical models to describe four

ecological systems; more specifically in each case study I aim to evaluate questions specific to population and/or disease dynamics. Each case study corresponds to a chapter which contains an extensive literature review and background. Therefore in this main introduction I will give a brief historical overview to some of the most significant contributions to the field of mathematical ecology, then a short description of the aims of each chapter and some of the techniques used.

1.1 Historical overview to mathematical models in ecological systems

One of earliest mathematical observations regarding human population demographics was made in the 19th century by Thomas Robert Malthus who proposed that the population grew exponentially (Murray, 2002). In 1838, Pierre Verhulst challenged this idea and suggested that the population is more likely to saturate at some density due to resource limitation (i.e. food production). He proposed an ordinary differential equation model whereby the growth rate of a species is restricted as the density increases and it is still commonly used in many mathematical models today, normally under the name of the logistic equation. (This restriction can be interpreted as interspecies crowding - resources are limited as the population density increases.)

Over the next century many mathematicians turned their attention to the modelling the trophic web; more specifically the interaction between multiple wildlife species that can be classified as predator-prey, competition or symbiotic (Murray, 2002). One of the earliest attempts to mathematically simulate the population dynamics of wildlife were the Lotka-Volterra equations in 1926. These equations were initially proposed by Alfred Lotka to describe chemical reactions (Lotka, 1910), however 16 years later Vito Volterra realised the theoretical principles reflected predator-prey dynamics reasonably well. This novel approach uses two ordinary differential equations to simulate the rate of change in the respective prey and predator populations which are linked by the assumption that the predator growth is proportional to the consumption of the prey (Murray, 2002).

In recent years there has been many attempts to improve the assumptions of this framework, for instance the inclusion of inter-specific competition and logistic growth terms (Jungck, 1997), saturation in the contacts between species (Holling, 1966), time lags (Cushing, 1976), and stochasticity (Bahar and Mao, 2004). However in absence of these variations the solutions of the Lotka-Volterra equations are interesting since when the prey and predator co-exist they can experience cyclic population dynamics (Murray, 2002). Population cycles are widely recognised within many wildlife systems and understanding their drivers is a large research area within mathematical ecology

today (Berryman, 2002). Predator-prey interactions are only one of the many hypotheses presented to explain cycling population dynamics (Korpimäki and Krebs, 1996) others include the weather, genotypic and phenotypic physiology, behavioural changes and resource seasonality (Berryman, 2002; Korpimäki and Krebs, 1996).

Analysis of population cycles can help build a greater understanding of the interaction between different species and their environment. This can identify the main drivers causing the cycles which, in turn, may highlight the dependence on other species and/or environment for regulation (Bowers et al., 1993). Moreover, population cycles may sometimes reach low densities which increase the risk of extinction; therefore understanding the mechanisms which trigger the oscillations may identify ways to mitigate the threat of extinction. A practical reason for understanding population cycles is it may help to develop methods to control pests (Briske et al., 2010). For example, many insect species can undergo large population cycles in which, at their peak, they can become pests. This can create potential for ecological (Lovett et al., 2006) and economical (Ginzburg and Taneyhill, 1994) side effects on the surrounding biosphere.

At a similar time to the evolution of the Lotka-Volterra equations, Kermack and McKendrick (see the re-release of the original work Kermack and McKendrick (1991)) developed a compartmental model to mathematically describe infectious disease in a population (Diekmann et al., 1995; Murray, 2002). The framework, proposed in 1927, was a set of three ordinary differential equations - coined the Susceptible-Infected-Recovered (SIR) model - whereby hosts were partitioned dependent on their infection status. Individuals can change class by becoming infected or recovering; disease transmission is simulated by a mass action term to represent the interaction between the susceptible and infected classes and infected individuals recover at some constant rate. This framework was also used to calculate the number of susceptible hosts needed for an epidemic outbreak to occur (often called the epidemic threshold and related to basic reproductive ratio of the disease, R_0) (Hethcote, 2000).

Around the 1980s Roy Anderson and Robert May published several novel papers extending epidemiology research to consider the population dynamical consequences of different parasites and to compare theoretical finding to experimental and field data (Anderson and May, 1979, 1981; May and Anderson, 1979). Their work concluded that parasitic infections can regulate vertebrate and invertebrate populations and also drive population cycles - thereby adding infection to the list of possible causes of cycles (Anderson and May, 1979; May and Anderson, 1979). By extending the compartmental models of Kermack and McKendrick they explored several models set-ups to highlight the most important factors contributing to cyclic population dynamics. For example in Anderson and May (1981) model A extends an Susceptible-Infected-Susceptible (SIS) model to include demographics and pathogen induced mortality,

and through analysis they concluded that high pathogenicity (relative to the intrinsic host growth rate) was the leading term contributing to population cycles. Another framework (which is used in this thesis in Chapter 2) is model G which extended model A to include the free-living stages of a pathogen. This showed that the host-pathogen interaction could cause high period population oscillations and may explain the cycles observed in forest insect systems - which typically have a period of around 6-10 years.

These frameworks have been hugely influential in the field of mathematical epidemiology (Anderson et al., 1992; Hethcote, 2000; Keeling and Rohani, 2008; Murray, 2002). They underpin many of the more sophisticated model structures that include, for example, age and/or cohort structure, spatial structure, seasonality, and stochasticity, and that have been used to represent ecological systems. Moreover the development of these techniques has allowed the precise ecological dynamics relating to a specific system and/or disease to be translated into mathematical language which in turn can be used to obtain a greater understanding of the systems processes. These classical model structures underpin the model frameworks that are developed in this thesis and an extended discussion of each of our model systems will be presented in each chapter.

1.2 Aims

Each chapter represents a self-contained case-study and includes an extensive background description of the ecology and mathematical modelling techniques. To avoid repetition I shall only highlight the main aims of each study here.

In Chapter 2 we extend the deterministic host-pathogen framework of Anderson and May (1981) to include a maternal effect on disease resistance. A maternal effect encompasses the idea that the quality of the maternal environment can affect the phenotype of the offspring (Bernardo, 1996; Gutterman, 2000). Many empirical studies, on a range of taxa, have considered the impact of maternal effects by controlling the parental environment through food quality and crowding (Boots and Roberts, 2012; Little et al., 2003; Mitchell and Read, 2005; Rossiter, 1991). A motivation for this project uses a recent study by Boots and Roberts (2012) who investigated the maternal effect in *Plodia interpunctella* in relation to a *granulosis* virus and concluded that disease resistance can be maternally inherited and is related to the quality of the maternal environment. Since maternal effects have been linked to population cycles, we consider the impact of maternally inherited disease resistance on the population dynamics in a host-pathogen framework. Our aim is to assess whether the maternal effect will increase or decrease the likelihood of population cycles.

In Chapter 3 we use mathematical models to measure the impact infection may

have on population size estimates using Capture-Mark-Recapture (CMR) studies. CMR studies are commonly used to gather information about small mammal species by recording the number of captures over a period of trapping sessions. The data can then be inputted into statistical models to estimate the population size in a bounded area (such as the programs CAPTURE and MARK, Pollock (1990)). In a recent study, Coltherd et al. (2010) concluded that parasitism can affect the rate of capture of wood mice and may be a source of heterogeneity in trapping studies. If this is possible population estimates may be biased if the heterogeneity remains undetected. We therefore use two mathematical models to simulate a series of infection dependent CMR data which can be inputted into statistical models to estimate the population size. The first model extends a classic deterministic Susceptible-Infected-Susceptible (SIS) model of Anderson and May (1979), whilst the second uses an individual-based, stochastic framework to replicate the disease and CMR process. We aim to assess whether modern statistical packages that estimate population density can account for the heterogeneity due to trapping rate depending on infection status. Importantly, we also use this case study as an opportunity to develop the mathematical techniques required to translate a model from a deterministic to stochastic set-up using the methodology of Keeling (1999) since this technique will be used in Chapters 4 and 5.

In the final two chapters we take advantage of inter-disciplinary collaboration to develop models to represent the population dynamics of the Eurasian red squirrel (*Sciurus vulgaris*) population on complex landscapes. Collaboration with an ecologist and the Forestry Commission Scotland allowed our models to be set-up with realistic assumptions to answer specific, real life problems. In both chapters we implement the technique developed in Chapter 3 which translates a deterministic framework to an individual-based, stochastic model but additionally include spatial structure (Judson, 1994). Real-life landscapes are represented using geographical information systems (GIS) which extrapolate woodland data from Forestry Commission databases, allowing habitat suitable for red squirrels to be identified. Creating a spatial, individual-based, stochastic model allows us to describe the heterogeneous distribution and connectivity of real-life landscapes which produce complex relationships with population abundance and persistence (Bienen, 2002).

Red squirrels have been in decline in mainland UK due to disease mediated invasion from the introduced North American grey squirrels (*Sciurus carolinensis*) in the 1900s. The emerging squirrelpox virus (SQPV) is critical in explaining the rapid replacement of reds since it causes high mortality in red squirrels and grey squirrels are avirulent carriers (Bosch and Lurz, 2012; Tompkins et al., 2003). In Chapter 4 we assess the potential spread of the disease in red squirrels on the Isle of Arran (which currently has no greys or SQPV) using a deterministic Susceptible-Infected (SI) framework and the techniques outlined in Chapter 3 we develop a spatial, individual-based,

stochastic SI model to simulate disease spread in red squirrel populations. Moreover by representing a real-life landscape we are able to provide a general understanding of the role of landscape connectivity in the spread and persistence of infectious disease. This work has been submitted as a paper.

In Chapter 5 we extend the framework in Chapter 4 to investigate how including seasonality in a spatial, individual-based, stochastic model will impact species introductions and population persistence (in the absence of disease). Habitat evaluation along with planning and monitoring is a critical part of re-introduction success as they can provide projections of species abundance in addition to being used to assess the impact of any landscape alterations. Moreover habitat can undergo multi-year cycles in seed crops which can impact dispersal corridors and persistence (Kelly et al., 2008). However it is only recently that spatial models have considered the inclusion of representing real-life landscapes (Armstrong and Seddon, 2008; Rout et al., 2007; Sarrazin and Barbault, 1996; Seddon et al., 2007; IUCN, 1987) and the impact of seasonality on landscape connectivity and the affect this may have on species introduction has not been previously studied. Our aim is to assess how landscape connectivity and fluctuations in resource abundance affect the spread and persistence of red squirrels. This work informs conservation strategies which aim to maintain a viable population of red squirrels on the Isle of Arran and can be used to assess the potential success of introducing red squirrels on the Isle of Mull. Such isolated stronghold populations may support viable red squirrel populations in the long-term and may be critical should red populations in mainland UK continue to be replaced by grey squirrels.

In the discussion we highlight the key findings and explore areas where the work in this thesis could be extended.

Chapter 2

The population dynamical consequences of a maternal effect on disease resistance

2.1 Introduction

An individual's phenotype is dependent on multiple factors. One such factor - termed the maternal effect - recognises that the quality of the maternal environment impacts the phenotype of an offspring (Bernardo, 1996; Gutterman, 2000). Maternal effects were initially studied in plants circa 1900 and it is now widely accepted that the next generation is heavily dependent on the conditions experienced by the maternal plant (Gutterman, 2000; Roach, 1987). Over the last two decades research suggests that the maternal effect can be detected in an extensive range of taxa with offspring life history traits such as size, growth rate, mortality and disease resistance being impacted (Bernardo, 1996; Boots and Roberts, 2012; Little et al., 2003; McCormick, 1998; Mitchell and Read, 2005; Rossiter, 1991).

Rossiter (1991) examined the effect that variable parental food quality had on offspring of the gypsy moth *Lymantria dispar*. A range of phenolic and defoliation values of parental habitat was measured, and the length of the pre-feeding period, development time, and pupal weight of the offspring was recorded. Rossiter (1991) found offspring attained a greater pupal weight when their mother fed on trees with higher damage levels. Furthermore mothers who fed on trees with greater condensed tannin levels resulted in production of daughters with a reduced pre-feeding period. Rossiter (1991) inferred that an increase in female pupal weight can result in an increase in fecundity levels and thus population natality; in addition a shorter pre-feeding period may increase the survival rate in early development. This example highlights that the nutritional experience of previous generations can impact the life history traits of future generations. Such changes in life history characteristics may

in turn affect the dynamics at a population level.

Maternal effects have been implicated in the generation of population cycles in a range of systems; for example the maternal effect hypothesis is a proposed driver of population cycles observed in northern European voles (Inchausti and Ginzburg, 1998, 2009). It is argued that maternal effects act as a general mechanism that can induce delayed density dependent feedbacks, since the effect of the maternal environment will not be expressed until their offspring reproduce. Furthermore, delayed density dependence is a known mechanism that can produce population cycles (Beckerman et al., 2002; Inchausti and Ginzburg, 2009). Rossiter (1991) proposes that the maternal effect acting upon offspring fecundity and survival may induce population cycles since a time lag is created. In these systems maternal quality can alter an offsprings growth rate; therefore the impact of a poor or good environment translates over several generations. This may lead to rapid population increases or population crashes which can drive multi-year cycles.

In addition to affecting demographic parameters, maternal effects can impact the level of inherited resistance to infectious disease. Innate immunity is the first line of defence in all mammals as it supplies macrophages (phagocytic white blood cells) to the infected area very quickly (Beck and Habicht, 1996). Vertebrate species acquire additional immunity from previous infections, which provide a faster, more specific immune response to any secondary attacks. Conversely, invertebrate species lack this immunological memory which provides acquired immunity against specific pathogens (Barnes and Siva-Jothy, 2000; Beck and Habicht, 1996). However, recent evidence suggests the level of resistance to pathogens in invertebrates may be maternally inherited depending on the environmental conditions experienced by the mother (Boots and Roberts, 2012; Little et al., 2003; Mitchell and Read, 2005).

Little et al. (2003) tested the hypothesis that offspring of the water flea *Daphina Magna* could acquire strain specific immunity to the bacterial pathogen *Pasteuria ramosa* if their mothers had prior exposure to the same strain. *Daphina magna* were split into two maternal groups and exposed to two strains, referred to as strain A and strain G. The offspring of each group were then further divided into groups that were challenged with each strain creating four classes of offspring: two with homologous exposure (mother and offspring experience the same strain) and two with heterologous exposure (mother and offspring challenged with different strains). Little et al. (2003) found that offspring whom experienced the same strain as their mother had a lower infectivity rate than those who had heterologous challenges, demonstrating acquired strain specific immunity of *Daphina magna* to *P. ramosa* dependent on maternal exposure.

Another study by Mitchell and Read (2005) found that offspring of the female *Daphnia magna* produced under poor conditions (low food availability and high pop-

ulation density) have a higher resistance to the bacterial pathogen *Pasteuria ramosa* than offspring produced in favourable conditions. A low level of resources is often used as a proxy for high density (Fryxell et al., 1991) and may translate into to a higher probability of infection. As *Daphnia magna* life span is short, offspring are likely to experience similar conditions to their parents, thus benefiting from an increased resistance when pathogen levels are high (Mitchell and Read, 2005). It may seem unintuitive that more effort is put into increasing resistance of offspring when resources are low due to the increased energy that this would require, however *Daphnia magna* have been found to optimise their reproductive allocation strategy by producing fewer but more resistant offspring. Mitchell and Read (2005) also inferred that maternal effects acting to increase disease resistance can impact host-pathogen population dynamics. When the population is at high density, there will be an increase in host resistance and therefore a reduction in disease transmission. This may act to reduce the propensity for population cycles in host-pathogen systems (Mitchell and Read, 2005).

Recently, a study by Boots and Roberts (2012) found a maternal effect in relation to viral infection of *Plodia interpunctella* by a *granulosis* virus. The study considered five different maternal populations subject to different food quality. The offspring of each population were dosed with a virus solution and their response was monitored. The study found offspring from the lowest quality maternal environment had the greatest resistance to the virus, providing evidence of inherited pathogen specific resistance in invertebrates. Moreover the offsprings were also found to have an increased phenoloxidase activity which is linked to an invertebrates ability to initiate a generalised immune response (Boots and Roberts, 2012; Soderhall and Cerenius, 1998). This may suggest that inheritance of non-strain specific resistance dependent on the maternal environment is possible.

Maternal effects acting on survival and growth have been shown to be a potentially key driver of population dynamics. It is clear that strain or non-strain specific inheritance of disease resistance can be maternally inherited, which may impact the host population dynamics (Beckerman et al., 2002; Benton et al., 2001; Mitchell and Read, 2005). Thus in this chapter we investigate the impact of a maternal effect acting on resistance on the population dynamics of host-pathogen systems; more specifically we are interested in whether the maternal effect acts to increase or decrease the propensity for population cycles.

To investigate this we first use the host-pathogen framework of Anderson and May (1981) (see also Bowers et al. (1993); White et al. (1996)) in the absence of any maternal effect. A stability analysis of this system provides baseline results from which we can understand the impact of the maternal effect. We extend this framework to include a representation of the level of resistance inherited at birth due to the maternal

environment in two ways. First the level of inherited resistance is linked to maternal host density. Second the level of inherited resistance is linked explicitly to the level of resources in the maternal environment. These two models capture the scenarios that have been tested in empirical studies (Boots and Roberts, 2012; Mitchell and Read, 2005). Using AUTO bifurcation software (Doedel, 1981; Doedel and Oldeman, 1981) we undertake stability analysis for the framework with a maternal effect and compare the results with the baseline study to examine whether a maternal effect on disease resistance increases or decreases the propensity for host-pathogen population cycles.

2.2 Host-pathogen model framework

2.2.1 Methods

In many invertebrate systems pathogens take the form of free-living infective stages. These stages have a high survival rate outside the host. Examples include a *nuclear polyherosis* virus of the Douglas-fir Tussock Moth (*Orgyia pseudotsugata*) and the *granulosis* virus of cabbage butterfly (*Pieris brassicae*) which can remain infective in the environment for several years (Anderson and May, 1981). The pathogen stages are ingested by the host, then replicate within the host where they can cause considerable damage and potentially host death. The pathogen stages are then shed by the host as free-living infective stages and the process can repeat.

To represent such invertebrate host-pathogen systems Anderson and May (1981) extended a classical Susceptible-Infected-Susceptible (SIS) differential equation model to represent a pathogen with free-living infective stages, known as Model G. In the SIS framework transmission is due to direct contacts between susceptible and infected individuals. Model G alters the disease transmission term to depend on the interaction between the susceptible hosts and free-living infective stages. Subsequently, Bowers et al. (1993) modified model G to include a density dependent birth rate (forcing the host population to saturate to a carrying capacity as a result of limited resources) and examined the sensitivity of population cycles to model parameters. In particular they assessed whether host-pathogen interactions could drive the population fluctuations observed in many forest insect systems. We use this framework as our baseline model which we will extend to include maternal effects acting on resistance.

The model of Bowers et al. (1993) considers the dynamics of the susceptible host population X, infected host Y and a pathogen with a population of free-living infected stages W given by

Parameter	Definition	Baseline value
a	Host birth rate	$a = 4.3\text{yr}^{-1}$
q	Intra-species competition	$q = 1/4.3$
b	Natural host death rate	$b = 3.3\text{yr}^{-1}$
ν	Transmission coefficient of disease	$\nu = 10^{-4}\text{yr}^{-1}$
α	Rate of disease induced mortality	$\alpha = 0$ *
ζ	Rate at which infected hosts produced free-living infective stages	$\zeta = 0$ *
μ	Natural decay of free-living infected stages	$\mu = 3\text{yr}^{-1}$
r	Intrinsic growth rate	$r = a - b$

Table 2.1: List of parameter definitions used in Equations (2.1). The baseline parameter values are taken from Bowers et al. (1993). * denotes parameters that are varied to find the stability regions (parameter space); their initial values are given.

$$\frac{dX}{dt} = a(X+Y)(1-q(X+Y)) - bX - \nu XW \tag{2.1a}$$

$$\frac{dY}{dt} = \nu XW - (b+\alpha)Y \tag{2.1b}$$

$$\frac{dW}{dt} = \zeta Y - \mu W \tag{2.1c}$$

The per capita maximum birth rate, a, is modified due to crowding through the parameter q which is related to the host carrying capacity K in the absence of the disease by $K = (a-b)/(aq)$. Natural host death occurs at rate b. Infective stages are produced by infected hosts at rate ζ and decay naturally at rate μ. Susceptible hosts become infected by consumption of infective free-living stages with transmission coefficient ν. Once infected, hosts have an additional mortality at rate α due to the pathogen.

In line with the study of Bowers et al. (1993) we assume there is no recovery from infection (insect populations do not have a developed immune system and so in most systems infection is fatal (Barnes and Siva-Jothy, 2000; Beck and Habicht, 1996)). In addition, evidence suggests additional mortality of the free-living infective stages due to uptake by hosts is negligible compared to natural decay of the pathogen (Dwyer, 1994; White et al., 1996), thus the uptake term which appears in the original model framework is excluded (Anderson and May, 1981; Bowers et al., 1993). The parameters in the model are defined in Table 2.1.

It is sometimes convenient to consider the total host population, $H = X + Y$ as

follows:

$$\begin{aligned}
\frac{dH}{dt} &= \frac{dX}{dt} + \frac{dY}{dt} \\
&= a(X+Y)(1-q(X+Y)) - b(X+Y) - \alpha Y \\
&= H\left((a-b) - aqH\right) - \alpha Y \\
&= rH\left(1 - \frac{aq}{r}H\right) - \alpha Y \\
&= rH\left(1 - \frac{H}{K}\right) - \alpha Y \qquad (2.2)
\end{aligned}$$

where $r = a - b$ and $K = r/(aq)$. Solving Equations (2.1) numerically with the parameters given in Bowers et al. (1993), results in a free-living infective stage density typically 7 orders of magnitudes greater than the host population. We therefore rescale Equations (2.1) by setting $V = 10^{-7}W$ to produce the following

$$\frac{dX}{dt} = a(X+Y)(1-q(X+Y)) - bX - \beta XV \qquad (2.3a)$$

$$\frac{dY}{dt} = \beta XV - (b+\alpha)Y \qquad (2.3b)$$

$$\frac{dV}{dt} = \lambda Y - \mu V \qquad (2.3c)$$

where $\beta = 10^{7}\nu$ and $\lambda = 10^{-7}\zeta$. We now use these Equations (2.3) to produce the baseline stability regions for the host-pathogen framework.

2.2.2 Steady state and stability analysis

Equations (2.3) has three biologically realistic steady states: the trivial steady state in which all classes are zero ($X = 0, Y = 0, V = 0$), the disease-free steady state in which there are no infected hosts or pathogen and the susceptible host is at the carrying capacity ($X = (a-b)/(aq) = K, Y = 0, V = 0$) and a co-existence steady state in which the host and pathogen have positive density ($X = X_C, Y = Y_C, V = V_C$) where

$$X_C = \frac{\mu(b+\alpha)}{\beta\lambda} \tag{2.4a}$$

$$V_C = \frac{\lambda}{\mu} Y_C \tag{2.4b}$$

$$0 = (aq){Y_C}^2 + \left((\frac{\lambda\beta}{\mu} + 2qa)X_C - a \right) Y_C + (a(qX_C - 1) + b)\, X_C. \tag{2.4c}$$

Y_C is found by solving the quadratic equation (2.4c) for the positive root. To determine the stability of the steady states we calculate the eigenvalues using the Jacobian which is given by

$$J = \begin{bmatrix} a(1-2qH) - b - \beta V & a(1-2qH) & -\beta X \\ \beta V & -(b+\alpha) & \beta X \\ 0 & \lambda & -\mu \end{bmatrix} \tag{2.5a}$$

where $H = X + Y$.

Eigenvalues for the trivial equilibrium are $\theta_1 = (a-b) = r, \theta_2 = -(b+\alpha)$ and $\theta_3 = -\mu$. Therefore whenever the host growth rate r is positive (which we assume) the trivial equilibrium is unstable.

The eigenvalues for disease free equilibrium are $\theta_1 = -(a-b) = -r$ and $\theta_{2,3} = -(b+\mu+\alpha)/2 \pm \sqrt{((b-\mu+\alpha)^2)/4 + (\beta\lambda(a-b))/(aq)}$. θ_1 and θ_3 are clearly negative and real when the growth rate r is positive, as all other parameters are positive. If the product of θ_2 and θ_3 is positive then θ_2 is negative and therefore the steady state is stable. This occurs when

$$\theta_2\theta_3 = \mu(b+\alpha) - \frac{\beta\lambda r}{aq} > 0$$

which we write as

$$R_0 = \frac{\beta\lambda K}{\mu(b+\alpha)} < 1 \tag{2.6}$$

The disease free steady state is therefore stable if the basic reproductive rate of the pathogen, R_0, is less than unity. This can be interpreted as the pathogen failing to produce enough free-living stages to sustain itself in an environment of susceptible hosts at the carrying capacity.

It is not possible to explicitly determine the eigenvalues for the co-existence equilibrium and so we utilise the methods of Bowers et al. (1993) to determine stability. By examining the Routh-Hurwitz stability criterion it is possible to show that for

stability it is required that $R_0 > 1$, leaving the disease-free equilibrium unstable. The Routh-Hurwitz stability criterion are applied to the characteristic equation (of the form $z^3 + Az^2 + Bz + C = 0$) of the Jacobian at the steady state. If the trace ($A = -\text{ trace}(J)$) and determinant ($C = -\det(J)$) are both negative and $AB - C$ is positive the steady state is stable (Bowers et al., 1993). Analysing the trace and the determinant algebraically is complicated and so instead we use numerical methods to trace the stability boundary representing the Hopf-bifurcation curve marking the region where the co-existence equilibrium becomes unstable (which occurs when $AB - C = 0$). The stability boundaries in $\lambda - \alpha$ parameter space for different values of disease transmission are shown in Figure 3.1. This figure shows that reducing the disease transmission coefficient β (which represents an increase in host resistance to infection) leads to a reduction in the size of the region where population cycles are exhibited.

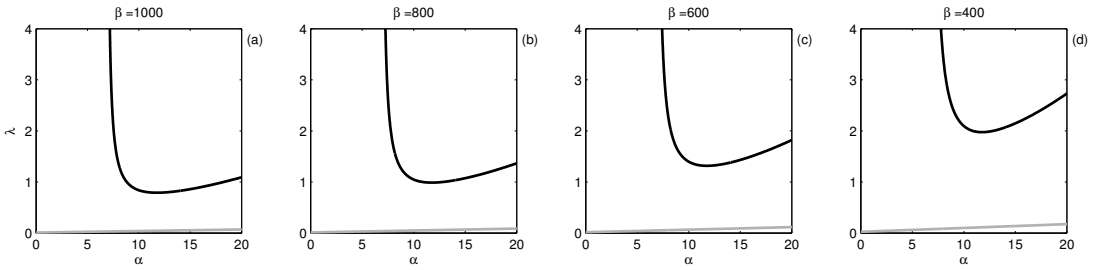

Figure 2.1: Equations (2.3) are analysed in $\lambda - \alpha$ parameter space with the stability boundaries $R_0 = 1$ (grey) and Hopf-bifurcation curve (black) displayed. Below $R_0 = 1$ the disease-free equilibrium is stable, above $R_0 = 1$ and below the Hopf-bifurcation curve the co-existence steady state is a stable point equilibrium, above the Hopf-bifurcation curve the host and pathogen exhibit population cycles. The disease transmission coefficient is varied in (a) $\beta = 10^3$, (b) $\beta = 800$, (c) $\beta = 600$, and (d) $\beta = 400$. Other parameter values are taken from Bowers et al. (1993) and are $r = 1, b = 3.3, \mu = 3.0, K = 1$.

In Figure 2.2 we illustrate a time series of the susceptible and infected host and free-living pathogen densities for a fixed parameter set in each stability region identified in Figure 3.1. It is clear from Figure 2.2 (c) that when the host and pathogen population exhibit large amplitude oscillations they may spend a substantial period of time close to zero.

Life-history theory has long recognised the importance of trade-offs which arise, for instance, due to energetic constraints (Boots and Begon, 1993; Kawecki and Stearns, 1993). In line with Mitchell and Read (2005), who found *Daphnia magna* optimise their reproductive allocation strategy by producing less but more resistant offspring,

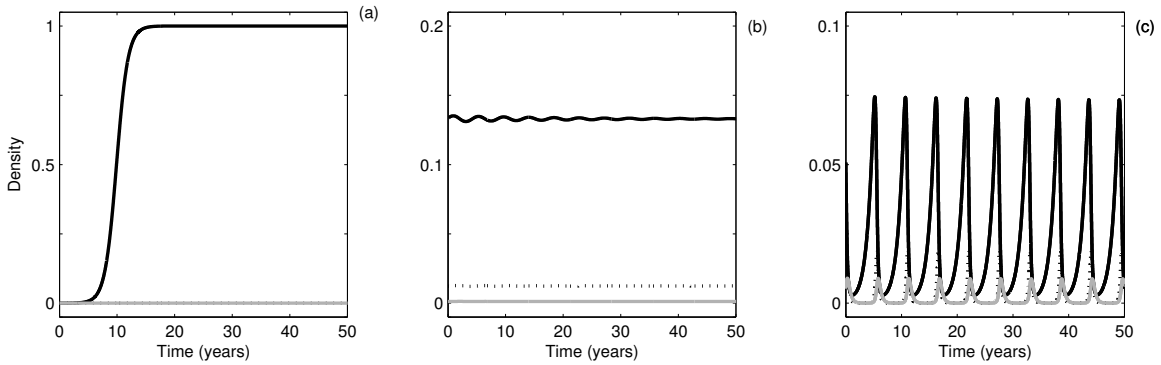

Figure 2.2: The time series illustrates the different population dynamics presented in Figure 3.1(a) with the susceptible host X (solid black), infected host Y (dotted black) and the free-living pathogen V (grey). Parameters are consistent with Figure 3.1(a) with $\alpha = 10$ and the shedding rate varied to represent each region where (a) $\lambda = 0.001$ is below $R_0 = 1$, (b) $\lambda = 0.3$ is between $R_0 = 1$ and the Hopf-bifurcation curve and (c) $\lambda = 2$ is above the Hopf-bifurcation curve.

we assume that offspring that benefit from increased resistance to infection will pay a cost in terms of a reduced birth rate. Before we extend our framework to include a maternal effect on pathogen resistance, we examine the impact of reducing the host birth rate in the original Equations (2.3). We proceed as before by tracing the Hopf-bifurcation curve identifying the boundary between the stable and cycling host-pathogen dynamics for a range of birth rate values with the result is shown in Figure 2.3. (Note we have removed the pathogen extinction boundary, $R_0 = 1$, for clarity.)

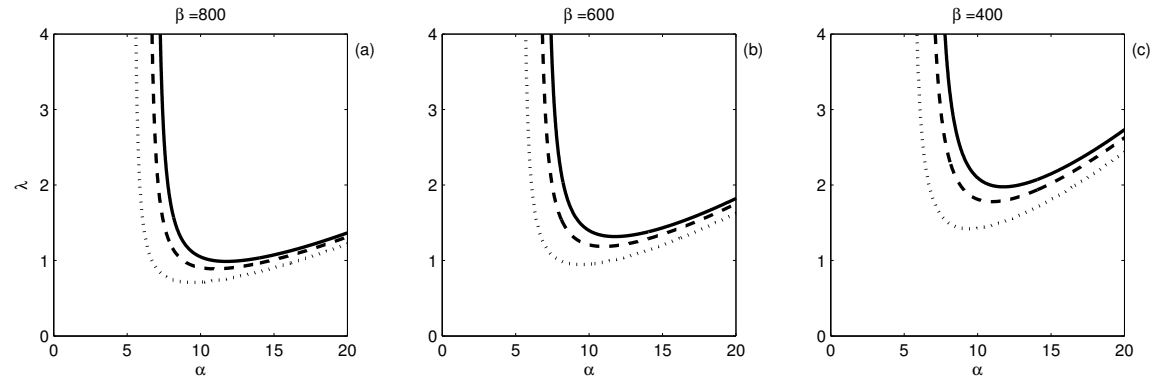

Figure 2.3: The Hopf-bifurcation curves of Equations (2.3) are plotted in $\lambda - \alpha$ parameter space for with changes in the host birth rate where $a = 4.3$ (thick), 4.085 (dashed) and $a = 3.655$ (dotted). Disease transmission coefficient is varied in (a) $\beta = 800$, (b) $\beta = 600$, and (c) $\beta = 400$ and other parameter values are consistent with Figure 3.1.

Figure 2.3 highlights that decreasing the host birth rate in Equations (2.3) in-

creases the size of the parameter region over which cycles are exhibited. This suggests that when an increase in host resistance is bought at a cost of a reduction in host birth rate, the effect on the population dynamics will depend on the strength of the trade-off between these parameters.

2.3 Host-pathogen model with a maternal effect linked to host density

In the previous section we explored the effect of varying the disease resistance parameters and birth rate on the stability of a single host population. We now extend the host-pathogen framework in Equations (2.3) to include a maternal effect that is linked to host density.

2.3.1 Methods

We begin by splitting the host density into two cohorts with corresponding susceptible host classes X_1, X_2 (where $X = X_1 + X_2$), and infected host classes, Y_1, Y_2 (where $Y = Y_1 + Y_2$). We assume hosts in cohort 1 have parameters as defined by Bowers et al. (1993) (see Figure 3.1) while hosts in cohort 2 have an increased resistance ($\beta_2 < \beta_1$) but may also have a reduced birth rate due to a trade-off ($a_2 < a_1$). The proportion of births into each cohort is dependent on the current (maternal) host density and is controlled by the switching functions E_1 and $E_2 = 1 - E_1$. Thus the adapted host-pathogen model is given by

$$\frac{dX_1}{dt} = a_1 E_1(X_1 + X_2 + Y_1 + Y_2)(1 - q(X_1 + X_2 + Y_1 + Y_2)) - bX_1 - \beta_1 X_1 V \quad (2.7a)$$

$$\frac{dX_2}{dt} = a_2 E_2(X_1 + X_2 + Y_1 + Y_2)(1 - q(X_1 + X_2 + Y_1 + Y_2)) - bX_2 - \beta_2 X_2 V \quad (2.7b)$$

$$\frac{dY_1}{dt} = \beta_1 X_1 V - (b + \alpha)Y_1 \quad (2.7c)$$

$$\frac{dY_2}{dt} = \beta_2 X_2 V - (b + \alpha)Y_2 \quad (2.7d)$$

$$\frac{dV}{dt} = \lambda(Y_1 + Y_2) - \mu V \quad (2.7e)$$

where parameter definitions are given in Table 2.2.

In our model we assume that the inheritance of disease resistance is instantaneous. In the studies we examined, Boots and Roberts (2012) kept the maternal environment

constant throughout adulthood and the time they were laying eggs. However, in Mitchell and Read (2005) the maternal environment was altered, but they found that the adult environment was most important when considering maternal transfer of disease resistance (e.g. poor maternal environment when an adult increased the disease resistance given to the offspring whereas a poor maternal environment when a juvenile did not have as great an effect on the inheritance of disease resistance). We also assume that at an individual is born with a fixed resistance (dependent on the maternal environment), which may be expressed when challenged by the infection. We therefore assume that the time between the laying eggs and the birth of the offspring is short and so omit any analysis of time lags. Whilst the inclusion of a time lag may be more accurate, this adds additional complexity to our model.

Parameter	Definition	Baseline value
a_1	Host birth rate for cohort 1	$a_1 = 4.3\text{yr}^{-1}$
a_2	Host birth rate for cohort 2, $a_2 = \epsilon a_1$	$a_2 = 4.3\text{yr}^{-1}$
E_1	Proportion of births in cohort 1	$E_1 = 1$
E_2	Proportion of births in cohort 2	$E_2 = 0$
p	The strength of the maternal effect	$p = 0$ *
q	Intra-species competition	$q = 1/4.3$
b	Natural host death rate	$b = 3.3\text{yr}^{-1}$
β_1	Transmission coefficient of disease for cohort 1	$\beta_1 = 10^3\text{yr}^{-1}$
β_2	Transmission coefficient of disease for cohort 2, $\beta_2 = \eta\beta_1$	$\beta_2 = 10^3\text{yr}^{-1}$
α	Rate of disease induced mortality	$\alpha = 10\text{yr}^{-1}$
λ	Rate at which infected hosts produced	
	free-living infective stages	$\lambda = 0$ *
μ	Natural decay of free-living infected stages	3.0yr^{-1}
r	Intrinsic growth rate	$r = a_1 - b$
η	Increased resistance of cohort 2, $0 < \eta < 1$	$\eta = 1$
ϵ	Reduction in the birth rate of cohort 2, $0 < \epsilon \leq 1$	$\epsilon = 1$

Table 2.2: List of parameter definitions used in Equations (2.7). Parameters for hosts in cohort 1 are taken from Bowers et al. (1993) and are the same as in Table 2.1. A range is given for parameters of hosts in cohort 2, with the baseline values given in column 3 (these are chosen so that Equations (2.7) reduce to baseline Equations (2.3). * denotes parameters that are varied to find the stability regions (parameter space); their initial values are given.

When there is no maternal effect ($\beta_1 = \beta_2$ and $a_1 = a_2$) and Equations (2.7) reduce to baseline Equations (2.3) as follows

$$\begin{aligned}\frac{dH}{dt} &= \frac{dX_1}{dt} + \frac{dX_2}{dt} + \frac{dY_1}{dt} + \frac{dY_2}{dt} \\ &= aH(1-qH)(E_1+E_2) - bH - \alpha Y \\ &= rH\left(1 - \frac{H}{K}\right) - \alpha Y \end{aligned} \tag{2.8a}$$

$$\begin{aligned}\frac{dY}{dt} &= \frac{dY_1}{dt} + \frac{dY_2}{dt} \\ &= \beta(X_1+X_2)V - (b+\alpha)(Y_1+Y_2) \\ &= \beta XV - (b+\alpha)Y \end{aligned} \tag{2.8b}$$

$$\frac{dV}{dt} = \lambda Y - \mu V \tag{2.8c}$$

where $K = r/(aq)$.

2.3.2 Stability analysis

In order to analyse the steady states and stability of Equations (2.7), we first define functions E_1 and E_2 which allocate the proportion of births to each cohort depending on the host density. When the population density is low there is little investment in additional resistance and therefore the majority of births are into the X_1 cohort. When the population density is high there is greater investment into resistance producing an increase of births in X_2 and consequent decrease of births in X_1. E_1 and E_2 are defined as follows:

$$E_1 = \max[1 - p(H_1 + H_2), 0] \tag{2.9a}$$

$$E_2 = \min[p(H_1 + H_2), 1] \tag{2.9b}$$

where p determines the slope of the functions and is thus a measure of the strength of the maternal effect. Functions E_1 and E_2 are displayed in Figure 2.4 for a range of p values, and it is clear that increasing the strength of the maternal effect increases the proportion of hosts which are born in the more resistant X_2 cohort.

We can now conduct stability analysis of Equations (2.7) and compare the resulting

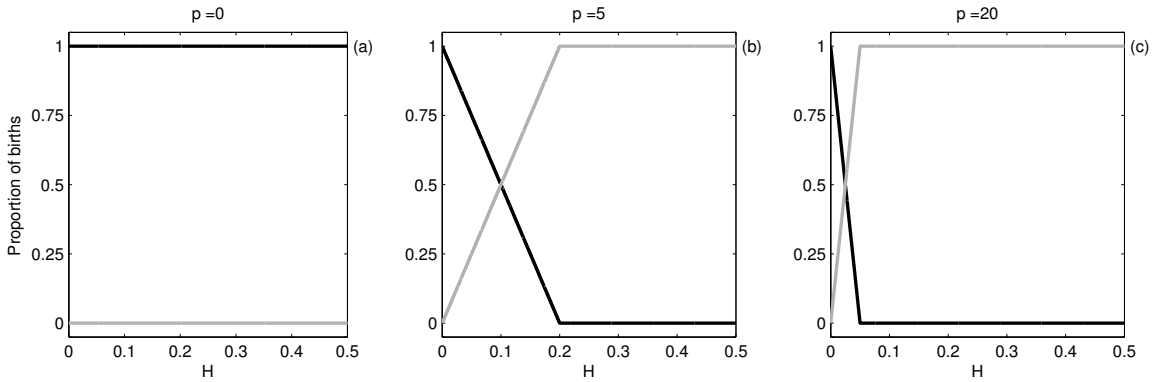

Figure 2.4: Functions E_1 (black) and E_2 (grey) specify the relationship between host density and the proportion of offspring born into cohorts 1 and 2 respectively and are defined in Equations (2.9). The functions are shown for three measures of maternal effect strength (a) $p = 0$ (there is no maternal effect and all hosts are born in the X_1 cohort), (b) $p = 5$ and (c) $p = 20$.

stability boundaries with those produced from fixed levels of host resistance. Initially we manipulate two parameters which contribute to the maternal effect directly: the strength of the maternal effect p and the increased resistance of the host born into cohort 2 through parameter η (where $\beta_2 = \eta\beta_1$).

Solving the system of Equations (2.7) is analytically intractable, thus we use numerical continuation software (AUTO, Doedel (1981); Doedel and Oldeman (1981)) to locate and trace the stability boundaries in the $\lambda - p$ parameter space. Initially we examine the impact of the maternal effect on resistance in the absence of a trade-off and therefore without the concurrent reduction in birth rate. The stability regions of the framework including a maternal effect on resistance defined by Equations (2.7) are shown in Figure 2.5 (a). The parameter space is partitioned into different regions depending on the population dynamics. Note that on the intercept with the vertical axis in this figure the maternal effect is absent ($p = 0$), and the model of Section 2.2 is recovered. We also include the Hopf-bifurcation curve for the framework in absence of maternal effect (Equations 2.3) for the two disease resistance values β_1 and β_2 to allow comparison.

Figure 2.5 indicates that the maternal effect can lead to changes in population stability. To the left of the $H_1 = 0$ extinction line (regions 1,2, and 3) both host cohorts exists; above the Hopf-bifurcation curve (region 1) there are population cycles, below the Hopf-bifurcation curve and above the $H_1 = 0$ boundary (region 2) we have stable co-existence of both cohorts and the pathogen and below the $V = 0$ boundary (region 3) there is stable host co-existence of both cohorts in the absence of the pathogen. To the right of the H_1 extinction line the system reduces to Equations (2.3) in which transmission is at level β_2 (this is why the dashed black line stops at the H_1 extinction boundary). In region 4, the host cohort 2 and the pathogen experience cycles, in region 5 the host cohort 2 the pathogen coexist at a stable equilibrium and in region 6 the

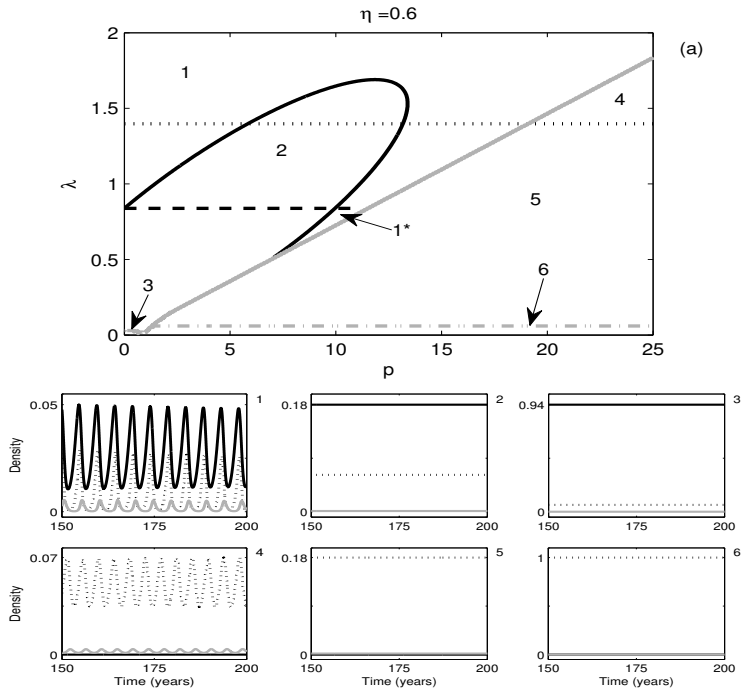

Figure 2.5: Equations (2.7) are analysed in the $\lambda - p$ parameter space and the Hopf-bifurcation (solid black), disease extinction (dot-dashed grey) and $H_1 = 0$ (solid grey) boundaries are shown in (a). The hopf-bifurcation curves for the system in absence of a maternal effect (Equations (2.3)) with β_1 (dashed black) and β_2 (dotted black) are included. The different regions of stability in (a) are numbered and their corresponding time series for fixed λ and p are shown in the remaining figures identified by the top right-hand number with H_1 (solid black), H_2 (dotted black) and V (solid grey). Here, cohort 1 has $\alpha = 10, a_1 = a$ and $\beta_1 = \beta$ (as in Figure 3.1 (a)) and cohort 2 has $\eta = 0.6$ and $\beta_2 = \eta\beta_1$ and $a_2 = a$. The different stability regions are discussed in the main text.

host cohort 2 stabilises to its carrying capacity in the absence of the pathogen.

It can be seen that for much of parameter space, where both host cohorts coexist, the maternal effect stabilises the dynamics compared to the case without a maternal effect (Figure 2.5). This is because the Hopf-bifurcation curve is generally above the line that partitions where cycles occur in the model without the maternal effect (region 2). The exception is a small region 1^* in which the maternal model predicts cycles whereas the model without a maternal effect would be a host-pathogen stable point.

The stabilising impact of the maternal effect can be seen more clearly in Figure 2.6. As the level of resistance conveyed to host cohort 2 is increased, the region of parameter space that exhibits stable host-pathogen co-existence also increases. In particular stable point dynamics are exhibited well above the Hopf-bifurcation for the model with no maternal effect (dashed line). Moreover in Figure 2.6 (b)-(c) the Hopf-bifurcation boundary for the maternal model extends beyond the Hopf-bifurcation boundary when all host are given increased resistance (dotted line). This suggests that

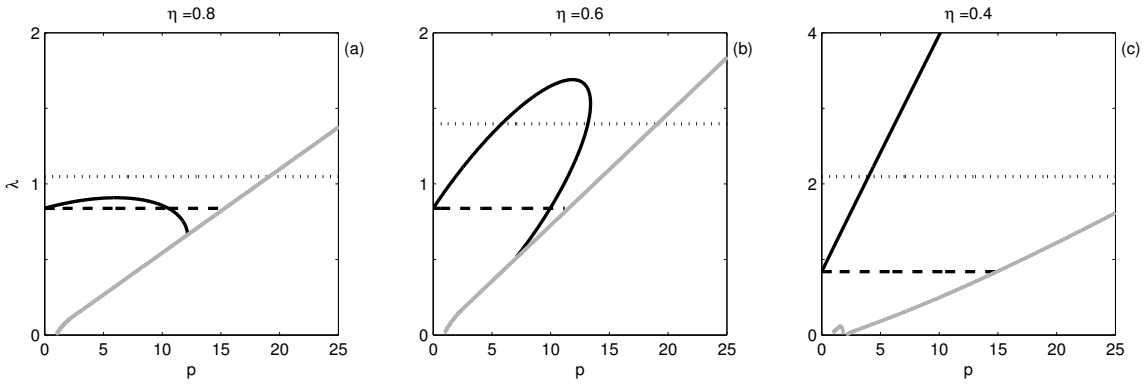

Figure 2.6: Equations (2.7) are analysed in $\lambda - p$ parameter space displaying the stability boundaries for different levels of resistance in cohort 2 where (a) $\eta = 0.8$, (b) $\eta = 0.6$, and (c) $\eta = 0.4$. The lines styles and parameter values are consistent with those defined in Figure 2.5 (a).

selectively conveying resistance through the maternal effect has a greater stabilising effect than if all hosts were fixed at a higher level of resistance.

Figure 2.7 shows the average host density (and maximum and minimum value when the host experiences cycles) as a function of the strength of the maternal effect p for different shedding rate values (λ). By decreasing λ in Figure 2.7 we can pass through different regions of stability. The vertical lines indicate where a stability boundary is crossed and typically the dynamics switch from cycles to stable point equilbria (or vice versa). Overall increasing the strength of the maternal effect results in an increase in the density of the H_2 population and total host H. In Figures 2.7 (b)-(d) crossing the $H_1 = 0$ boundary forces the system to revert to a model with only a single host cohort H_2 at a stable equilibrium (which is therefore independent of p).

In general we have shown that the greater the increase in resistance of the second cohort and the greater the strength of the maternal effect the larger the region of population stability.

2.3.3 Trade-offs: costs to increased resistance

In Section 2.2.2 we noted the importance of including a trade-off in which an increase in disease resistance is bought at a cost of a reduction in the birth rate of the host. We now analyse the impact of a trade-off in model framework that includes a maternal effect on host resistance. In line with observations in experimental insect pathogen systems (Boots and Begon, 1993) we assume an increase in resistance leads to a reduction in the birth rate (i.e. $\beta_1 > \beta_2$ and $a_2 = \epsilon a_1$ where $0 < \epsilon \leq 1$).

We trace the stability regions for different birth rate reductions in cohort 2 and different levels of resistance in Figure 2.8 (a)-(c). The trade-off which reduces the birth rate of cohort 2 acts to reduce the region in which cycles are exhibited. This

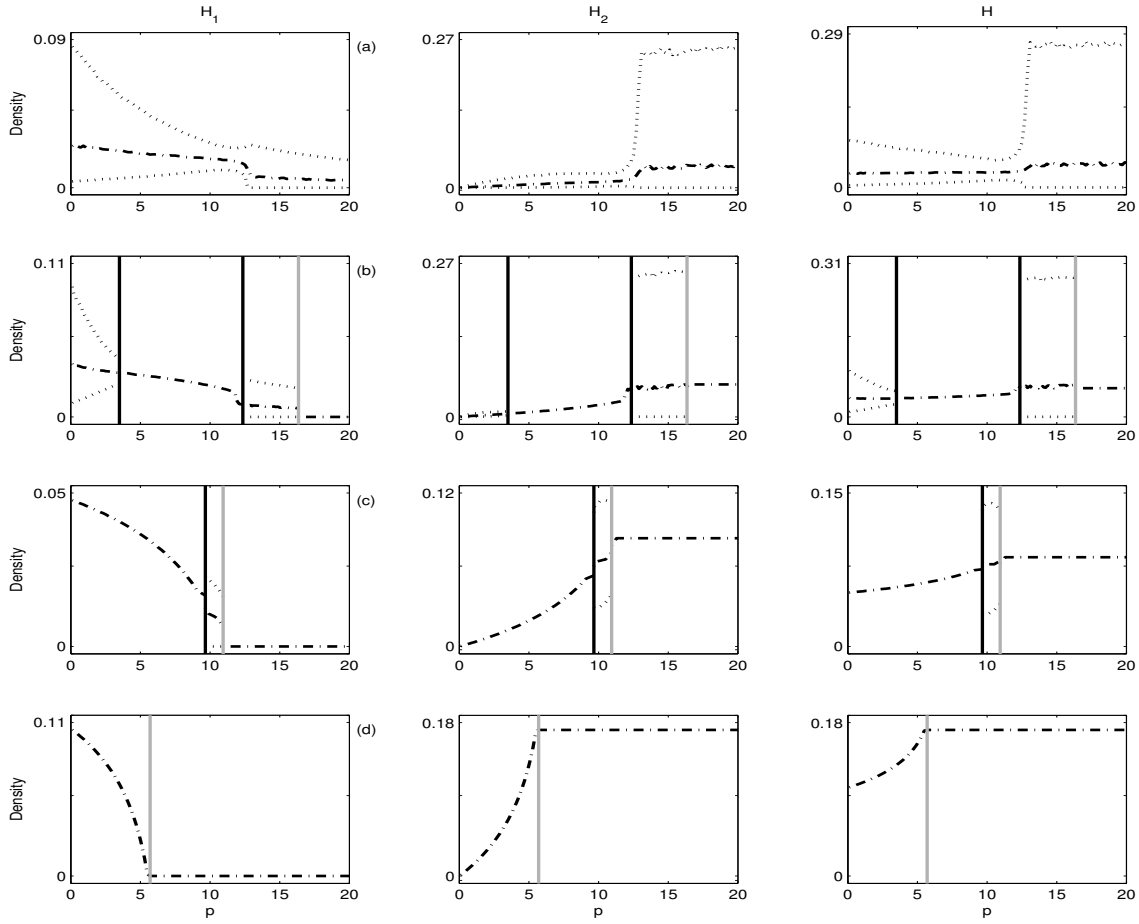

Figure 2.7: Equilbrium values (dot dashed black) of the host populations H_1 (left column), H_2 (middle column) and $H = H_1 + H_2$ (right column) as a function of the strength of the maternal effect, p are shown. The vertical lines represent passing through the Hopf-bifurcation (black) and $H_1 = 0$ boundary (grey) in Figure 2.6 (b) with each row corresponding to shedding rate (a) $\lambda = 1.8$, (b) $\lambda = 1.2$, (c) $\lambda = 0.8$ and (d) $\lambda = 0.4$. When the population is cycling, the maximum and minimum of population cycles are included (dotted black). Other parameter values are defined in figure 2.5 (a).

contrasts with the results in the absence of a maternal effect where a reduction in the birth rate resulted in an increased region of cycles (Figure 2.3). This highlights a key result indicating that a framework which includes the dynamical maternal effect linked to host density can greatly enlarge the region of stable equilibrium dynamics in the co-existing host-pathogen system. In addition, the inclusion of costs which reduce host birth rate increases the region of stable equilibrium (region 2) further; more specifically the region supporting stable equilibrium dynamics can greatly exceed the region that would support such dynamics if all offspring had additional resistance (dotted line in Figure 2.8 (d)-(f)).

The stabilising impact of the maternal effect with costs is further highlighted in Figure 2.9. Once the costs exceed a threshold then cycles are only exhibited for low strengths of the maternal effect (small p). It is interesting to note that the overall

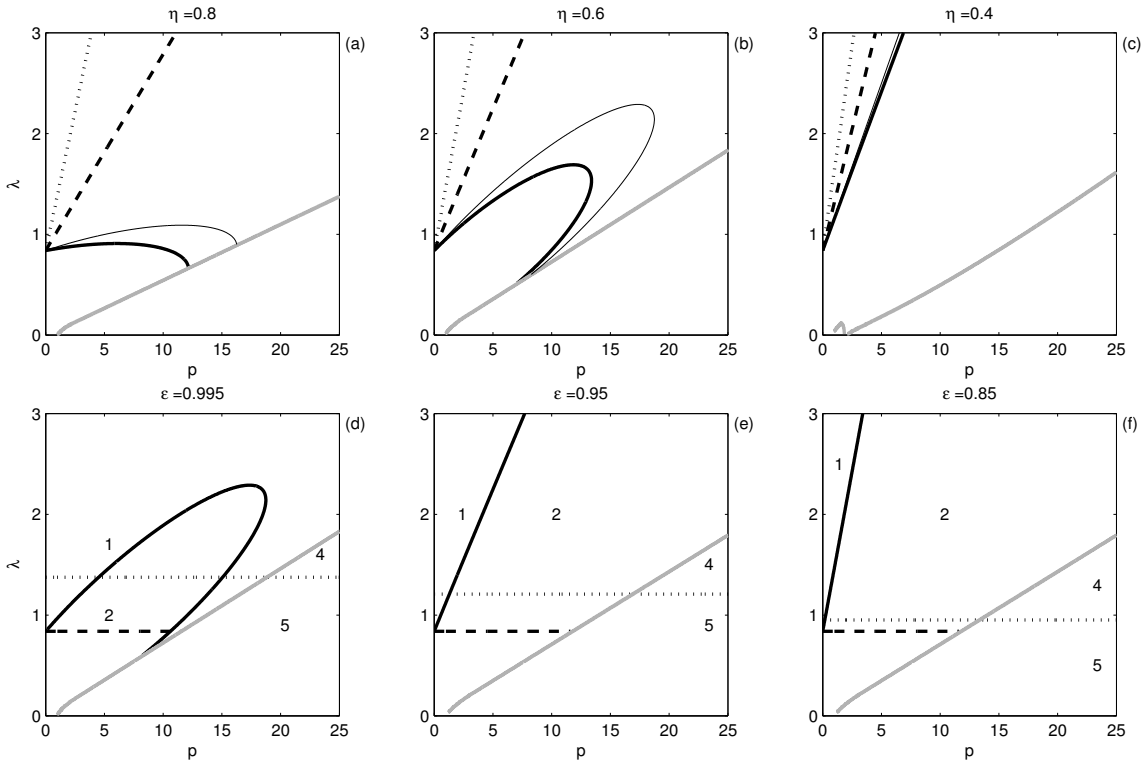

Figure 2.8: Equations (2.7) are analysed in $\lambda - p$ parameter space and the Hopf-bifurcation curves (black) and $H_1 = 0$ boundary (grey) are shown for disease transmission of cohort 2 (a) $\eta = 0.8$, (b) $\eta = 0.6$, and (c) $\eta = 0.4$. The Hopf-bifurcation is potted for a range of trade-offs in (a)-(c) $\epsilon = 1$ (thick black), $\epsilon = 0.995$ (thin black), $\epsilon = 0.95$ (dashed black), and $\epsilon = 0.85$ (dotted black). The results in (b) are highlighted in more detail below where (d) $\epsilon = 0.995$, (e) $\epsilon = 0.95$, and (f) $\epsilon = 0.85$. Furthermore, (d)-(f) include the $H_1 = 0$ boundary (grey) and Hopf-bifurcation boundaries for the system in absence of a maternal effect with β_1 and a_1 (dashed black) and β_2 and a_2 (dotted black) defined in Equations (2.3). The stability regions and other parameter values are consistent with Figure 2.5 (a).

host density increases as a result of the maternal effect even though there is a cost to resistance of a reduced birth rate. This suggests that the loss due to the reduced birth rate is exceeded by the reduction in mortality through reduced infection.

Overall the maternal effect framework given in Equation (2.9) predicts an increase in the region of host-pathogen stabilisation and an increase in host density.

2.3.4 Sensitivity analysis of the parameters

To examine the generality of our findings we conduct a sensitivity analysis by varying key model parameters and examining the resultant parameter space portraits and stability boundaries (Figure 2.10).

When the level of resistance conveyed to cohort 2 increases (Figure 2.10 (d)-(f)) the region in which a stable equilibrium is exhibited increases. The region in which population cycles are exhibited increases as the natural death rate (b) increases

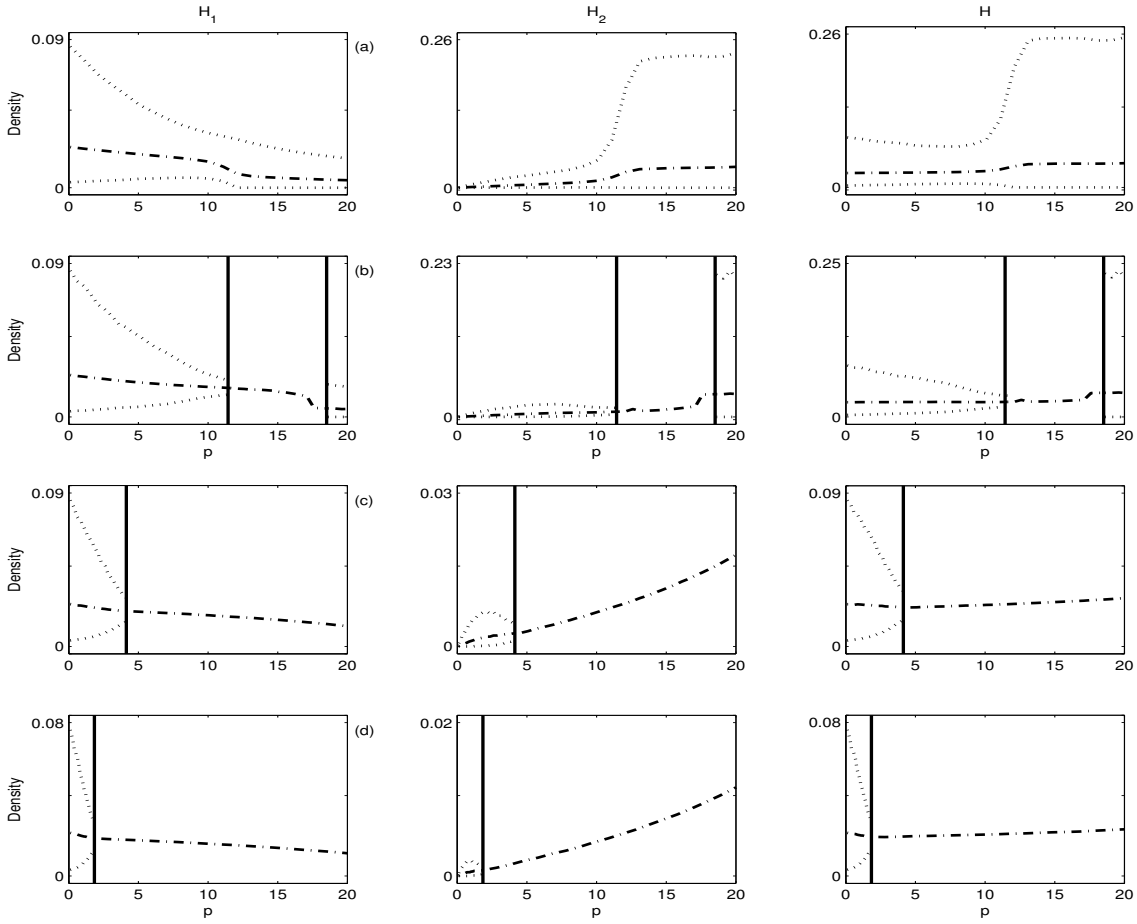

Figure 2.9: Equilbrium values of the host classes in Figure 2.8 (b) with a fixed shedding rate $\lambda = 2$ and each row corresponding to different costs to resistance with (a) $\epsilon = 1$, (b) $\epsilon = 0.995$, (c) $\epsilon = 0.95$ and (d) $\epsilon = 0.85$. Line styles are consistent with Figure 2.7 and parameter values are defined in Figure 2.5 (a).

(Figure 2.10 (a), (e) and (i)). Similarly, Figure 2.10 (b), (e) and (h) highlights that as the disease induced mortality rate (α) increases, the region in which population cycles occur increases. Increasing the pathogen decay rate (μ), reduces the free-living pathogen density and has the effect of reducing the region of cycles Figure 2.10 (c), (e) and (g). These results correspond to previous findings that examined how population cycles depend on model parameters in models that do not include a maternal effect (Anderson and May, 1981; Bowers et al., 1993; White et al., 1996).

The overall pattern shown in Figure 2.10 is consistent; the maternal effect stabilises the population dynamics and population cycles are less likely to occur as the strength of the maternal effect and the level of maternally conveyed resistance or the cost to resistance increase. (An exception is shown in Figure 2.10 (c) when the pathogen decay rate is low and where the maternal effect could induce cycles since the Hopf-bifurcation curve (black line) decreases with p.)

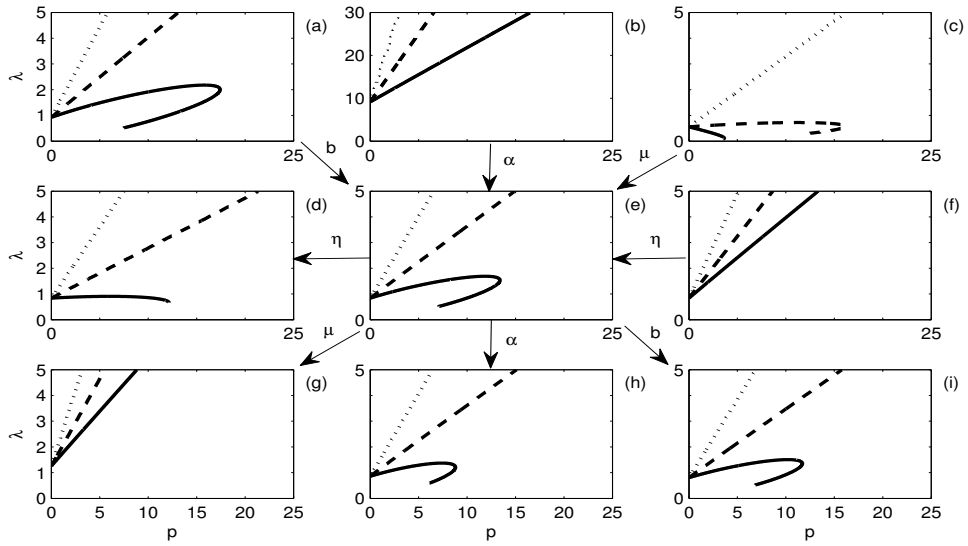

Figure 2.10: Hopf-bifurcation curves of Equations (2.7) are plotted in $\lambda - p$ parameter space including cost to resistance with $\epsilon = 1$ (solid black), $\epsilon = 0.95$ (dashed black), and $\epsilon = 0.85$ (dotted black) for various changes in parameter values. Figures (d)-(f) are the original plots from Figure 2.8 (a)-(c) with the reduction in disease transmission parameter η increasing from right to left (d) $\eta = 0.8$, (e) $\eta = 0.6$ and (f) $\eta = 0.4$. In the remaining plots $\eta = 0.6$ is fixed, with the arrow displays the direction of the parameter being increased with (a), (e), and (i) natural death rate $b = 2.5, 3, 4$, (b), (e), and (h) virulence, $\alpha = 7, 10, 15$, and (c), (e), and (g) pathogen decay $\mu = 1, 3.3, 5$. Other parameter values are as in Figure 2.5 (a).

2.4 Host-pathogen model with a maternal effect linked to resource

In experimental studies a correlation between the level of resource and the level of resistance conveyed to host offspring has been reported (Little et al., 2003; Mitchell and Read, 2005; Rossiter, 1991). In particular a low resource maternal environment led to an increased level of resistance in offspring. In this section we use the same techniques as in Section 2.3 but extend our analysis to consider the resource level, R, linked to the maternally conveyed level of host resistance. We initially investigate the behaviour at fixed resource levels only therefore R will act like an additional parameter.

2.4.1 Methods

The host-pathogen framework introduced in Equation (2.7) considers two cohorts (H_1 and H_2) with the hosts in cohort 2 incurring an increased pathogen resistance ($\beta_2 > \beta_1$). Whereas in the previous framework births into the different cohorts was dependent on host density, we now assume births are dependent on the level of resource

R which acts on functions E_1 and E_2 as follows.

$$E_1 = R \tag{2.10a}$$

$$E_2 = 1 - R \tag{2.10b}$$

As before E_1 and E_2 are constrained between zero and unity. Here a reduction in resource leads to an increase in offspring being born into the resistant cohort.

2.4.2 Stability analysis

We trace the Hopf-bifurcation curve for this framework in $\lambda - R$ parameter space for different levels of cohort 2 disease resistance and show the results in Figure 2.11. Furthermore we include the Hopf-bifurcation boundaries for the original one cohort Equations (2.3) with no host investment and total host investment in increased resistance so we can compare the impact of the maternal effect framework.

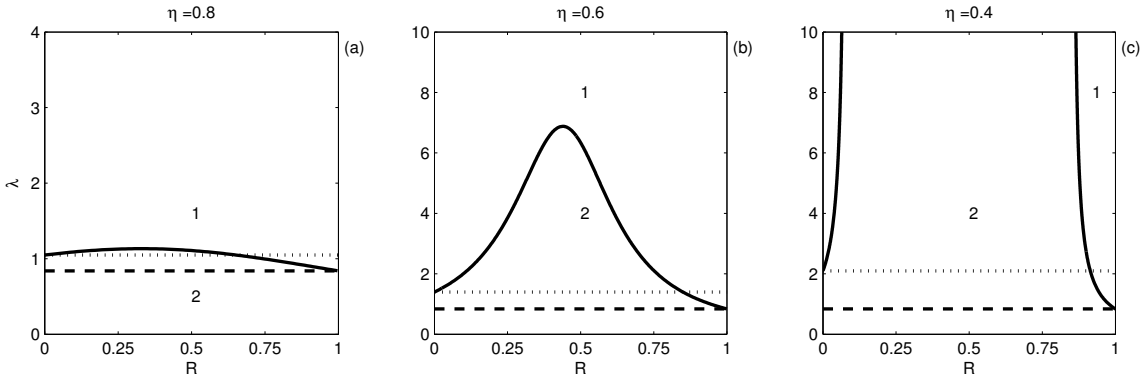

Figure 2.11: Equations (2.7) are analysed in $\lambda - R$ parameter space and the stability boundaries are displayed for different levels of resistance of hosts in cohort 2 (a) $\eta = 0.8$, (b) $\eta = 0.6$ and (c) $\eta = 0.4$. The lines styles and parameter values are consistent with those defined in Figure 2.5 (a).

When there is no resource (very poor quality environment) all hosts invest in resistance ($E_1 = 0$ and $E_2 = 1$ in Equations (2.10)), thus the Hopf-bifurcation of the resource dependent model shown meets the stability boundary of the original framework with all hosts investing in increased resistance (see Equations (2.3)) at $R = 0$ in Figure 2.11 (a)). Similarly, when the resource is at its maximum ($R = 1$), all hosts are born into cohort 1 without any increased resistance. Between these resource levels the maternal effect leads to a reduction in the region in which cycles

are exhibited. As the level of resistance conveyed by the maternal effect increases so does the region of parameter space where a stable equilibrium is exhibited (Figure 2.11 (a)-(c)).

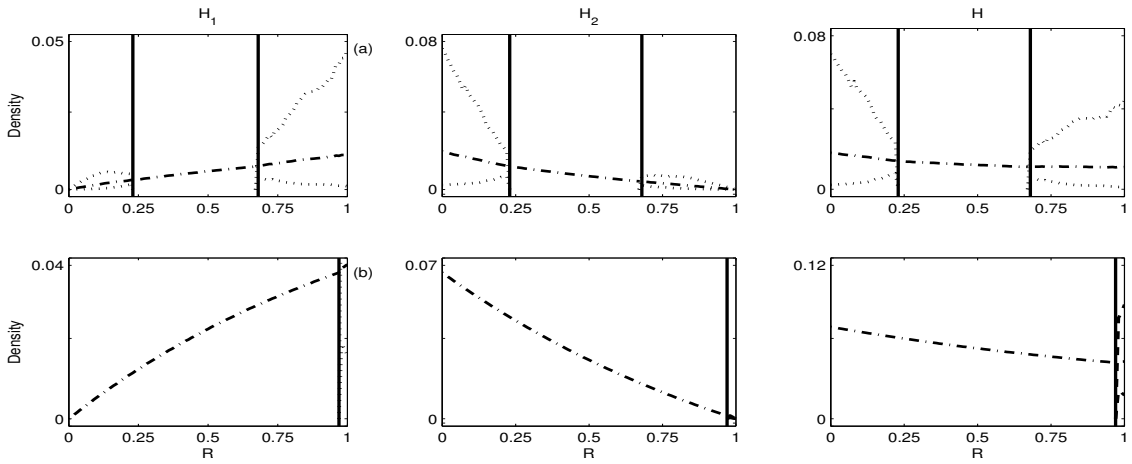

Figure 2.12: The average density (dot dashed black) of the host populations H_1 (left column), H_2 (middle column) and $H = H_1 + H_2$ (right column) as a function of the quantity of resource, R are shown. The vertical lines represent passing through the Hopf-bifurcation curve in Figure 2.11 (b) with a shedding rate (a) $\lambda = 4$ and (b) $\lambda = 1$. In addition, when the population is cycling the maximum and minimum of population cycles are included (dotted black). Other parameter values are defined in Figure 2.5 (a).

We can examine the population dynamics further and in particular how the host density changes as the level of fixed resource increases by tracing the host density (and maximum and minimum value if the host is cycling) for different shedding rates in Figure 2.12. Increasing the resource results in a decrease of births allocated to cohort 2 and an increase in the allocation to cohort 1, this is reflected appropriately in the density changes in Figure 2.12 (a)-(b). A notable result is that average host density decreases when the resource quality is increased which reflects an increase in the proportion of cohort 1 which have a lower resistance to disease.

When we include a cost to resistance in terms of a reduction in birth rate (as in previous sections) the overall finding that the maternal effect reduces the propensity to cycle is still exhibited Figure 2.13. However, the trend as the cost is increased is not so clear. In the previous section we noted that as costs increased the region exhibiting a stable equilibrium increased whereas in this model the pattern is not universal. With costs to resistance the total host population still shows an increase as the resource level drops but this increase is less marked as the costs are increased in Figure 2.14 (a)-(c).

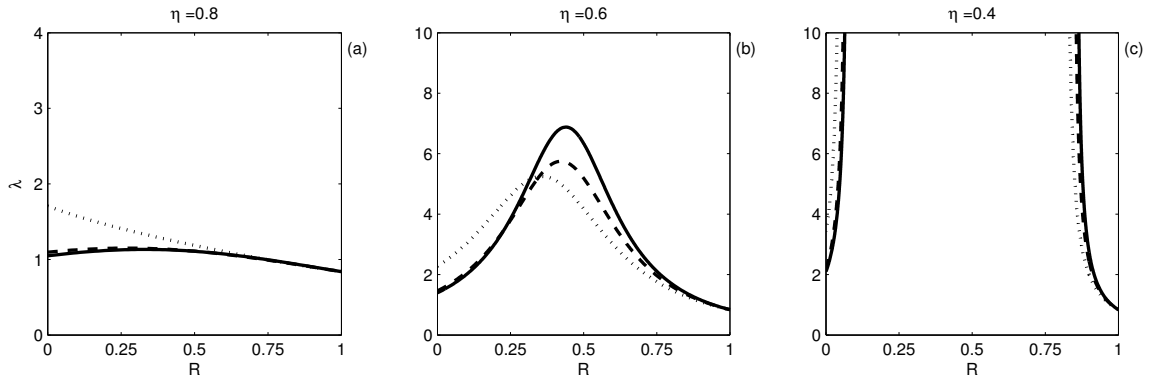

Figure 2.13: Equations (2.7) are analysed in $\lambda - R$ parameter space and the Hopf-bifurcation curves including a cost to resistance acting on the birth rate such that $\epsilon = 1$ (thick black), $\epsilon = 0.95$ (dashed black), and $\epsilon = 0.85$ (dotted black). The disease transmission coefficient of cohort 2 is varied (a) $\eta = 0.8$, (b) $\eta = 0.6$ and (c) $\eta = 0.4$. The other parameter values are consistent with Figure 2.5 (a).

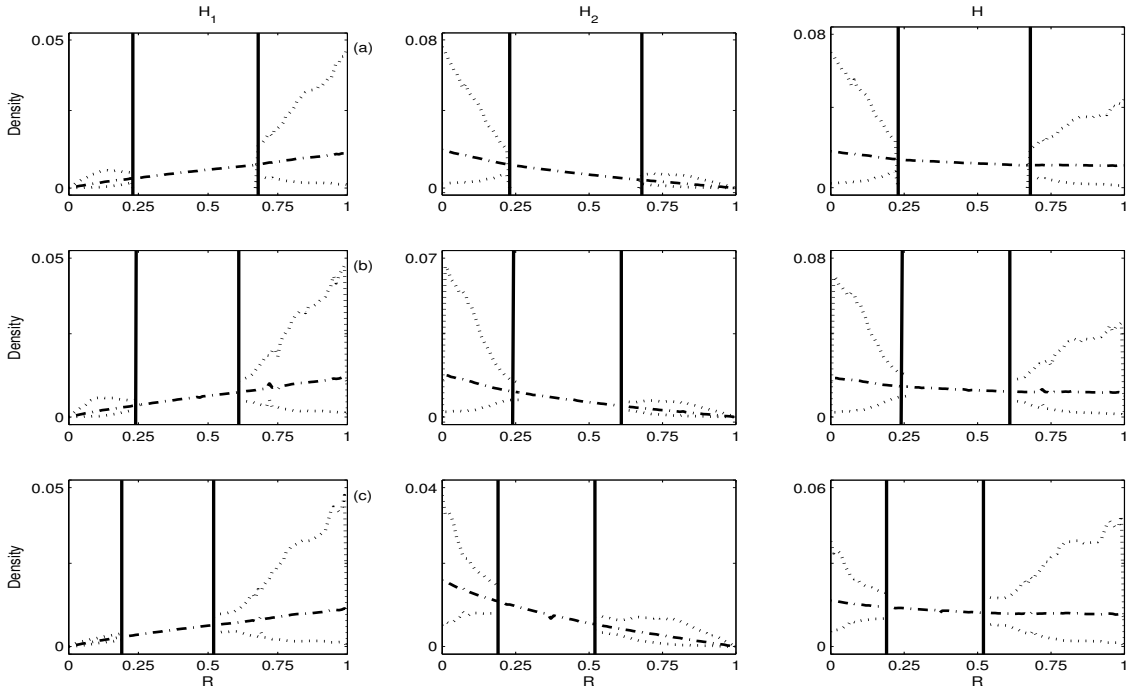

Figure 2.14: The average density (dot dashed black) of the host populations classes in Figure 2.13 (b) with the shedding rate $\lambda = 4$ and each row corresponding to a cost to resistance (a) $\epsilon = 1$, (b) $\epsilon = 0.95$ and (c) $\epsilon = 0.85$. The layout and line style is consistent with Figure 2.12 and other parameter values are defined in Figure 2.5 (a).

In summary, we have shown that a system including a maternal effect which acts to increase the resistance of offspring based on a fixed level of resource, can increase the parameter region over which a stable host and pathogen equilibrium is exhibited (Figure 2.11). When hosts with increased resistance incur a cost in terms of a reduced birth rate, the region of the parameter space exhibiting a stable equilibrium can be reduced (compared with the framework in absence of costs and at higher resource levels). However when compared to the original model without maternal effects, the

impact of the maternal effect is stabilising (Figure 2.13).

2.5 Host-pathogen model framework with a dynamic resource

In this section we extend the model framework to consider a dynamical resource. We assume the resource exhibits logistic growth but can also be consumed by the host. In addition the birth rate of the host is proportional to the rate of consumption of the resource.

2.5.1 Methods

We revise the framework in Equation (2.3) to explicitly include a dynamic resource (R) and a resource dependent host birth rate. The adapted model is given by

$$\frac{dR}{dt} = \rho R\left(1 - \frac{R}{\kappa_R}\right) - cRH \tag{2.11a}$$

$$\frac{dX}{dt} = a_R cRH - bX - \beta XV \tag{2.11b}$$

$$\frac{dY}{dt} = \beta XV - (b + \alpha)Y \tag{2.11c}$$

$$\frac{dV}{dt} = \lambda Y - \mu V \tag{2.11d}$$

where the resource has growth rate ρ and saturates at carrying capacity κ_R. Resource depletion can occur due to consumption by the host with coefficient c. The host has a net birth rate proportional to the conversion efficiency of the host a_R and the consumption of the resource cRH. Other components in the system are consistent with Equations (2.3). To keep host densities consistent with the original framework we compare the coexistence equilibrium of Equations 2.3 (without R) and Equations 2.11 (see Appendix A for details). This also provides a means of defining the unknown resource parameters. As before we conduct stability analysis of Equations (2.11) before the inclusion of a maternal effect to define baseline stability regions.

2.5.2 Stability analysis

We first conduct stability analysis in absence of disease by setting $Y = V = 0$ in Equations (2.11), leaving a system of two Ordinary Differential Equations (2.11a)-(2.11b) with $H = X$. There are three equilbria: trivial steady state in which all

classes are zero ($R = 0, H = 0$), the resource only steady state in which the resource is at carrying capacity in absence of the host ($R = \kappa_R, H = 0$) and a co-existence steady state ($R = R_C, H = H_C$) where

$$R_C = \frac{b}{a_R c} \tag{2.12a}$$

$$H_C = \frac{\rho(a_R c\kappa_R - b)}{a_R c^2 \kappa_R} \tag{2.12b}$$

We note that the co-existence steady state is only valid for positive densities, thus $a_R c\kappa_R - b > 0$ must hold.

To determine the stability of the steady states we calculate the eigenvalues using the Jacobian which is given by

$$J = \begin{bmatrix} \rho(1 - \frac{2R}{\kappa_R}) & -cR \\ a_R cH & a_R cR - b \end{bmatrix} \tag{2.13a}$$

Eigenvalues for the trivial equilibrium are $\theta_1 = \rho$ and $\theta_2 = -b$, which is unstable since we assume the resource growth rate, ρ, is positive. The eigenvalues for the resource only equilibrium are $\theta_1 = -\rho$ and $\theta_2 = a_R c\kappa_R - b$, which is asymptotically stable when $a_R c\kappa_R - b$ is negative. The eigenvalues for the resource and host co-existence steady state are

$$\theta_{1,2} = -\frac{b\rho}{2a_R c\kappa_R} \pm \sqrt{\frac{b^2\rho}{a_R c\kappa_R}\left(1 + \frac{\rho}{4a_R c\kappa_R}\right) - b\rho_R} \tag{2.14}$$

Since all parameters are positive, θ_2 is always negative. If the product of θ_1 and θ_2 is positive then θ_2 must be negative and therefore the steady state is stable. This occurs when

$$\theta_1\theta_2 = \frac{\rho b(a_R c\kappa_R - b)}{a_R c\kappa_R} > 0$$

which holds when the co-existence steady state is positive (since that requires $a_R c\kappa_R - b > 0$).

Using the parameters values defined in Appendix A the term under the square root in Equation (2.14) is negative which produces imaginary eigenvalues ($-0.3837 \pm 0.7875i$). However the real part of the eigenvalue is negative (and the absolute value is strictly less than one) therefore the co-existence steady state is stable with dynamics shown in Figure 2.15.

We now consider how the addition of disease may impact the dynamics of Equa-

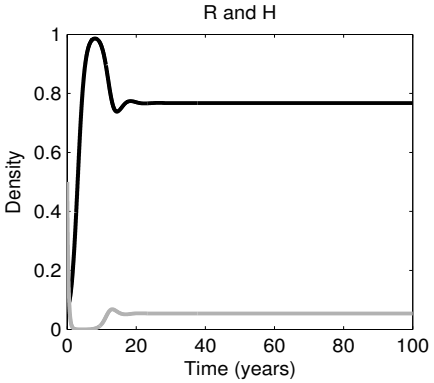

Figure 2.15: The time series plots of the co-existence steady state given by Equations (2.11a-2.11b) for the resource (black) and the host (grey) in absence of disease. Parameter values are estimated in Appendix A with $a_R = 1, c = 4.3, \kappa_R = 1, b = 3.3$ and $\rho = 3.3$.

tions (2.11). Firstly, we note that Equations (2.11) produce a number of equilibrium points. We are primarily interested in the boundary where the host and pathogen dynamics change from stable point to cycling; therefore we use AUTO we locate and trace the Hopf-bifurcation in $\alpha - \lambda$ parameter space as before.

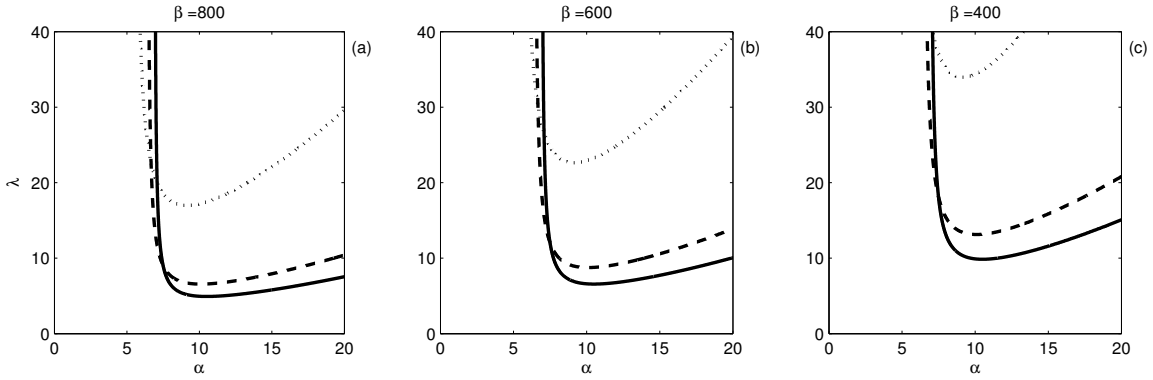

Figure 2.16: Stability boundaries of Equations (2.11) in $\lambda - \alpha$ parameter space for different levels of resistance (a) $\beta = 800$, (b) $\beta = 600$, and $\beta = 400$. A trade-off in terms of reduced birth rate is included in each plot $a_R = 1$ (solid), $a_R = 0.95$ (dashed), and $a_R = 0.85$ (dotted line). Above the Hopf-bifurcation the resource, host and pathogen exhibit population cycles and below the resource, host and pathogen tend to a stable steady state. Other parameter values are given in Appendix A and Figure 2.3

Figure 2.16 displays the stability boundaries for the host-pathogen framework including a dynamic resource (Equations (2.11)). As resistance to the pathogen is increased the region that exhibits stable point equilibrium (below the Hopf-bifurcation) increases considerably, mirroring the result produced by the original framework in

absence of a dynamic resource (Figure 2.3). However the inclusion of costs, in terms of a reduction in birth, increases this region further, which contrasts with the results for the model without a dynamic resource (Figure 2.3).

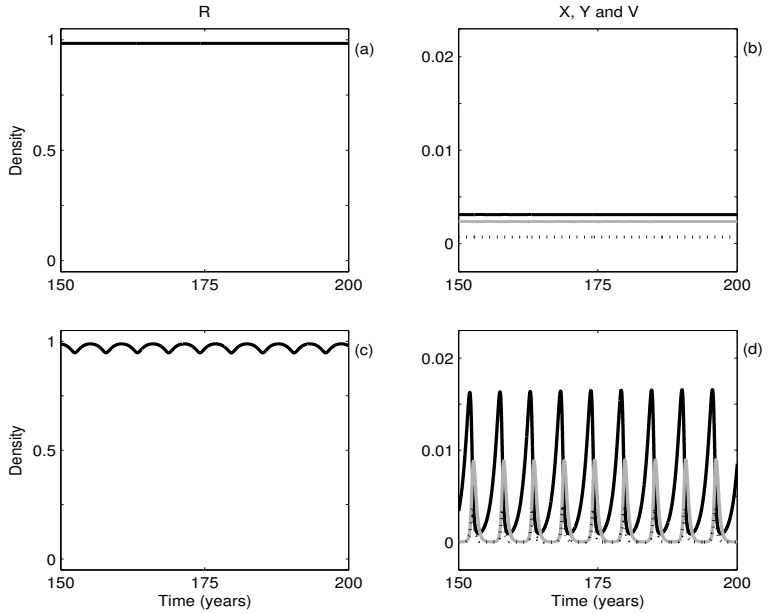

Figure 2.17: Time series plots illustrate the population dynamics of the stability regions in Figure 2.16 (a) where the left column displays the resource and the right column the susceptible (solid black), infected (dotted black) hosts and the free-living pathogen (grey). Parameter values are consistent with Figure 2.16 (b) with $\lambda = 10$ and $a_R = 1$, and (a)-(b) $\alpha = 5$ and (c)-(d) $\alpha = 10$.

In Figure 2.17 we show a time series highlighting the stability regions. Figure 2.17 (d) displays the system exhibiting large amplitude population cycles, where the host spends a substantial period of time close to zero.

2.6 Host-pathogen model with a maternal effect linked to a dynamic resource

2.6.1 Methods

We modify Equations (2.11) to include a maternal effect triggered by a dynamic resource. The host population is separated into 2 cohorts giving the following model:

$$\frac{dR}{dt} = \rho R\left(1 - \frac{R}{\kappa_R}\right) - cRH \tag{2.15a}$$

$$\frac{dX_1}{dt} = E_1\left(a_{R1}cRH\right) - bX_1 - \beta_1 X_1 V \tag{2.15b}$$

$$\frac{dX_2}{dt} = E_2\left(a_{R2}cRH\right) - bX_2 - \beta_2 X_2 V \tag{2.15c}$$

$$\frac{dY_1}{dt} = \beta_1 X_1 V - (b+\alpha)Y_1 \tag{2.15d}$$

$$\frac{dY_2}{dt} = \beta_2 X_2 V - (b+\alpha)Y_2 \tag{2.15e}$$

$$\frac{dV}{dt} = \lambda(Y_1 + Y_2) - \mu V \tag{2.15f}$$

As before hosts belonging to cohort 1 have parameters consistent with those defined in Equation (2.11) while hosts in cohort 2 incur an increased resistance ($\beta_2 < \beta_1$) and reduced birth rate due to a trade-off ($a_{R2} < a_{R1}$). The main difference between the dynamic resource model and the model linked to host density (Equation (2.7)) is that the host consumes resource (term cRH) which is subsequently turned into births with efficiency a_{R1} or a_{R2}.

The maternal effect on resistance is linked to the level of resource with the proportion of births into each cohort controlled by the functions E_1 and E_2 as follows:

$$E_1 = \max[1 - p_R(1-R), 0] \tag{2.16a}$$

$$E_2 = \min[p_R(1-R), 1] \tag{2.16b}$$

where parameter p_R determines strength of the maternal effect (see Figure 2.18).

2.6.2 Stability analysis

We follow the same approach as in Section 2.3 where we used AUTO to trace the Hopf bifurcation in $\lambda - p$ parameter space. Here we trace the stability regions for Equations (2.15) in the $\lambda - p_R$ parameter space for different levels of resistance, η, and display the results in Figure 2.19. The trends displayed are consistent with before when the maternal effect was linked to host density (Figure 2.6); as the strength of the maternal effect increases the region where a stable equilibrium is exhibited (region 2) increases. Furthermore the resource dependent maternal effects stabilises the system

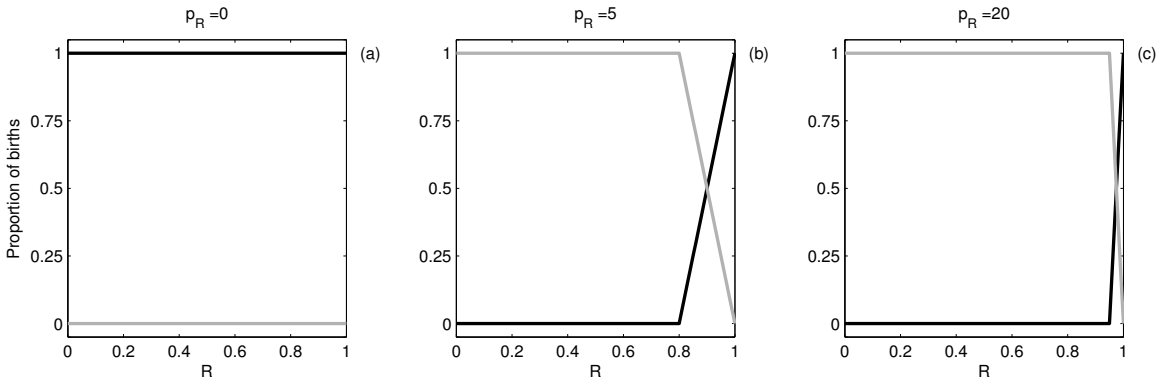

Figure 2.18: Functions E_1 (black) and E_2 (grey), defined in Equations (2.16) specify the relationship between resource density and the proportion of offspring born into cohorts 1 and 2 respectively. Results are shown for three levels of the strength of the maternal effect (a) $p_R = 0$ (absence of a maternal effect thus all host births occur in X_1), (b) $p_R = 5$ and (c) $p_R = 20$.

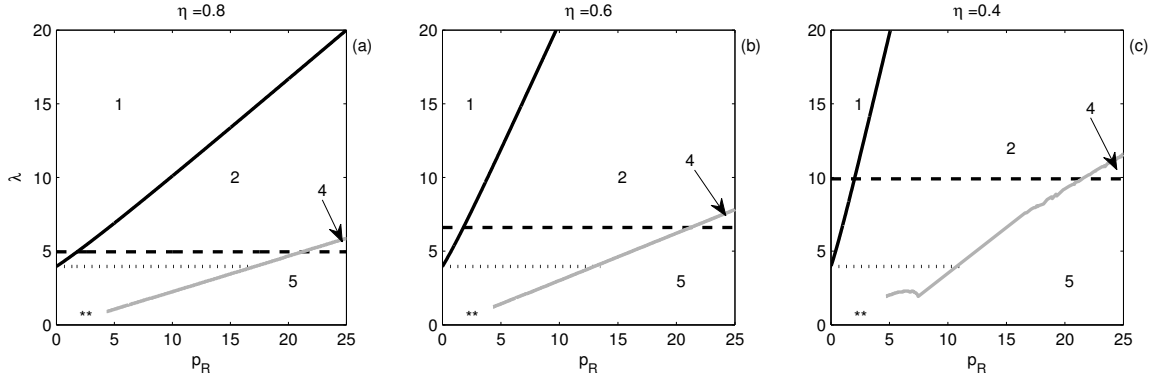

Figure 2.19: Equations (2.15) are analysed in $\lambda - p_R$ parameter space displaying the stability boundaries for different levels of resistance of hosts in cohort 2 (a) $\eta = 0.8$, (b) $\eta = 0.6$ and (c) $\eta = 0.4$. The lines styles are consistent with those defined in Figure 2.5 (a), in addition an area close to the origin $**$ denotes a section of the parameter space where various equilbria can exist in the absence of the pathogen, dependent on initial conditions. For simplicity we omit these regions. Other parameter values are $\rho = 1, \kappa_R = 1, c = 4.3, a_{R1} = a_{R2} = 1, b = 3.3, \beta_1 = 10^3, \beta_2 = \eta\beta_1, \alpha = 10, \mu = 3$.

much further than the baseline framework in absence of a dynamical maternal effect (Equations (2.3) with $\beta = \beta_1$ or β_2). As the level of resistance conveyed to host cohort 2 is increased the area where the host and pathogen tend to a stable point equilibrium (region 2) increases (Figure 2.19 (a)-(c)).

The average host density (in addition to the maximum and minimum densities) for different shedding rates λ is shown in Figure 2.20 against the strength of the maternal effect p_R. This figure confirms the change in the population dynamics as the boundaries in Figure 2.19 (b) are crossed. It also highlights the tendency for the total host population to increase in density as the strength of the maternal effect increases. In summary the inclusion of a maternal effect linked to a dynamic resource increases the region where host and pathogen tend to a stable equilibrium (Figure 2.19).

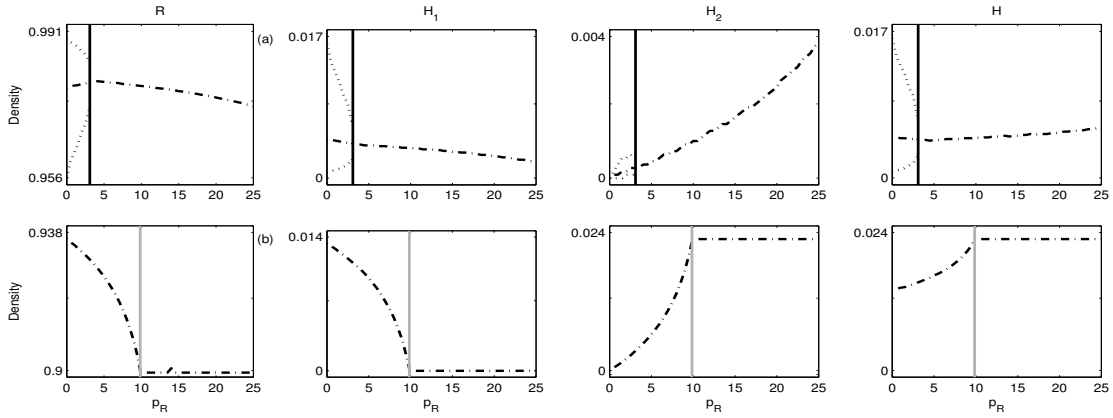

Figure 2.20: Average density (dot dashed black) of the resource R (1st column) and host populations H_1 (2nd column), H_2 (3rd column) and $H = H_1 + H_2$ (4th column) as a function of the strength of the maternal effect p_R. The vertical lines represent passing through the Hopf-bifurcation (black) and $H_1 = 0$ boundary (grey) with each row corresponding to shedding rate (a) $\lambda = 10$ and (b) $\lambda = 3$. When the population is cycling, the maximum and minimum of values are included (dotted black) with other parameter values consistent with Figure 2.19.

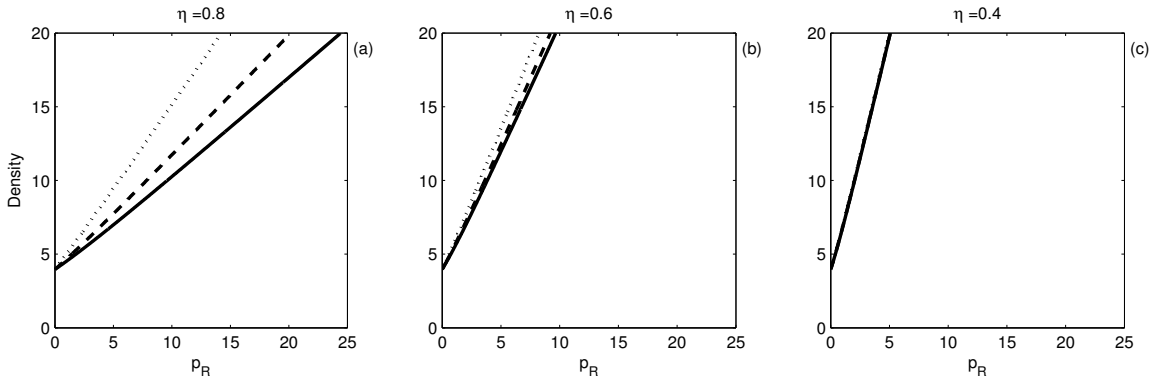

Figure 2.21: Equations (2.15) are analysed in $\lambda - p_R$ parameter space displaying the stability boundaries including a trade-off for different levels of resistance of hosts in cohort 2 (a) $\eta = 0.8$, (b) $\eta = 0.6$ and (c) $\eta = 0.4$. A trade-off in terms of reduced birth rate is includede in each plot where $\epsilon = 1$ (solid), $\epsilon = 0.95$ (dashed) and $\epsilon = 0.85$ (dotted) where $a_{R2} = \epsilon a_{R2}$. Other parameter values are defined in Figure 2.19.

Figure 2.21 displays the stability regions when we assume there are costs to the increased level of resistance conveyed on cohort 2 (we assume $a_{R1} > a_{R2}$). When the increase in resistance of cohort 2 is small (Figure 2.21 (a)) the inclusion of costs increases the region over which a stable equilibrium is exhibited. As the increase in resistance to cohort 2 increases inclusion of costs has a reduced effect (Figure 2.21 (c)). A similar trend to Figure 2.20 where the total host density increases as the strength of the maternal effect increases also occurs when we include costs to resistance.

2.7 Discussion

A maternal effect, whereby the life history properties of offspring are dependent on the maternal environment, has been observed in a wide variety of taxa (Bernardo, 1996; Boots and Roberts, 2012; Little et al., 2003; McCormick, 1998; Mitchell and Read, 2005; Rossiter, 1991). Recent studies have shown that a maternal effect may be responsible for an increase in disease resistance exhibited in invertebrates (Boots and Roberts, 2012; Mitchell and Read, 2005). In a study by Mitchell and Read (2005) the host was challenged with an infection in maternal environments which differed in density and resource levels whereas in the study by Boots and Roberts (2012) only resource levels differed. In this study we examine the impact that a maternal effect on resistance could have on the host-pathogen population dynamics. Since the experimental studies have linked the maternal effect to changes in both density and resources we consider two model frameworks. The first links the level of resistance in offspring to the maternal host density. The second explicitly represents the levels of resource and links the level of resistance inherited by offspring to the level of resources in the maternal environment. Our main result is that a maternal effect that increases disease resistance acts to stabilise the population dynamics. This is true for both model set-ups. In particular as the strength of the maternal effect increases the region of parameter space that exhibits population cycles decreases (and therefore the region that exhibits a stable point equilibrium increases).

Previous studies have highlighted how a maternal effect could lead to changes in population dynamics (Rossiter, 1991; Inchausti and Ginzburg, 1998; Beckerman et al., 2002; Inchausti and Ginzburg, 2009). In these studies the maternal effect led to changes in the growth rate of offspring and theory showed that the maternal effect could increase the propensity for population cycles (Beckerman et al., 2002; Inchausti and Ginzburg, 2009). The explanation is that maternal effects lead to a delayed density dependent feedback since the environment experienced by previous generations determines the life-history traits of the current generation. Biologically the mechanism operates as follows. In a good maternal environment high quality (highly reproductive) offspring are produced whereas a poor environment results in poor quality offspring. If the environment varies there will be situations in which highly reproductive offspring occur in poor environments and low reproducing individual occur in good environments. This mismatch between phenotypes and environment can lead to densities overshooting capacity or slow population recovery from low density. This delayed density dependence promotes population cycles (Beckerman et al., 2002; Inchausti and Ginzburg, 2009).

In contrast our results - where the maternal environment is linked to disease resistance - show that the maternal effect can reduce the propensity to cycle. Host-

pathogen cycles are caused when host population levels increase to levels that allow a disease epidemic. This reduces the host density to low levels and it takes time for the host to recover to sufficient density to trigger the next epidemic outbreak (Anderson and May, 1981; Bowers et al., 1993; White et al., 1996). In our system the maternal effect increases resistance in the face of deteriorating environmental conditions that occurs as the population density increases. The maternal effect therefore leads to a reduction in disease transmission opportunities at high host density and so reduces the severity of an epidemic (and dampens the cycles). Mitchell and Read (2005) speculated that a maternal effect on disease resistance would lead to a reduction in the cycles and our results confirm this.

Our results also indicate that a maternal effect on resistance to infection can (generally) increase the total host density. This result has not been verified in experimental studies which focus solely on whether increased resistance is inherited. Increased host density and stable equilibrium population dynamics may be beneficial to the host and may also be important in the evolution of maternally inherited resistance where types/cohorts with increased fitness may evolve and replace those with a lower fitness.

The work in this chapter on maternally inherited resistance has similarities to theoretical studies that examine density dependent prophylaxis (DDP) (Reilly and Hajek, 2008; Reynolds et al., 2011; White and Wilson, 1999). Under DDP the level of resistance to infection depends on time delayed host density. When the delay is small DDP can lead to an increased propensity to cycle whereas if the delay is sufficiently large it can reduce the likelihood of cycles (Reynolds et al., 2011). In our system resistance is linked to host density but hosts will retain this level of resistance for their lifetime. This mechanism may act in a manner similar to a long delay in the DDP system as here the findings are comparable.

In summary we have developed frameworks which assess the impact of a maternal effect on disease resistance on the population dynamics of host-pathogen systems. Our findings indicate that when a maternal effect on resistance is linked to either host or resource density it acts to increase the stability of the host-pathogen system. Our theoretical work therefore supports claims deduced from laboratory studies that examine maternally inherited resistance to infection.

Chapter 3

Population estimates using Capture-Mark-Recapture techniques with infection dependent capture rates

3.1 Introduction

Field data is often required to estimate the abundance of a small mammal population in a bounded area (Pollock, 1990). One method used to obtain the required data is Capture-Mark-Recapture (CMR) which consist of a series of trapping sessions in a closed area. Individuals who are trapped are marked and returned to the field thereby creating a trapping history (a record of occasions on which an individual was captured), which provides data that statistical methods interpret to estimate parameters like probability of capture and population size.

One of the earliest methods which use trapping data is the Lincoln-Peterson technique (1930). A simple two capture session study is used to estimate the total population in a closed area; individuals caught in the first session are marked and released and the total number is recorded, in the second session the number who are newly caught and who are re-captured are recorded (Marten, 1970; Seber, 1982; Shanker, 2000). An estimate of the total population is then based on the assumption that the proportion of the whole population captured in the first trapping round is the same as the proportion of individuals caught in the first trapping round that are recaptured in the second. The accuracy of this method is subject to data set assumptions such as closure of the population (no births, deaths or emigration), marks do not fall off and are not missed, and there is no heterogeneity (every individual has equal probability of capture) (Marten, 1970; Seber, 1982). The last assumption is commonly

broken through differences in individual behavioural responses which may occur if catchability is altered as a consequence of previous trapping making an individual 'trap-happy' (increased probability of re-capture) or 'trap-shy' (decreased probability of re-capture). Alternatively heterogeneity may arise between the difference in sex or age, whereby individuals have their own rate of capture, dependent on their current state (Pollock, 2002).

Over the last century there has been an increase in the development of statistical models which are able to identify and handle data sets arising in populations with a variety of structures (Schwarz and Seber, 1999). For instance the regression technique which can be applied to Capture-Removal (CR) data with multiple trapping sessions where individuals are only counted on their first capture (Seber, 1982). This technique requires the same assumptions as the Lincoln-Peterson model but boasts a graphical method which may be used to detect the presence of heterogeneity (Marten, 1970). Other models include: the Jolly-Seber model (1965) allowing the assumption of a closed population to be relaxed (Pollock, 1982; Seber, 1982); the Jackknife method (1978) which was one of the first to accept heterogeneous data (Burnham and Overton, 1978; Pollock, 2002); and more recently computational packages, such as Capture (Pollock, 1982; Rexstad and Burnham, 1991) or Mark (White and Burnham, 1999) that enable multiple statistical models to be implemented on CMR data with different heterogeneities.

Recently a study by Coltherd et al. (2010) examined the effects of the nematode *Heligmosomoides polygyrus* on the capture rates of wood mice *Apodemus Sylvaticus* and found that parasitism affects the rate of capture of wood mice. *H. polygyrus* displays a high prevalence of infection in wood mice and parasite infections are positively correlated with poor host nutritional status, therefore the easy access to food in traps may explain the increase in infected individuals' capture rates (Coltherd et al., 2010). This study suggests that the infection status of individuals may influence the probability of capture and act as a source of heterogeneity in CMR studies.

In this chapter we are motivated by the study by Coltherd et al. (2010) to examine the impact infection dependent heterogeneity in capture rates may have on population estimates. We generate simulated data sets using two frameworks. This allows us to control the level of heterogeneity and to compare estimates produced by the regression technique and by the Capture program with the underlying true values known from the models. The first framework is a deterministic model which simulates the disease and Capture-Removal (CR) process at a population level. This produces the total number of captures after each trapping session which can only be used in the regression technique, since the program Capture requires an individual trapping history

An aim of this chapter is therefore to use the deterministic model and the regression technique to identify any heterogeneity and estimate the population size when

the capture rates are infection dependent. Whilst this model is relatively easy to implement it does not include the stochasticity found in populations with disease nor the natural variability in capture studies (Black and McKane, 2012; Grimm, 1999; Judson, 1994). We therefore use this case study as an opportunity to learn the techniques required to create an individual-based, stochastic framework.

Individual-based models have been used in ecology since the 1970s and have a range of benefits such as being able to incorporate the discrete nature of population dynamics (i.e. increased risk of extinction at small population densities) and it is arguably easier to include additional information such as age and sex (Black and McKane, 2012; Grimm, 1999). By developing this framework we are able to simulate the CMR and disease process at an individual level thus creating a full CMR trapping history which can be used in Capture to estimate the population size. Therefore a second aim of this chapter is to use the individual-based model to examine the accuracy of the population estimates using the program Capture.

3.2 Methods

We first describe a deterministic framework in Section 3.2.1 which simulates CR field data when infection is present. In Section 3.2.2 we produce a stochastic version of the deterministic model which will create individual trapping CMR history data. Finally in Section 3.2.3 we introduce the regression technique and the program Capture which use the trapping data created in Sections 3.2.1 and 3.2.2 to estimate the population size for various levels of infection parameters.

3.2.1 The deterministic framework

To understand the impact of infection related changes in capture rates we first develop a system of Ordinary Differential Equations (ODEs) which simulate the infection and capture process. This outputs data at a population level which is sufficient for the regression technique. We use a Susceptible-Infected-Susceptible (SIS) model (Anderson and May, 1980; Diekmann et al., 1995) in which the total population consists of a susceptible S and infected I classes with dynamics given by

$$\frac{dS}{dt} = -\beta SI + \gamma I \tag{3.1a}$$

$$\frac{dI}{dt} = \beta SI - \gamma I \tag{3.1b}$$

Infection occurs through mass action between susceptible and infected classes where β is the transmission coefficient. Infected individuals recover at a rate γ with no

immunity and thus return to the susceptible class. The total population is closed ($N = S + I$) and has stable endemic equilibrium $(\bar{S}, \bar{I}) = (\gamma/\beta, N_0 - \gamma/\beta)$ where $N_0 = S_0 + I_0$ is the initial population.

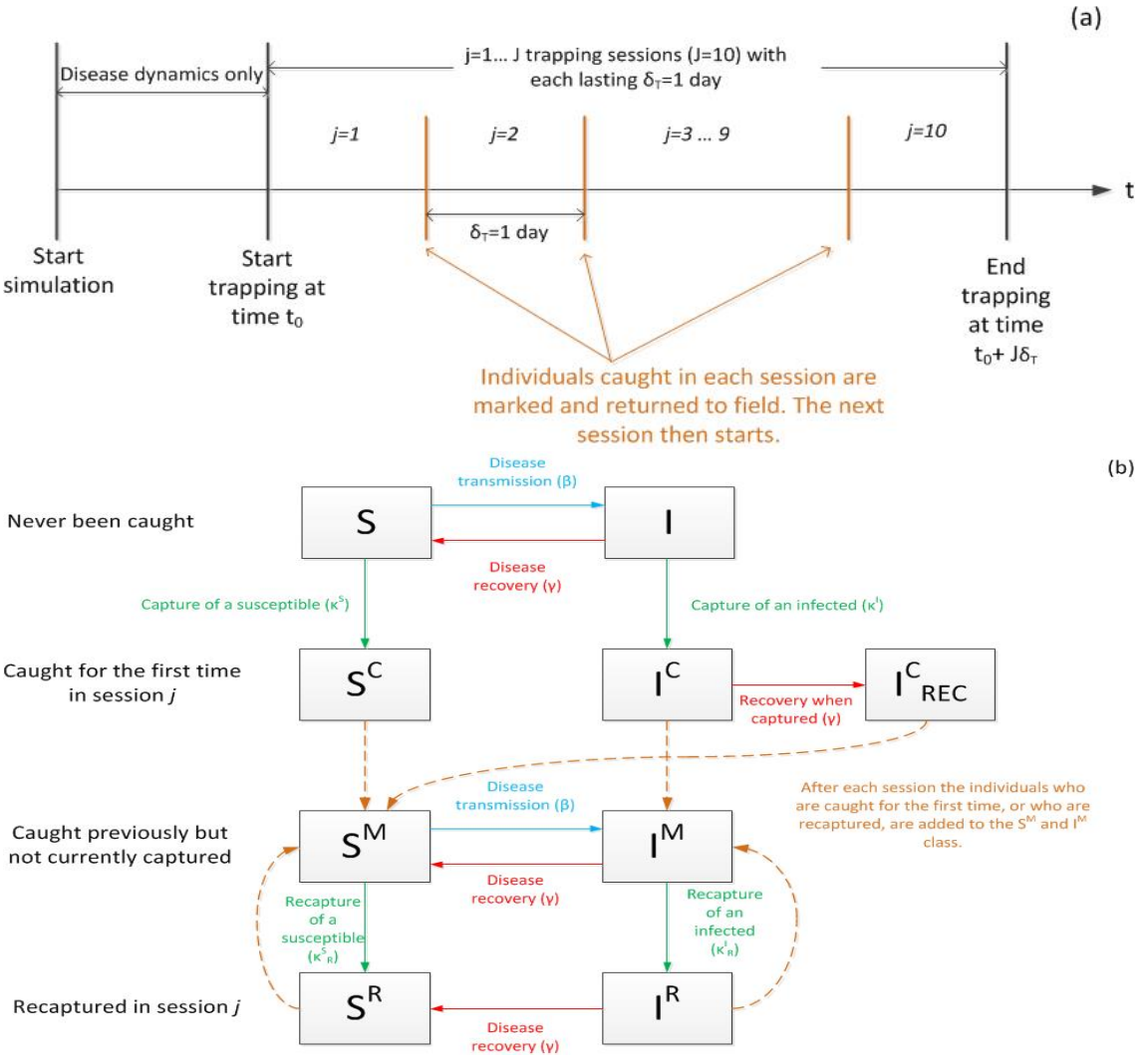

Figure 3.1: The capture-removal process is shown for $j = 1...J$ sessions where $J = 10$ and the length of each session is $\delta t = 1$ day. This process is shown in (a). The flow chart in (b) shows the capture and disease process corersponding to classes in Equation (3.2). Rectangle boxes represent a state (for example S^C shows the total number of individuals who are currently caught for the first time). The solid arrows indicate infection or capture dynamics and the changing of states: blue arrows for infection, red arrows for recovery and green arrows for capture. The dashed orange lines indicate releasing trapped individual once each session is over. We note that before trapping, $t < t_0$ in (a), the only processes occuring are disease transmission and recovery as shown on the top row of (b). Once trapping has begun the whole process in (b) occurs for each of the trapping sessions in (a) - more detail is given in the main text.

To incorporate a Capture-Removal (CR) process we assume there are J trapping sessions labelled $j = 1...J$, where only naive captures are counted (i.e. individuals who are caught are returned to the population with a mark and any recaptures are not included). Figure 3.1 (b) shows the capture process where by each trapping session lasts one day and the next trapping session begins immediately after, and the flow chart in Figure 3.1 (c) shows the process within each session.

The basic model in Equation (3.1) is extended to include the multiple classes which represents this process in Equation (3.2). The number of susceptible and infected individuals who have never been caught are given by the classes S and I respectively. Classes S^C and I^C represent the number of naive susceptible and infected captures (caught for the first time) in the jth trapping session. After each trapping session the individuals caught (S^C and I^C) are returned to the field, however in order to identify re-captures in our model they enter the corresponding 'marked' classes S^{M} and I^{M} respectively (i.e. the individuals in these classes have been previously caught but are not currently caught). Classes S^{R} and I^{R} represent the susceptible and infecteds who are re-captured; at the end of each trapping session these individuals are returned to the marked class S^{M} and I^{M} respectively (since we are only using the CR data we do not specify the session in which individuals have been re-captured). Finally the last class ${I^C}_{\mathrm{Rec}}$ represents infected individuals who recover whilst being caught (I^C); at the end of each trapping session these individuals are returned to the marked susceptible (S^M) class (separating this group allows us to determine the number of infected and susceptible individuals at the point of capture as opposed to the end of the trapping session - we expand on this later). We note that the total number of individuals uncaught are therefore $S + S^M$ and $I + I^M$ respectively. Updating our SIS framework we produce

$$\frac{dS}{dt} = -\beta S(I + I^M) + \gamma I - \kappa^S S \tag{3.2a}$$

$$\frac{dS^C}{dt} = \kappa^S S \tag{3.2b}$$

$$\frac{dS^M}{dt} = -\beta S^M(I + I^M) + \gamma I^M - \kappa_R^S S^M \tag{3.2c}$$

$$\frac{dS^R}{dt} = \gamma I^R + \kappa_R^S S^M \tag{3.2d}$$

$$\frac{dI}{dt} = \beta S(I + I^M) - \gamma I - \kappa^I I \tag{3.2e}$$

$$\frac{dI^C}{dt} = -\gamma I^C + \kappa^I I \tag{3.2f}$$

$$\frac{dI^M}{dt} = \beta S^M(I + I^M) - \gamma I^M - \kappa_R^I I^M \tag{3.2g}$$

$$\frac{dI^R}{dt} = -\gamma I^R + \kappa_R^I I^M \tag{3.2h}$$

$$\frac{dI^C_{\text{Rec}}}{dt} = \gamma I^C \tag{3.2i}$$

We first describe the disease dynamics. Disease transmission can only occur between individuals that are not currently captured; more specifically uncaught susceptibles (S and S^{M}) can become infected by contact with uncaught infecteds at rate $\beta S(I + I^{\text{M}})$ and $\beta S^{\text{M}}(I + I^{\text{M}})$ and individuals are moved to the appropriate class upon becoming infected (i.e. S to I and S^{M} to I^{M}).

Individuals in any infected class can recover at a *per capita* rate γ where they enter the corresponding susceptible class when uncaught (i.e. I to S, I^{M} to S^{M}). When an individual is caught for the first time and recovers within that session they leave class I^C and enter a temporary class I^C_{Rec} where, at the end of the session, they will be added to the S^{M} class. Since we are not recording re-captures individuals who recover when re-captured (I^{R}) are returned to the susceptible class S^{R} directly.

We now describe the parameters attributed to the CR process in Equation (3.2). Naive captures occur at rate κ_j^S and κ_j^I where susceptible and infected individuals leave class S and I and enter classes S^C and I^C respectively. At the end of the session caught individuals are added to the marked classes (S^{M} and I^{M}), where they can be re-caught at rate κ_R^S and κ_R^I (and enter classes S^{R} and I^{R} respectively). We are not required to record the number of re-captures per session therefore we set the

re-capture rate to be consistent with the capture rate from the second trapping session onwards producing

$$\kappa_R^{S,I} = \begin{cases} \kappa^{S,I} & \text{when } (T_0 + \delta_T) < t \leq (T_0 + J\delta_T) \\ 0 & \text{when } 0 < t \leq T_0 + \delta_T. \end{cases} \tag{3.3}$$

where T_0 marks the time of the first session and δ_T is the fixed length of each trapping session. In this study we assume that there are 10 trapping sessions ($J = 10$) where each session lasts 1 day ($\delta_T = 1$). In field studies, traps are checked after the session, individuals are marked and released then the traps are reset. We represent this in our model, by session $j+1$ starting immediately after session j. This means that trapping lasts for 10 consecutive days. This is a relatively short period of time in comparison to the time-scale of disease (the infectious period of an individual is 30 days) thus the number of hosts changing infectious states during trapping is very small. We discuss the impact of the infection dynamics during trapping in Section 3.2.3 when considering chronic and acute infections.

As before, at the end of every session the re-captured individuals are returned to their respective marked classes (S^{M} and I^{M}). To include infection dependent heterogeneity we fix $\kappa^I > \kappa^S$ so that an infected is more likely to be caught that a susceptible.

The initial conditions for Equations (3.2) are simply given by $S = S_0$ and $I = I_0$ (so that $N_0 = S_0 + I_0$) and all other classes zero. We let densities tend to equilibrium then commence trapping at time T_0, therefore at the end of each capture session, most of the classes are updated creating boundary conditions

$$S(T_j) = S(\tilde{T}_{j-1}) \tag{3.4a}$$

$$S^C(T_j) = 0 \tag{3.4b}$$

$$S^M(T_j) = S^M(\tilde{T}_{j-1}) + S^C(\tilde{T}_{j-1}) + S^R(\tilde{T}_{j-1}) + I^C_{\text{Rec}}(\tilde{T}_{j-1}) \tag{3.4c}$$

$$S^R(T_j) = 0 \tag{3.4d}$$

$$I(T_j) = I(\tilde{T}_{j-1}) \tag{3.4e}$$

$$I^C(T_j) = 0 \tag{3.4f}$$

$$I^M(T_j) = I^M(\tilde{T}_{j-1}) + I^C(\tilde{T}_{j-1}) + I^R(\tilde{T}_{j-1}) \tag{3.4g}$$

$$I^R(T_j) = 0 \tag{3.4h}$$

$$I^C_{\text{Rec}}(T_j) = 0 \tag{3.4i}$$

where $\tilde{T}_{j-1}$ represents the time at the end of a trapping session (e.g. $S^C(\tilde{T}_{j-1})$ would give the number of susceptible individuals caught at the end of trapping session $j-1$). Using the boundary conditions in Equation (3.4) we can solve Equation (3.2) in a piecewise manner and record the number of susceptible (S^C) and infected individuals ($I^C + I^C_{\text{Rec}}$) caught in each session.

The CR data produced from the deterministic framework can be used to estimate the population size using the regression technique identified in Section 3.2.3.

3.2.2 The stochastic framework

A drawback of using a deterministic framework is that it is unable to represent the discrete individual variation found in a natural system particularly when we are dealing with populations at small densities (Black and McKane, 2012; Grimm, 1999). We therefore create an individual-based, stochastic SIS model which can simulate the disease and CMR process in addition to providing a full capture history for each individual within the system. We follow the methodology proposed in Keeling and Rohani (2008) to implement Gillespie's algorithm which generates random event sequences given rate parameters for the events (Gillespie, 1977), therefore forming an individual-based, stochastic SIS version of Equation (3.2) except we now include recaptures.

As before classes S and I represent the number of uncaught susceptible and infected individuals respectively and S^C and I^C denote the number of individuals caught

Description	Population	Probability
Disease transmission	$S \to S-1$, $I \to I+1$	$:[\beta I]/R$
Recovery uncaught individual	$S \to S+1$, $I \to I-1$	$:[\gamma]/R$
Recovery caught individual	$S^C \to S^C+1$, $I^C \to I^C-1$	$:[\gamma]/R$
Capture of a susceptible	$S \to S-1$, $S^C \to S^C+1$	$:[\kappa^S]/R$
Capture of an infected	$I \to I-1$, $I^C \to I^C+1$	$:[\kappa^I]/R$

Table 3.1: A list of the events in the individual-based, stochastic, SIS model described in Section 3.2.2. For each event the outcome at a population level is given in column 2. S and I are the total number of uncaught susceptible and infected individuals respectively and the inclusion of the index ^{C} denotes the captured classes. The associated probability is calculated in column 3 where the rate of an event, in the square brackets, is divided by the sum of all the rates $R = \Sigma\ [rates]$ across the total population.

in the current trapping session from each infection class. Unlike the deterministic model, where those who are caught entered a marked class at the end of each trapping session, the captured individuals are returned to the appropriate S and I classes at the end of each session. Each individual in our system is assigned a subscript i (where $i = 1...N$) which permits their infection and trapping status to be tracked.

The events and their associated probabilities now depend on the infection and capture state of individuals; for instance a susceptible individual S_i can undergo two possible events, infection or capture, whereas a captured susceptible S_i^C has no associated events until they are released at the end of the trapping session. As before infection can only be transmitted by individuals who are not caught (I), but recovery can occur whilst in a trap (however the infection status of a captured individual is recorded at the point of capture). We translate the rates given in Equations (3.2) to probabilities by dividing the individual rates by the sum of all the rates, R (see Table 3.1). An event is then selected at random and the corresponding individual's infection status, the population total and event probabilities are updated. The time is also updated by assuming that the time step between events is an exponentially distributed random variable (Renshaw, 1993), this is generated by the transformation $-\ln(\psi)/R$ where $\psi \in U(0,1)$. Repeating this process simulates events over time and the status of each individual can be tracked. This method simulates the random variability seen in natural systems. Thus each run (known as a realisation) of the model generates a different result, and the statistical properties of the expected or mean behaviour must now be formed as the average of a number of realisations.

This method allows us to extract the individual CMR trapping histories which can be used in complex statistical programs such as Capture. Additionally we can exclude any recaptures in the data sets which permit the use of the regression method.

3.2.3 Models for estimating the population size

In Section 3.2.1 and 3.2.2 we developed two frameworks to simulate CR and CMR data. The first produces the total number of naive captures in each session using a deterministic framework whilst the second uses a stochastic framework to produce a full individual CMR history. We now highlight two techniques which we use to estimate the population size for a range of infection parameters.

This first is the regression method which requires naive capture data from a Capture-Removal (CR) process (any re-captures are disregarded). This method was initially used in fisheries where populations are large and those caught were permanently removed (Marten, 1970). Underpinning the regression method is that continued CR sampling would remove the total population (or leave no unmarked individuals) and thus reveal the population size. Assuming that the probability of capture per individual is constant in each trapping session, the number caught is then proportional to the number remaining. Thus, for a homogeneous population, a plot of the number caught in each session, n_j, against the cumulative number caught, x_j, would achieve a population estimate, $\hat{N}$, by extrapolating the best fit line at $n_j = 0$. Moreover the gradient of the best fit line produces the probability of capture $\hat{p}$ (Pollock, 2002), thus giving estimates

$$\hat{N} = \bar{x} - \frac{\bar{n}}{\hat{p}} \tag{3.5a}$$

$$\hat{p} = \frac{\sum_{j=1}^{J}(n_j - \bar{n})(x_j - \bar{x})}{\sum_{j=1}^{J}(x_j - \bar{x})} \tag{3.5b}$$

where $\bar{n}$ and $\bar{x}$ represent the mean number caught and the mean cumulative number caught per session respectively. This technique is reasonably accurate when the following assumptions hold: the population is closed (there are no births, deaths or migration), no marks fall off or are overlooked by the observer, and there is no heterogeneity (more specifically individuals have equal catchability throughout the study). Despite these limitations, an advantage of the regression techniques is that it can be used to identify population data heterogeneity by plotting and estimating the best fit for $\log(n_j)$ vs $(j-1)$ (Marten, 1970). If the best fit is a decreasing straight line it can be assumed there is no heterogeneity and the least squares estimates are assumed accurate (Marten, 1970). Alternatively if a bias is present in the capture data, the individuals with a higher probability of capture are likely to be caught first resulting in a small but visible stepwise change in the $\log(n_j)$ plot. Under these conditions Equations (3.5) would produce inaccurate estimates.

By applying the regression technique to the CR data created by the deterministic

framework in Section 3.2.1, we analyse the data for heterogeneity to see if the presence of infection could be inferred if it were not already known. More specifically we evaluate whether the heterogeneity can be identified by comparing the estimates using the susceptible and infected data sets separately ($\hat{S}$ and $\hat{I}$) to the total data set ($\hat{N}$). When the disease is dynamic the susceptible and infected capture data sets will lose the assumption of closure, since individuals who are trapped cannot become infected (due to no disease transmission opportunities) but can recover. This may produce an error in the $\hat{S}$ and $\hat{I}$ estimates. We therefore examine two scenarios: the first is fixing disease over the trapping period (i.e. no transmission or recovery) and the second is including a dynamic disease (i.e. permitting transmission and recovery). By fixing infection dynamics this may be representative of a chronic disease with slow transmission and recovery; moreover this reduces Equations (3.4) since $I_j^{\text{Rec}} = 0$ as individuals cannot recover when trapped. Alternatively, dynamic infection may represent an acute infection with fast transmission and recovery; we try to limit the bias produced by recording the number caught in each class at the point of capture (hence the use of I_j^{Rec} class), therefore those that recover from infection in the trap are still counted as caught infected (using $I_j + I_j^{\text{Rec}}$). Simulating both scenarios allows us to examine the flexibility of the regression estimate when the assumptions of closure and homogeneity are relaxed.

Before using the data sets in Capture we first validate the stochastic model by comparing the regression estimates in both the stochastic and deterministic frameworks. We can then use the full CMR data sets in Capture which has multiple statistical models able to estimate the size of a closed population with different systematic effects such as heterogeneity of trapping probabilities in the population, behavioural response after initial capture and time dependence in trapping probabilities (Pollock, 1982; Rexstad and Burnham, 1991).The final aim of this chapter was to examine the accuracy of the population estimates produced by the program Capture for the data sets produced by the individual-based, stochastic model for a range of infection parameters. As before, we do this through the use of the susceptible, infected and total data sets for both fixed and dynamic infections.

3.3 Results

3.3.1 The regression model

In this section we first explore whether the regression model is able to identify heterogeneity in CR data when the capture rates are infection dependent. We simulate CR data for a range of infection parameters and use the regression method to identify bias in the data by plotting $\log(n_j)$ vs $(j-1)$. We first fix the disease dynamics

and show the susceptible, infected and total population data sets in Figure 3.2. The best fit for the susceptible and infected data is clearly linear indicating no detectable heterogeneity; moreover their population estimates using Equation (3.5) are accurate ($\hat{S} + \hat{I} = N_0$, as expected since the data sets are both closed and homogeneous). However, despite the capture rates being infection dependent, using the linear best fit for the log of the total catch is still reasonable (Figure 3.2 (a)) with only a marginal amount of bias being detected; although Equation (3.5) produces a 6% underestimation of the population size. The deterministic model provides us with precise CR data and it is therefore reasonable to assume the added variability of the stochastic model is likely to make the small levels of heterogeneity in Figure 3.2 undetectable.

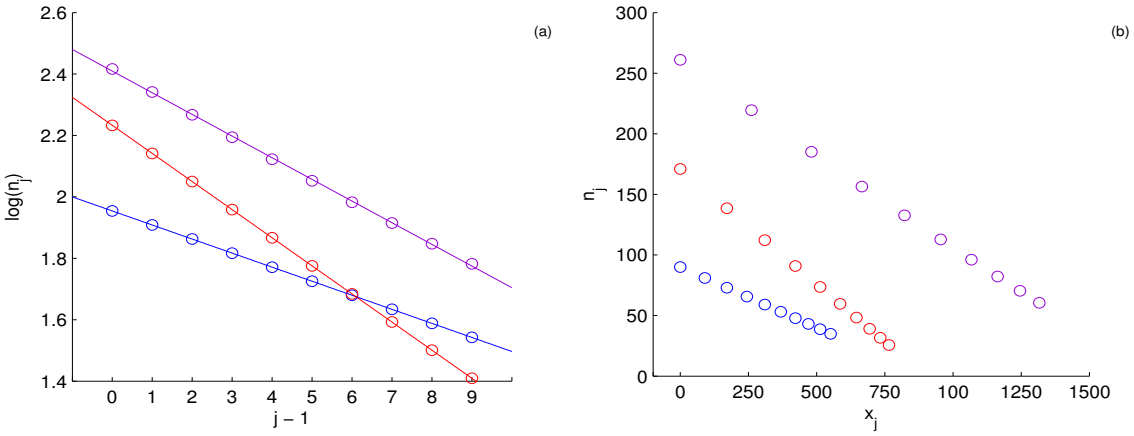

Figure 3.2: We simulate a CR process using the deterministic framework in Equations (3.2) for fixed disease dynamics with the susceptible (blue) and infected (red) and total population (purple). The number caught in the jth session is denoted n_j and the cumulative number caught is x_j. Data sets displayed are (a) $\log(n_j)$ against the $j-1$ session and (b) n_j against x_j. The initial population is $S_0 = I_0 = 900$ and capture rate is given by $\kappa^{S,I} = -\log(1 - P^{S,I})$ where $P^{S,I}$ is the proportion of the population that is caught on the first trapping session for susceptible and infected populations respectively. Here we have $P^S = 0.1$ and $P^I = 2 \times P^S$ (giving $\kappa^S = 0.10536$ and $\kappa^I = 0.22314$).

Figure 3.2 suggests that infection dependent capture rates are unlikely to be detected by the regression technique for fixed dynamics as the deviation from a straight line is negligible. When the disease is fixed the population estimate given by the separate data sets ($\hat{S} + \hat{I}$) is accurate. However, the error in the regression estimate when using the combined data can be considerable, as shown in Figure 3.3 (a)-(c), where the error is plotted for a range of prevalence values and capture rates. It can be seen that regressing on the total catch, Equation (3.5) consistently underestimates

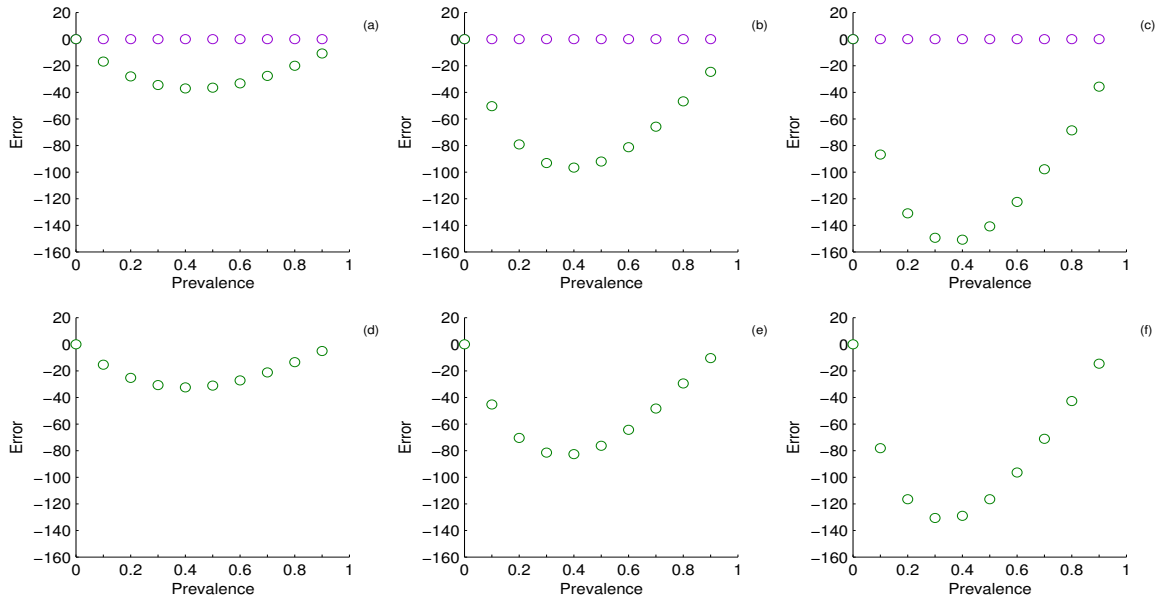

Figure 3.3: Population estimates using Equation (3.5) for a range of disease prevalence (defined by $I_0/(S_0+I_0)$) and infected capture rates (a) and (d) $P^I = 1.5\times P^S$, (b) and (e) $P^I = 2 \times P^S$, and (c) and (f) $P^I = 2.5 \times P^S$. The error is plotted using the total catch $(\hat{N}-N_0)$ (dark green) and the susceptible and infected catches $(\hat{S}+\hat{I}-(S_0+I_0))$ (purple). We examine the cases of (a)-(c) no recovery or transmission ($\beta = \gamma = 0$) and (d)-(f) dynamic disease ($\gamma = 1/30$ and $\beta = \gamma/S_0$). Other parameters are given in Figure 3.2.

the population density ($\hat{N}$), with the error increasing as the difference between capture rates increases (Figure 3.3 (a)-(c)). The negative bias is created because infected individuals are likely to be caught first since they have an increased probability of capture. This results in increasing the slope of the best fit line (Figure 3.2 (b)), and the probability of capture for the total population using Equation (3.5b), subsequently decreasing the estimate of population size using Equation (3.5a).

When we assume a dynamic infection process the error trends are qualitatively similar to those in the static prevalence case when using the total population data (Figure 3.3 (d)-(f)). We note however that the $\hat{S}+\hat{I}$ estimate is subject to error because both classes are no longer closed (and so these estimates are removed from Figure 3.3 (d)-(f)). In both disease scenarios Figure 3.3 reveals the error for the total catch $\hat{N}$ is consistently greatest at intermediate prevalence values because the proportion of the infected population is roughly split, maximising heterogeneity in the capture rates. Conversely when the prevalence is high or low, the majority of the population is either infected or susceptible respectively, thus a smaller error in the estimate is present.

Since the stochastic model includes random noise we use the average of 200 realisations and include 95% confidence intervals. In Figure 3.4 we show both results are in close agreement, with relatively small confidence intervals. In an attempt to

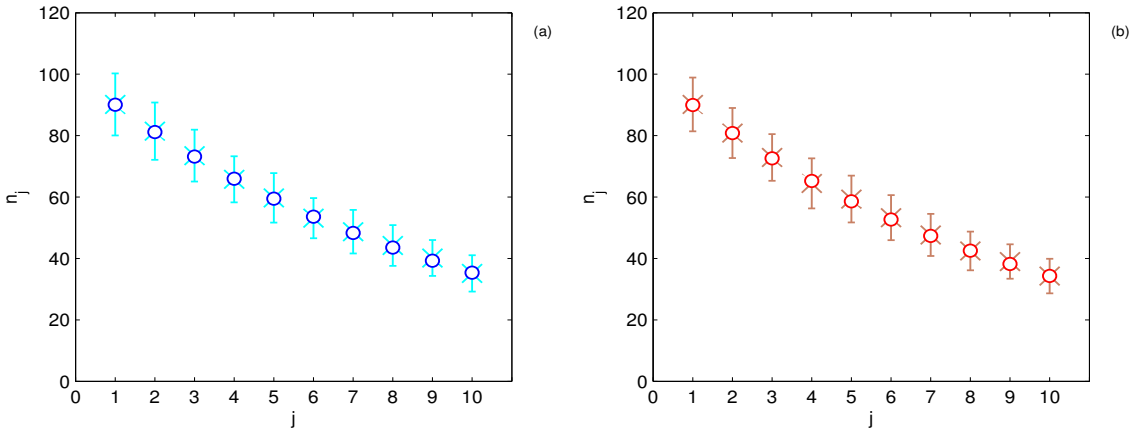

Figure 3.4: The number of naive captures in a ten trapping session study using the deterministic framework (∘) and stochastic framework (×) for (a) susceptibles and (b) infecteds. The stochastic model displays the average of 200 simulations with 95% confidence intervals. The initial population is $S_0 = I_0 = 900$ and parameters $\gamma = 1/30$, $\beta = \gamma/S_0$ and equal capture rates $P^{S,I} = 0.1$.

identify heterogeneity in the stochastic data when $\kappa_I > \kappa_S$, the best fit of the log of the number caught is plotted however the results are similar to Figure 3.2 revealing no visible bias (so the results are not given here). This permits us to assume estimates using Equation (3.5) are accurate. We note that when using a single run of the stochastic model, the added noise in the capture data may increase the difficulty of identifying heterogeneity.

In Figure 3.5 the regression technique is used to estimate the population size estimate using both the deterministic and stochastic data for fixed disease dynamics. It is clear that the average error in total population estimate produced by the stochastic model shows a similar pattern when compared with deterministic model. However, the 95% confidence intervals are relatively large which indicates that the small variance in the number caught from a single run in the stochastic model (see Figure 3.4) is amplified in Equation (3.5). The stochastic data sets are representative of the variability seen in a natural system and Figure 3.5 clearly shows that a small amount of noise in the data can produce large errors in the population estimate when using the regression method. (Note when the disease was dynamic we achieved a similar outcome to Figure 3.3 (d)-(f) for both the deterministic and stochastic models.)

These results indicate that identifying infection dependent heterogeneity using the regression technique is difficult (the slope for the total population in Figure 3.2 is close to a straight line). When this is the case it permits the use of Equations (3.5) to estimate the population size. However, these equations will underestimate the population size if there is heterogeneity in capture rates between infected and uninfected individuals that is not identified. If heterogeneity is identified, treating the susceptible and infected individuals separately (i.e. as separate homogeneous

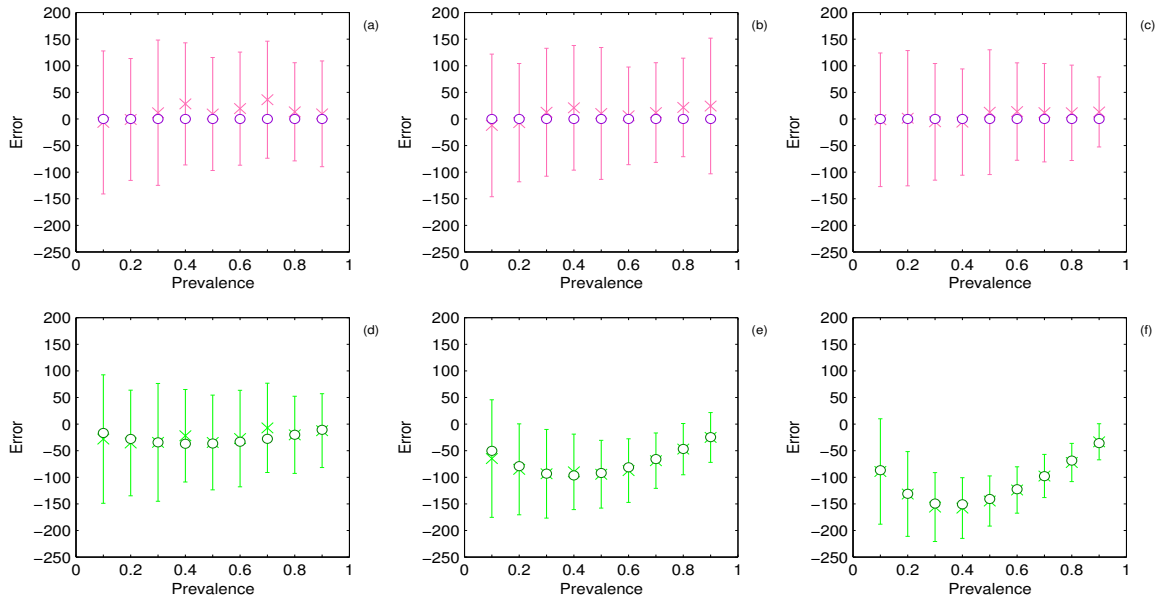

Figure 3.5: The regression method estimates using data from the deterministic model (purple and dark green, ∘) and stochastic model (pink and light green, ×) for (a)-(c) $\hat{S}+\hat{I}$ and (d)-(e) $\hat{N}$. The capture rate for an infected individual is (a) and (d) $P^I = 1.5 \times P^S$, (b) and (e) $P^I = 2 \times P^S$, and (c) and (f) $P^I = 2.5 \times P^S$. The estimate for the stochastic model is the average of 200 runs with 95% confidence intervals and the disease dynamics are fixed $\gamma = \beta = 0$ and $P^S = 0.1$.

data sets) can substantially reduce or eliminate this error.

3.3.2 Program Capture

As we have seen the regression technique is only accurate for homogeneous data sets we therefore now examine the population estimates produced by program the Capture using the individual CMR histories simulated by the individual-based, stochastic, SIS framework. There are several models in Capture which are able to identify different types of heterogeneity and still maintain reasonable accuracy in their estimates. The models that are relevant to our study are labelled: M_0 which assumes no heterogeneity; M_h which allows for individual heterogeneity; and M_{th} which allows individual and temporal heterogeneity.

In the first scenario we consider fixed disease dynamics therefore model M_0 is appropriate when we consider the susceptible and infected data separately and model M_h for the total population data. In Figure 3.6 (a)-(c) we show the error in the population estimates using the M_0 estimator for the susceptible and infected classes $(\hat{S}+\hat{I})$ for a range of prevalence and infection dependent capture rates. It is evident that the approximations are very good and produce similar margin of errors to the estimates from the regression technique. We include the estimates using M_0 for the total data set since it is interesting to note that the error trend is similar to that

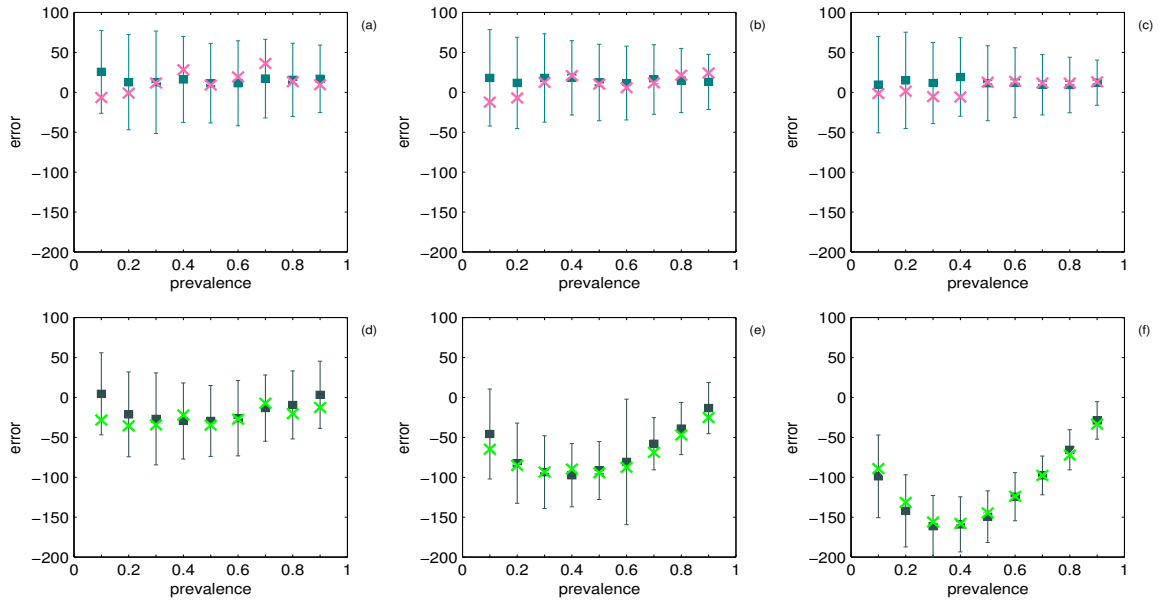

Figure 3.6: Model M_0 in Program Capture is used to estimate the average population density of 200 simulations (teal □) for the (a)-(c) susceptible and infected data set $\hat{S}+\hat{I}$ and (d)-(f) the total population data set $\hat{N}$. We include 95% confidence intervals for estimates using M_0 and include the average estimate using the regression method (×) (on the same data sample). Infection capture rates and other parameters are the same as in with Figure 3.5.

produced by the regression technique (Figure 3.6 (d)-(f)).

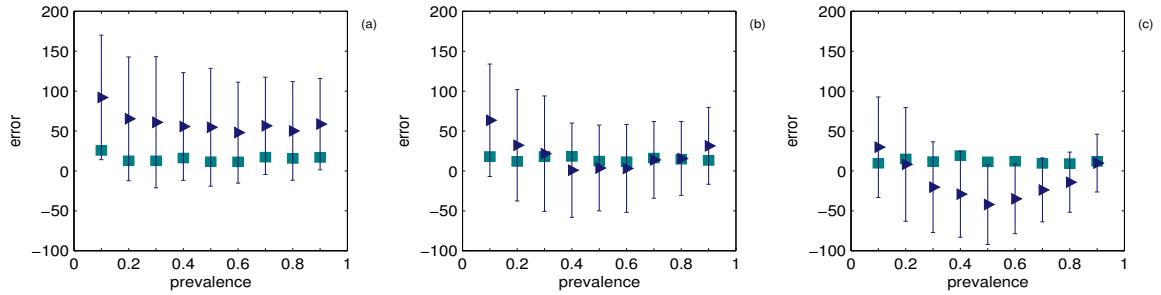

Figure 3.7: Model M_h in Program Capture is used to estimate the population density using the total data set $\hat{N}$ (navy △) for a range of prevalence values. The estimate shown is the average of 200 simulations with 95% confidence intervals. The average estimate of $\hat{S}$ and $\hat{I}$ using M_0 (teal □) is also included for comparison. Infection capture rates and other parameters are the same as in with Figure 3.5.

When there is no disease transmission there may still be heterogeneity present in the data due to different initial conditions and capture probabilities for infected individuals. Model M_h allocates a distinct capture probability to each individual, and Capture applies a statistical test to determine whether these probabilities differ

from one another sufficiently that including heterogeneity by using M_h is necessary. The results using this estimator are displayed in Figure 3.7 where it can be seen that model M_h is sensitive to the level of heterogeneity in the data. The error in the population size varies from overestimation when the level of heterogeneity is small (Figure 3.7 (a)) to underestimation when the heterogeneity is high (Figure 3.7 (c)). Moreover, it can be seen that the estimates from model M_h are more accurate than the regression method for larger differences in capture rates (compare to Figure 3.6 (d)-(f)). However the errors are further reduced when model M_0 or the regression technique is used on the susceptible and infected data sets separately ($\hat{S} + \hat{I}$) (Figure 3.7 and Figure 3.6 (a)-(c)).

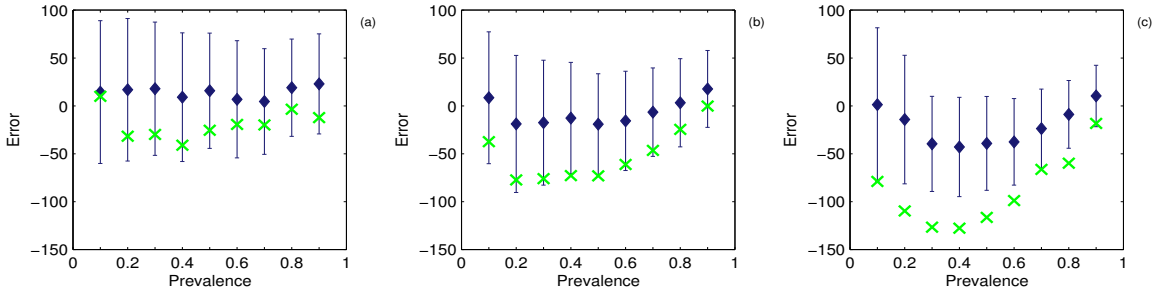

Figure 3.8: Model M_{th} in Program Capture is used to estimate the average population density using the total population data set $\hat{N}$ (navy $\diamondsuit$). The average of 200 simulations is shown with 95% confidence intervals. The regression estimate for the total population $\hat{N}$ (green $\times$) is also included. $\gamma = 1/30$, $\beta = \gamma/S_0$ other parameters figure layout is the same as in Figure 3.5.

When we consider a disease which is dynamic over the trapping period the assumption of closure for the susceptible and infected data sets is broken. Therefore, we only examine the total population estimate using model M_{th} which incorporates individual and temporal heterogeneity allowing individuals to change infection state at any time throughout the trapping periods. Figure 3.8 shows that the error in the total population size $\hat{N}$ produced by model M_{th} is small in comparison to the regression method estimate. As the difference in capture rates is increased there is a shift in error qualitatively similar to the estimate given by Model M_h in Figure 3.7; more specifically small levels of heterogeneity result in overestimation and large levels in underestimation.

Using the individual-based, stochastic framework we are able to create CMR trapping data and have shown that Program Capture is able to produce reasonably accurate population estimates despite infection dependent capture rates; however this is dependent on the appropriate model being identified. We therefore argue that to

achieve the best estimate of the population size identifying any heterogeneity due to the infection status is critical.

3.4 Discussion

Capture-Mark-Recapture (CMR) studies create individual trapping histories which can be used in combination with various statistical techniques to estimate the population size. Most of these techniques require assumptions regarding the data to hold (arguably one of the most important is that of homogeneous capture rates). In this chapter we use a study by Coltherd et al. (2010) - which found that infected mice were more likely to be captured than those who were uninfected - to motivate the evaluation of infection dependent capture rates on the population estimates using the regression technique and program Capture. The data was simulated by two frameworks which replicated the disease and trapping process.

The first framework was a deterministic model which recorded the number of naive captures in each trapping session for a range of disease parameters. When we applied the regression method to this data we found that it produced a large negative bias in the total population when the total catch was used, however when considering the susceptible and infected data sets separately the approximation was reasonably accurate (Figure 3.3). One of the conditions of the regression technique is that of homogeneous data. Using the log plots should show heterogeneity as a deviation from a straight line relationship, however this deviation was difficult to observe in the data generated here, despite the fact that using the total population data gave significant errors.

Data produced from a deterministic model does not include any natural variation; we therefore used this study to develop an individual-based, stochastic, SIS model to incorporate the effect of such variability on the analysis. Using a stochastic model has many advantages, such as the ability to track key characteristics of a population at the individual level. By following the methodology of Gillespie (1977) we simulated the disease and trapping process to create data which could be used in the regression technique (by ignoring re-captures) and in Program Capture which is able to handle heterogeneity. Comparing CR data in Figure 3.4 we demonstrated that our model had, on average, similar output to the deterministic framework, however when using the regression technique, the small level of noise in the number caught resulted in wide confidence intervals for the population size estimate, suggesting that this method is not reliable means of detecting and handling heterogeneity. The overall trend in the average estimate produced using the stochastic framework was consistent with the deterministic model (Figure 3.5), with the maximum error occurring at medium prevalence values and increasing with the difference between capture rates.

We manually selected the appropriate models in Capture dependent on the data sets and found that, in general, the appropriate models produced good estimates of the population size. The infection status is generally assumed not to be known, however when trapping is carried out in combination with diagnostic tests this information could be provided. For fixed disease dynamics it is generally best to split the population into the susceptible and infected groups and use model M_0, however using the total data set model M_h produced relatively small errors (Figure 3.7). A fixed disease may represent a chronic infection with slow transmission and recovery where trapping process occurs over a much shorter period than the disease dynamics. Alternatively, when disease is dynamic, individuals can change their infection state, as for example in an acute infection. In this case we found the total population estimate using model M_{th} was relatively accurate (Figure 3.8).

The aim of this chapter was to analyse the impact of infection dependent capture rates on the total population size estimate. We have shown how the sophisticated statistical methods used in the program Capture, can account for heterogeneity in data and in particular can produce a good estimate of total population size when infected individuals have an (undetected) increased capture probability. To undertake the analysis in this chapter we developed stochastic model representations of underlying deterministic models. These techniques will be used in subsequent chapters when we consider the conservation of red squirrels (see Chapters 4 and 5).

Chapter 4

Disease spread on complex dispersal landscapes: Assessing the potential threat of squirrelpox to red squirrels on the Isle of Arran

4.1 Abstract

Emerging infectious diseases and disease-mediated invasions are a substantial threat to native populations. The spread of disease through naive native populations will depend on life history and disease parameters and on habitat suitability and connectivity. Using the potential spread of squirrelpox virus (SQPV) on the Isle of Arran as a case study, we develop mathematical models to examine the impact of an emerging disease on a complex landscape. Our findings indicate that a SQPV outbreak on Arran is likely to be short lived and localised to the point of introduction allowing recovery of reds to pre-infection densities. This has important consequences for the conservation of red squirrels. By considering a range of disease parameters we infer more generally how complex landscapes interact with disease characteristics to determine the spread and persistence of disease. We find the extent of disease spread is dependent on the rare passage of infection through poor quality corridors connecting good quality habitats. Acute, highly transmissible infectious disease is predicted to spread rapidly causing high mortality. Nonetheless the disease typically fade-outs following local epidemics and is not supported in the long-term. An equivalent chronic infectious disease is predicted to spread more slowly but can remain endemic in the population. This allows the disease to spread more extensively in the long-term as it increases the chance of spread between poorly connected populations. Our results highlight how a detailed understanding of landscape connectivity and the nature of

the threat from emergent infectious disease is crucial when considering conservation strategies to protect native species.

4.2 Introduction

Emerging infectious diseases (EIDs) contribute to species extinction (Smith et al., 2006) and are a global threat to biodiversity (Morse, 1995; Daszak, 2000; Daszak et al., 2001). Disease transmission may occur rapidly, impacting multiple hosts with factors such as climate change, agricultural and environmental alterations, and an increase in human activity facilitating the increased incidence of EIDs world-wide (Morse, 1995; Morens et al., 2004). Furthermore, the deliberate or accidental introduction of non-native species can aid the spread of infectious disease (Prenter et al., 2004). Morse (1995) proposes that EIDs are caused by a two-step process, the introduction of a new species and/or disease into a susceptible population, followed by the establishment within the new environment. The exposure of susceptible indigenous populations to novel and potentially fatal disease aids the invader and if it succeeds to thrive it may increase predation and competition for resources, alter habitat and decrease biodiversity (Manchester and Bullock, 2000).

There are a wide range of examples of emergent infectious diseases (Daszak, 2000). For example the fungal pathogen *Chalara fraxinea* is believed to have emerged in Poland in 1992 and has since caused widespread die back in Ash species (up to 90% mortality) across Europe (Forestry Commission Scotland, 2013). An example of a disease-mediated invasion is the introduction of crayfish species from Northern America - *Orconectes limosus* in 1890, *Pacifastacus leniusculs* and *Procambarus clarkii* both in $1950-60$s (Parvulescu et al., 2012) - to Europe which threaten native crayfish populations (*Astacus astacus* and *Austropotamobiums pallipes*). The invasive species are resistant carriers to a fungal plague *Aphanomyces astaci* which causes epidemics and mortality aiding local extinction of the native crayfish. Disease-mediated invasion is widespread (Strauss et al., 2012) and since it is likely that avirulent individuals survive trans-locations it makes identifying species harbouring potential lethal diseases difficult (Strauss et al., 2012). The invader can cause an epidemic in the naive native population which allows the invasive species to establish with reduced levels of competition for resources and can lead to the replacement of native species (Strauss et al., 2012; Prenter et al., 2004; Gheranrdi, 2006; Daszak, 2000). Understanding the spread of EIDs is therefore crucial to the conservation of native species and thus understanding how disease spreads in the environment can help reduce the impact of infectious disease in wildlife and humans (Patz et al., 2004).

The heterogeneous distribution and connectivity of suitable habitat has a complex relationship with population abundance and persistence (Bienen, 2002). When

habitat is sparse, isolated habitat patches can be formed dividing a population into several subpopulations (Hanski, 1991). Poor connectivity between patches may result in a reduction of movement between local populations which in turn can act to decrease patch biodiversity (Kareiva and Wennergren, 1995), fitness due to inbreeding (Chesser and Ryman, 1986) and population growth (Travis, 2003). Furthermore poor connectivity may lead to a higher probability of local extinction (Fahrig and Merriam, 1985; Henein and Merriam, 1990; Schumaker, 1996) and reduced likelihood of natural re-establishment via dispersal (Fahrig and Merriam, 1985; Andel and Aronson, 2012). Evidence therefore supports the maintenance of dispersal corridors to promote growth and local population persistence and diversity (Beier and Noss, 1998; Dobson et al., 1999; Lookingbill et al., 2010; Andel and Aronson, 2012). However, enhanced connectivity between subpopulations can increase the spread of infectious disease leading to detrimental impacts on native populations (Real and Biek, 2007; Hess, 1994).

The use of spatial frameworks in mathematical models to explore the impact of infectious disease in wildlife has been well established (Hanski, 1991, 1998; Keeling, 1999; Real and Biek, 2007; Rushton et al., 2000), however the incorporation of detailed landscape structure is less well explored (Ostfeld et al., 2005). Since landscape and habitat are infrequently homogeneous a representation of landscape structure will produce a fragmented mixture of high and low quality subpopulations with different levels of inter-population connectivity. Since, for directly transmitted parasites, susceptible individuals must encounter an infected individual for infection to spread (Riley, 2007) the inclusion of geographical data in spatial disease models may identify corridors trafficking infectious disease which in turn may be used to contain outbreaks (Beier and Noss, 1998; Dobson et al., 1999; Riley, 2007).

To illustrate the importance of modelling disease spread in complex environments we examine the impact of habitat distribution and connectivity on the spread of infectious disease in the Eurasian red squirrel (*Sciurus vulgaris*) on the Isle of Arran (Figure 4.1 (a)). The Eurasian red squirrel has been in decline in mainland UK since the introduction of the North American grey squirrels (*Sciurus carolinensis*) in 1900s. Initially competition alone was blamed for causing the reduction in the native population, however it is now accepted that disease-mediated invasion is a critical factor in the replacement of red squirrels (Daszak, 2000; Rushton et al., 2000; Tompkins et al., 2003). The emerging squirrelpox virus (SQPV) is likely to have been introduced to the UK with the grey squirrels (since it is largely avirulent in greys) (Bosch and Lurz, 2012). Squirrelpox causes high mortality in red squirrels and is critical in explaining the rapid replacement of reds (Tompkins et al., 2003). To prevent species extinction the UK Biodiversity Action Plan (Joint Nature Conservation Committee, 2012) have designated 35 red squirrel strongholds (18 in Scotland and 17 in England) and it is therefore important to understand the threat of SQPV in these strongholds. One such

stronghold, Arran, was chosen for its island status and lack of grey squirrel existence thus far (Lurz, 2012). Arran is roughly 32km by 20km in dimensions with 6803ha of fragmented woodland, predominately coniferous, with a mixture of high and low connectivity between local patches (Figure 4.1) (Lurz, 2012). Constructing a spatial disease framework based on red squirrels on Arran provides an ideal case study to examine the impact habitat connectivity has on the spread of infectious disease.

Our aims are therefore two-fold. Firstly, our case study provides species and location specific results that can directly inform conservation management and policy decisions. Secondly, we aim to provide a general assessment of the importance of replicating geographical information accurately in spatial models when analysing disease spread in complex landscapes. Therefore in addition to considering the spread of SQPV we modify the model to include a range of disease parameters - chronic and acute disease with high and low transmissibility - and so can infer how complex landscapes interact with disease characteristics to determine the spread and persistence of disease. Moreover, we include two levels of connectivity, one derived directly from GIS data and one which is additionally supplemented with ground-truthing from local experts that indicate additional barriers to dispersal. We therefore provide a general understanding of how landscape connectivity and infectious disease properties influences disease spread and persistence.

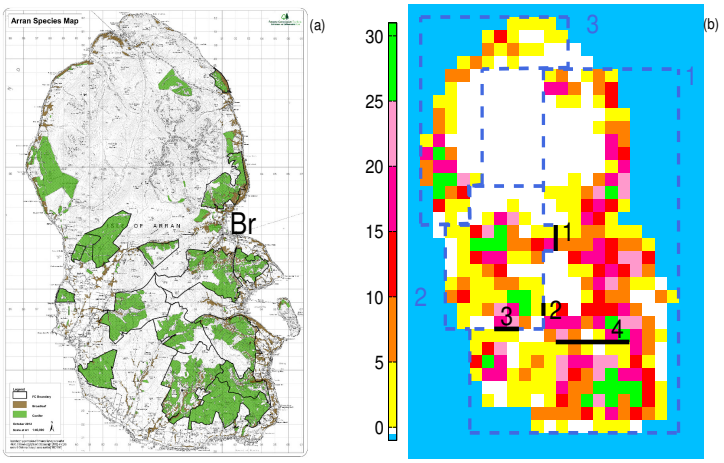

Figure 4.1: The Isle of Arran is shown in (a) (with permission from FCS) with the coniferous (green) and broadleaf (brown) woodland highlighted and 'Br' represents the main port Brodick. The carrying capacity of red squirrels (per km^2) is shown in (b) using estimates of 0.36/ha in coniferous and 0.6/ha in broadleaf. Cells which are well connected are grouped together by the dashed coloured blocks (labelled $1-3$); there is poor connectivity between the blocks. In addition, ground-truthing in collaboration with Forestry Commission Scotland, has identified routes which do not permit movement, identified by thick black lines.

4.3 Methods

4.3.1 Red squirrel carrying capacity

We extrapolate woodland data from the forest inventory maps for 2011 (provided by the Forestry Commission Scotland (FCS) website) using GRASS Geographical Information System (GIS) (Westervelt et al., 1992) (using similar methods to Rushton et al. (2000) and Lurz et al. (2003)). The island is divided into a 1km $\times$ 1km grid - since 1km is typically the maximum dispersal distance for red squirrels (Bosch and Lurz, 2012) and larger than the (approximately) 150m radius of core range activity (Bosch and Lurz, 2012). Within each grid cell habitat data identifying no coverage (thus unable to support red squirrels), coniferous and broadleaf woodland is determined from inventory records (shown in Figure 4.1 (a)). Using published densities of red squirrel abundance in different tree species from Lurz (2012) the carrying capacity is calculated for each cell dependent on the quantity and type of woodland cover (Figure 4.1 (b)). We use upper density estimates for abundance (to reflect a high seed year) with results for lower density estimates (poor seed year) shown in Appendix C.

4.3.2 The model

We assume that any grey squirrels/disease introduced to Arran would be the result of an accidental or deliberate release at the main port (Brodick) on the island (Figure 4.1 (a)). Contingency plans have been developed on Arran to trap and remove greys should they be sighted but this may not prevent disease transmission to the established local red squirrel population and so our initial conditions assume a local population of reds is infected. To assess the potential spread of the disease we reduce the deterministic model of Tompkins et al. (2003), who modelled red/grey/SQPV dynamics on mainland UK, to consider the interaction between the susceptible (S) and infected (I) reds only, with the following equations:

$$\frac{dS}{dt} = (a - qH)H - bS - \beta SI \tag{4.1a}$$

$$\frac{dI}{dt} = \beta SI - (b + \sigma)I \tag{4.1b}$$

where the total population is $H = S + I$. Reds are born susceptible with maximum reproduction rate a and natural mortality rate b. We assume the carrying capacity K is positive and relates to the crowding coefficient $q = (a - b)/K$ which acts to limit the birth rate when the density is high relative to the carrying capacity. Infection is directly transmitted with transmission coefficient β and infected red squirrels ex-

perience additional mortality (virulence) at rate σ due to the disease. There is no recovery class since SQPV is lethal to red squirrels (Tompkins et al., 2002).

We first conduct stability analysis of Equations (4.1). There are three equilbria: trivial steady state in which all host classes are zero ($S = 0, I = 0$), the disease free steady state in which the host is at carrying capacity in absence of the disease ($S = (a-b)/q = K, I = 0$) and a co-existence steady state ($S = S_C, I = I_C$) where

$$S_C = \frac{(b+\sigma)}{\beta} \tag{4.2a}$$

$$0 = q{I_C}^2 + ((2q+\beta)S_C - a)\, I_C + (qS_C + b - a)\, S_C. \tag{4.2b}$$

I_C is found by solving the quadratic Equation (4.2b) for the positive root. To determine the stability of the steady states we calculate the eigenvalues using the Jacobian which is given by

$$J = \begin{bmatrix} a - b - \beta I - 2qH & a - \beta S - 2qH \\ \beta I & \beta S - (b+\sigma) \end{bmatrix} \tag{4.3a}$$

where $H = S + I$.

Eigenvalues for the trivial equilibrium are $\theta_1 = (a-b) = r$ and $\theta_2 = -(b+\sigma)$. Therefore whenever the host growth rate r is positive (which we assume) the trivial equilibrium is unstable.

The eigenvalues for disease free equilibrium are $\theta_1 = -(a-b) = -r$ and $\theta_2 = (\beta(a-b) - q(b+\sigma))/q$. θ_1 is always negative for a positive growth rate, and θ_2 is negative when the reproductive number, $R_0 = (\beta K)/(b+\sigma)$, is less than one (see Appendix B.2 for more on reproductive number). This is interpreted as the pathogen failing to produce enough free-living stages to sustain itself in an environment of susceptible hosts at the carrying capacity.

It is analytically difficult to explicitly determine the eigenvalues for the co-existence equilibrium defined in Equations (4.2). We therefore fix the demographic parameter values (see Section 4.3.4), the carrying capacity to its maximum for the island ($K = 3755$) and examine the four disease parameter sets (Table 4.2) separately. For each scenario we find the equilibrium values are very small (e.g when $\beta = 0.6$ and $\sigma = 26$ Equations (4.2) give $S_C = 45$ and $I_C = 1$) in addition, the eigenvalues are complex with the real part negative. It can also be shown that the disease parameter sets have a large reproductive number, R_0, due to the carrying capacity being so large. When this is the case the co-existence equilrbrium is stable. However we note that the carrying capacities are variable across the landscape in this chapter (see Figure

4.1) which signficantly reduces the size of R_0 (Appendix B.2). The population in each cell may then have different stable equilbrium dependent on the carrying capacity.

As the carrying capacity is reduced however, the system is changed (reproductive number, R_0, decreases) and stability may alter. Additionally, we introduce only a small number of infected red squirrels so it is important to include the possibility of disease extinction or fade-outs which the deterministic framework does not include. Therefore we develop a stochastic version of the deterministic model (4.1) as this captures the random variability of infectious disease at low densities. Furthermore, in heterogeneous spatial environments the spread of infection may be dictated by rare dispersal events and spatial, individual-based frameworks can highlight these key dispersal routes. Therefore, within each 1km by 1km landscape patch (Figure 4.1 (b)) we represent the dynamics using a spatial, individual-based, stochastic, SI model. The rates of change in the deterministic model (4.1) are turned into probabilities of events (Table 4.1, see Renshaw (1991) and Keeling and Rohani (2008) for details on the methodology) which account for changes in abundance within each grid patch. In addition, the abundance within patches can change due to dispersal and disease spread between neighbouring cells.

We assume squirrels core movement has a range αkm (= 0.3km in this study) which may include crossing cell boundaries. Therefore infection can occur through susceptible infected contact within a focal cell (i, j) at rate $\beta S_{i,j} I_{i,j}$ and additionally through contact with neighbouring adjacent ΣI_a or corner ΣI_c cells (at rate $\beta S_{i,j}((\alpha/2)\Sigma I_a + (\alpha^2/4)\Sigma I_c)$, see Appendix B for more details). Core range activity is significantly less than the grid-cell dimensions and individuals are likely to return to their focal cell and so we ignore daily dispersal events. However we include long distance dispersals where an individual leaves the focal cell (i, j) and enters a neighbouring cell (i^*, j^*). We assume saturation dispersal such that individuals are more likely to disperse as cell density increase (which is appropriate for dispersal in mammals (Poethke and Hovestadt, 2002) by the following function:

$$D_{i,j} = d \exp\left(\frac{-(K_{i,j} - (S_{i,j} + I_{i,j}))}{0.5K_{i,j}}\right) \tag{4.4}$$

where d is the dispersal coefficient when the cell population is at its carrying capacity. There is no available data on the frequency of long distance dispersals, therefore we make an assumption that a squirrel will make approximately one long range dispersal in its lifetime (when the density is at carrying capacity), thus giving $d = b$. Once an individual disperses from the focal cell it enters one of the eight neighbouring cells at random dependent on their cell density and location to the focal cell (with appropriate scaling between adjacent and corner cells).

Using methods of Gillespie (1977) (see also Renshaw (1991) and Keeling and Ro-

Description	Outcome	Probability
Birth	$\Pr(S_{i,j} \to S_{i,j} + 1)$	: $[(a - q_{i,j}H_{i,j})H_{i,j}]/R$
Natural death of S	$\Pr(S_{i,j} \to S_{i,j} - 1)$	: $[bS_{i,j}]/R$
Natural death of I	$\Pr(I_{i,j} \to I_{i,j} - 1)$	: $[bI_{i,j}]/R$
Disease induced mortality	$\Pr(I_{i,j} \to I_{i,j} - 1)$	: $[\sigma I_{i,j}]/R$
Dispersal of S	$\Pr(S_{i,j} \to S_{i,j} - 1$ and	
	$\Pr(S_{i^*,j^*} \to S_{i^*,j^*} + 1)$	: $[D_{i,j}S_{i,j}]/R$
Dispersal of I	$\Pr(I_{i,j} \to I_{i,j} - 1$ and	
	$\Pr(I_{i^*,j^*} \to I_{i^*,j^*} + 1)$	: $[D_{i,j}I_{i,j}]/R$
Transmission of disease	$\Pr(S_{i,j} \to S_{i,j} - 1$ and	
	$\Pr(I_{i,j} \to I_{i,j} + 1)$	: $[\beta S_{i,j}\left(\frac{\alpha^2}{4}\Sigma I_c + \frac{\alpha}{2}\Sigma I_a + I_{i,j}\right)]/R$

Table 4.1: A list of all possible events in the spatial, individual-based, stochastic SI model described in Section 4.3.2. The outcome of each event in cell (i, j) is given in column 2 with the associated probability in column 3, where the rate (within square brackets) is divided by the total sum of the rates $R = \Sigma\ [rates]$ across all the cells. The dispersal of susceptible and infected individuals from the focal cell (i, j) to a neighbouring cell (i^*, j^*) is given by $D_{i,j}$ which is defined in Equation (4.4). The transmission of disease occurs when a susceptible individual comes into contact with an infected individual from the current cell (i, j) or from 8 neighbouring cells where ΣI_c and ΣI_a are the total infected individuals in the corners and adjacent cells respectively.

hani (2008)) we transform the rates into probabilities by dividing each rate by the sum of the total rates $R = \Sigma\ [rates]$ (see Table 4.1). The choice of event is determined at random and the time between events is defined as $\delta t = -\ln(\psi)/R$ where ψ is drawn from a uniform distribution between 0 and 1 (which assumes that time to the next event is an exponentially distributed random variable (Renshaw, 1991)). After each event grid cell densities and therefore probabilities are updated. By repeating this process the abundance of susceptible and infected individuals can be tracked over space and time.

4.3.3 Arran connectivity

GIS data provides habitat information that is transformed into a grid-cell carrying capacity and informs within cell epidemiological dynamics and between cell transmission and dispersal. In addition to the GIS data, ground-truthing in collaboration with Forestry Commission Scotland, has identified further routes of poor connectivity - highlighting, for instance, exposed mountain tops that would be a barrier to dispersal. This can be incorporated in the model by preventing dispersal between appropriate cells (shown by black lines in Figure 4.1 (b)). The ground-truthing information is likely to impact dispersal and disease spread predicted by our model since, for example, barrier 1 in Figure 4.1 (b) prevents east to west connectivity. In this study we compare two connectivity scenarios: the first includes all the connectivity information obtained from GIS and ground-truthing, whilst the second uses GIS data only. It is likely that the connectivity in most spatial models utilise GIS information only, so in comparing the two scenarios we aim to highlight the importance of incorporating local knowledge (if available) when modelling disease spread.

4.3.4 Parameter values

All demographic parameters are kept constant. The natural death rate, $b = 0.9$, is produced using adult mortality estimates presented in Barkalow et al. (1970). The growth rate for red squirrels is estimated at 0.6yr^{-1} (Tompkins et al., 2003) which translates into a birth rate $a = 1.5\text{yr}^{-1}$. The values of a and b combine with grid patch dependant carrying capacities to determine the susceptibility to crowding q in each patch. The dispersal rate $d = b$ and core movement has a range $\alpha = 0.3$km (Bosch and Lurz, 2012). Table 4.2 displays the four sets of parameter values used for evaluating disease spread on Arran. We explore a range of disease parameters to reflect the best estimate parameters for SQPV and to represent acute and chronic infections with high and low levels of transmissibility. There is a lack of data on red to red SQPV transmission and so the best estimate parameters for SQPV use the transmission coefficient derived for grey to grey interactions (we use the (high)

	Acute (high virulence)		Chronic (low virulence)	
Parameter	(SQPV) Low transmission	High transmission	Low transmission	High transmission
Transmission coefficient, β	0.6 *	12	0.6	12
Disease induced death, σ	26 *	26	0.445	0.445

Table 4.2: The disease parameters considered in this study. * denotes the baseline parameters.

virulence level defined for reds in Tompkins et al. (2003)). This allows us to simulate how SQPV would most likely spread if a local outbreak occurred on Arran (Table 4.2). Since red squirrels display visible symptoms of infection (and greys do not) it may be reasonable to assume red to red transmission is higher than the grey to grey rate and therefore we consider an acute disease with high transmission (Table 4.2). These scenarios combine to provide information on the spread of an acute infection with high and low levels of transmissibility.

To provide a general understanding of disease spread on our complex landscape we also consider disease parameters that represent chronic infections (low virulence) with low and high transmissibility (Table 4.2). Here virulence is chosen to maintain the same basic reproductive rate of the disease for the acute, high transmission and chronic, low transmission cases. Establishing these parameter sets allows us to examine the impact of different infectious disease characteristics on the spread and persistence of infection in fragmented habitats. (For further details on parameter estimation see Appendix B.)

4.4 Results

4.4.1 Squirrelpox spread on Arran

Using the best estimate SQPV parameters the spread of SQPV from its source of introduction is limited (Figure 4.2). This indicates that there may be no large scale threat to the population of red squirrels on Arran if an SQPV outbreak occurred. In most simulations the disease fails to spread and fades-out within 2 months of the initial introduction (Figure 4.2 (a)). In a few simulations (4 out of 25) there is limited disease spread to neighbouring cells but nevertheless the disease fade-outs within 6 months of the initial introduction (Figure 4.2 (c)). In all cases the population reduction due to the disease is relatively small (infection within a grid-cell reduces the density by at most 25%). Therefore the best estimate parameter set for SQPV does not permit the spread of disease or cause any significant reduction to the red squirrel

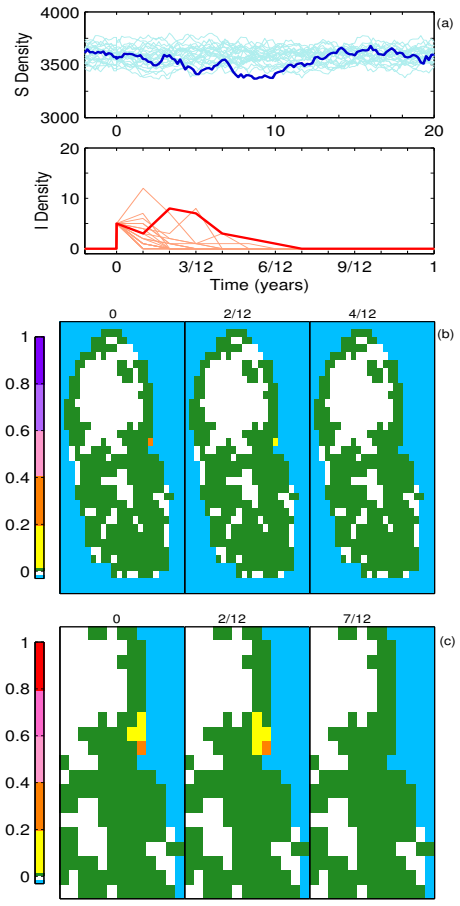

Figure 4.2: The spatial, individual-based, stochastic SI model using (best estimate) SQPV parameters (Table 4.2) where connectivity includes GIS information and ground-truthing. Once the total population has achieved quasi-steady state, 5 infected red squirrels are introduced at Brodick (Figure 4.1 (a)) at time 0. In (a) the total susceptible (blue) and infected (red) population densities are shown against time for 25 model realisations with a single realisation highlighted in bold. In (b) and (c), snap shots show the spatial distribution of disease at different time frames. We define the disease prevalence as the proportion of infected hosts in each cell ($Prev = I_{i,j}/(I_{i,j}+S_{i,j})$). In (b) we show the proportion of the 25 simulations that have a prevalence greater than 0.2 (for example a grid cell value of 1 translates to the prevalence being greater than 0.2 in all realisations). In (c) we show the prevalence for the realisation highlighted in bold in the time series (a) with an enlarged scale to focus on the region where the disease was introduced.

population on Arran. This is due to the high virulence and low transmissibility of the disease which in combination with the relatively low densities on Arran (around $0.1-0.5$ squirrels/ha around Brodick) means the basic reproductive rate of the disease (R_0) is not sufficiently high to promote large-scale disease spread or persistence (see Appendix B for analysis of R_0). (Since disease spread is limited with these parameter values there is no difference between the scenarios using GIS and ground-truthing and GIS information only.)

4.4.2 Acute infection with high transmissibility

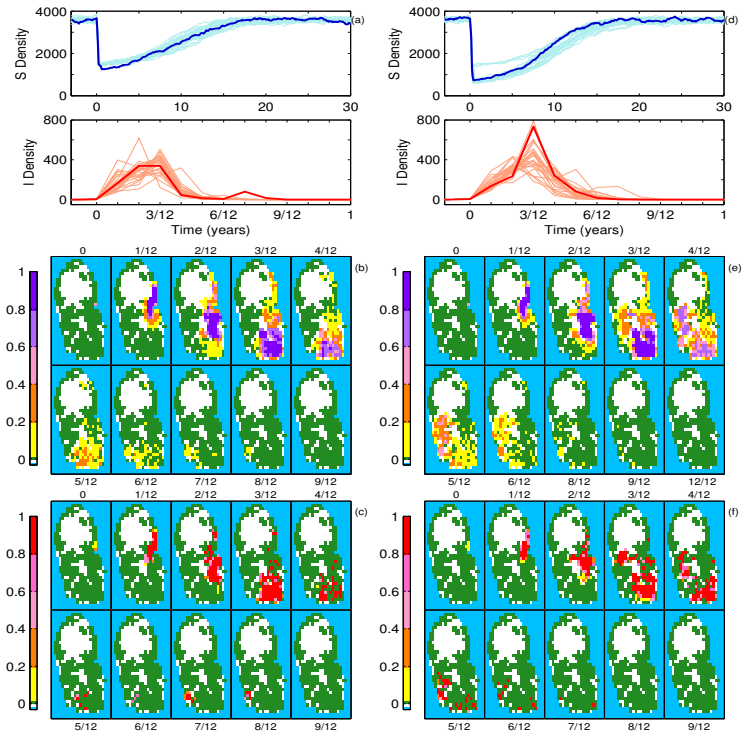

Figure 4.3: The spatial, individual-based, stochastic SI model with acute, high transmission parameters (Table 4.2) where in (a-c) connectivity includes GIS information and ground-truthing and in (d-f) GIS information only. Once the total population has achieved quasi-steady state, 5 infected red squirrels are introduced at Brodick (Figure 4.1 (a)) at time 0. In (a) and (d) the total susceptible (blue) and infected (red) population densities are shown against time for 25 model realisations with a single realisation highlighted. In (b) and (e) we show the proportion of simulations that have a prevalence greater than 0.2 and in (c) and (f) we show the prevalence for the realisation highlighted in (a) and (d) respectively (prevalence is defined in Figure 4.2).

Figure 4.3 shows the population dynamics and disease spread when the high virulence of SQPV is retained and transmission is increased (since parameterisation for red to red transmission is currently unavailable this also serves as a hypothetical worst-case scenario for SQPV). When restrictions to dispersal imposed by ground-truthing are included the disease spreads rapidly throughout the east and south of the island (region 1 in Figure 4.1 (b)). Disease outbreaks lead to a substantial reduction of up to 89% of local density. The density in region 1 is reduced to 15% and the total population is reduced to 42% of its pre-infection levels. The wavelike expansion in the distribution of the disease and the eventual containment of disease is dependent

on areas of high and low landscape connectivity. In areas of high connectivity the disease spreads quickly causing high mortality, however upon reaching regions of low connectivity the disease may fade-out as it rapidly exhausts the local pool of susceptible individuals and is rarely able to spread over poor quality (low density) habitat (this prevents the spread from region 1 to 2 as denoted in Figure 4.1 (b)). When the additional barriers to dispersal imposed by ground-truthing are removed the disease spread is more extensive and occurs across the majority of the island (since the connectivity between regions 1 and 2 is improved). There is high disease mortality in regions 1 and 2 and the total population is reduced to 22% of its pre-infection levels. Poor connectivity between regions 2 and 3 prevent disease outbreaks in region 3. In both connectivity scenarios the disease fades-out following an epidemic. Locally this takes $1-2$ months and has typically faded-out on the entire island within 7 months. Fade-out arises since the high virulence and rapid spread of the disease largely exhausts the local population of susceptibles. Following disease-fade out the population recovers to its pre-infection level through demographic processes. These simulations indicate that a highly virulent, highly transmissible disease can have marked impacts on the population density over a large scale. They also reveal how areas of low connectivity, through which the disease fails to spread, can safe-guard populations.

4.4.3 Chronic infection with low transmissibility

Figure 4.4 shows the impact of a chronic infection with low transmission when connectivity includes the information from ground-truthing (note, the basic reproductive rate of the disease, R_0, is the same in Figures 4.3 and 4.4). The disease initially spreads throughout region 1 reducing the population here to 17% of pre-infection levels, with the total population reduced to 43%. This is similar to the acute, high transmission scenario with connectivity from GIS and ground-truthing (Figure 4.3 (a)-(c)) except for the chronic disease the rate of spread is reduced. The key difference is that the disease persists under this chronic scenario in the long-term therefore a rare dispersal event eventually allows the disease to expand into region 2 in 80% and region 3 in 67% of realisations. Although, the disease persists in the long-term in a single realisation of the model the distribution of infection changes over time with periodic epidemics and fade-out out of the disease locally (Figure 4.4 (c)). (Results observed in the connectivity scenario in which the dispersal barriers imposed through ground-truthing are removed show a similar reduction to the host densities, but here the disease initially spreads to all regions.) A key difference between Figure 4.3 and Figure 4.4 is that the persistence of the chronic infection provides greater opportunity for dispersal and therefore it can eventually expand over a more extensive region.

Note, we did consider the chronic, high transmission scenario (Table 4.2). The parameters increase the basic reproductive rate of the disease greatly. Here, the

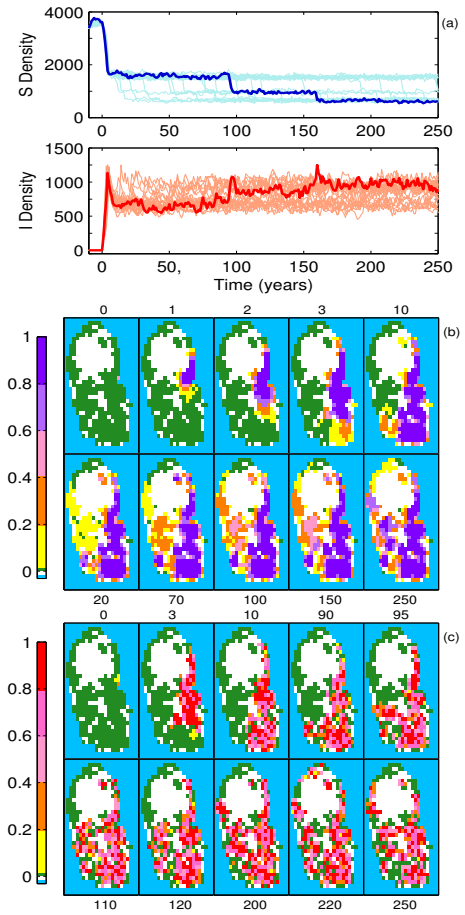

Figure 4.4: The spatial, individual-based, stochastic SI model with chronic, low transmission parameters (Table 4.2) where connectivity includes GIS information and ground-truthing. Once the total population has achieved quasi-steady state, 5 infected red squirrels are introduced at Brodick (Figure 4.1 (a)) at time 0. In (a) the total susceptible (blue) and infected (red) population densities are shown against time for 25 model realisations with a single realisation highlighted. In (b) we show the proportion of simulations that have a prevalence greater than 0.2 and in (c) we show the prevalence for the realisation highlighted in (a) (prevalence is defined in Figure 4.2).

disease spreads rapidly across the whole landscape, the total population abundance is reduced dramatically and most individuals become infected. This leads to the local extinction of populations. In the long term there are two possible outcomes. Either the entire population becomes extinct or the disease becomes extinct and the population recovers to pre-infection levels (for more information see Appendix C).

Results for all the scenarios presented here but with the low red squirrel density estimates used to determine grid-cell carrying capacities, are reported in Appendix C. The results for the low density scenarios are qualitatively similar to those for the high density scenarios although the effect of the lower density does reduces the severity of disease outbreaks and extent of disease spread (as at lower density the reproductive ratio of the disease, R_0 is reduced).

4.5 Discussion

Emerging infectious diseases (EIDs) and disease-mediated invasions are a substantial threat to native wildlife abundance and diversity (Morse, 1995; Daszak, 2000; Daszak et al., 2001). Through the use of mathematical models we addressed how infectious disease characteristics and landscape connectivity combined to influence disease spread and persistence. The model analysis allowed us to make system specific predictions on the potential threat of SQPV to red squirrels on the Isle of Arran that are being used to influence conservation management decisions (Macpherson et al., 2013). Further, the generality of our model framework allowed us to uncover broadly applicable findings on how different infection characteristics (acute or chronic infections) influence the spread and persistence of disease in realistic landscapes.

To protect the remaining populations of red squirrels 35 red squirrel strongholds in England and Scotland have been developed in which reds are isolated from grey squirrels (through control of greys or due to the isolated nature of the stronghold). However, SQPV remains a threat to stronghold red populations. For instance, high density red populations in Formby, Merseyside and in Whinfell, Cumbria have been protected by trapping and removal of greys since the launch of strongholds in 2006 (Parrott et al., 2009), but have suffered repeated SQPV outbreaks which has resulted in a marked reduction in population abundance (followed by disease fade-out and subsequent population increases). Using, best estimate SQPV parameters the model predicts the impact of disease on the low density populations on Arran will be limited to a short term, local outbreak focussed at the point of disease introduction. When considering a highly virulent, highly transmissible disease (which could represent SQPV if red-red transmission is sufficiently high but also could represents a system with best estimate SQPV parameters with a higher density host population) the disease spread is more widespread and a substantial reduction in population density is predicted due to disease induced mortality. However, disease spread does not occur between poorly connected regions and the disease fades-out leading to population recovery to pre-infection levels - supporting the observations of disease dynamics in high density stronghold populations (Parrott et al., 2009). In terms of the conservation of red squirrels on Arran the model suggests that if introduced, SQPV spread is likely to remain local to the point of introduction and will not cause an island-wide epidemic and as long as grey squirrels are removed from the island reds should recover.

The model results have broad implications for red squirrel conservation and more generally in the understanding of the spread of highly virulent EIDs through native populations. Our results support previous studies by Gurnell et al. (2006) and Duff et al. (2010) who concluded that in the absence of grey squirrels SQPV would not persist due to the increased mortality of reds reducing the chance of disease trans-

mission. This suggests that the disease cannot persist without an additional local reservoir of infection and emphasises that limiting grey squirrel introductions and/or preventing the further population expansion of grey squirrels may be critical to safeguarding the remaining red squirrel populations in the UK. The interface between the distribution of red and grey squirrels in the UK occurs in Highland Scotland and has been relatively stable for 40 years. Grey populations to the south of this interface are currently disease-free but recent surveys (Scottish Wildlife Trust, 2013) indicate that SQPV is spreading northwards from Southern Scotland and so there is a clear risk that SQPV will spread to grey populations at the interface. The model results here suggest the SQPV may cause epidemic outbreaks and mortality in red populations adjacent to the interface but that it is unlikely to spread extensively through the red (only) populations in Highland Scotland (north of the interface). However, the impact of the disease will increase the apparent competition from greys at the interface (Tompkins et al., 2003) and could allow greys to expand their distribution northwards (Bell et al., 2008). This would have detrimental implications for the conservation of red squirrels and it is therefore essential that it is a focus for further study.

The implication of landscape connectivity for wildlife viability and persistence is well studied with clear evidence that increased connectivity can increase population abundance and prevent extinction (Fahrig and Merriam, 1985; Henein and Merriam, 1990; Schumaker, 1996; Dobson et al., 1999; Lookingbill et al., 2010; Andel and Aronson, 2012). However, it has been argued that increased connectivity may also promote the spread of infectious disease (Hess, 1994; Bienen, 2002; Real and Biek, 2007). Our results indicate that disease can spread rapidly through (relatively) high density well connected regions and that disease spread is prevented or greatly reduced through poor habitat. Therefore, poor connectivity may provide a refuge from disease for a proportion of the population and so careful consideration of the threat from disease is required when considering habitat changes to improve connectivity. We have shown how model studies are useful tools in determining the level of connectivity, but also that it is essential to supplement the landscape data used in model analysis with expert knowledge on the ground.

Our modelling study provides a general understanding of how the speed and extent of disease spread is related to habitat quality, landscape connectivity and the specific characteristics of the disease. When the basic reproductive rate of the disease, R_0, is low (in our study due to a combination of a low density habitat, high virulence and low transmission) the disease fails to persist and spread is limited. When R_0 is increased disease spread is more marked and the long-term impact depends on the nature - acute or chronic - of the disease. Acute, highly virulent diseases can spread rapidly through well connected regions and cause severe population crashes. However, the short lived nature of infection reduces the chance of disease spread between

poorly connected regions and the disease fade-outs (provided there is not a reservoir of infection). Evidence for such epidemic outbreaks followed by disease fade-out has been observed in the high density stronghold red squirrel population in Formby, Merseyside (Parrott et al., 2009). Chronic disease spreads more slowly than the acute infection but has a longer infectious period and this allows it to remain endemic in the population. This increases the opportunity for (rare) disease spread across poorly connected regions and so in the long-term chronic disease can spread more extensively (and does not require a reservoir of infection). This may have similarities with squirrel Adenovirus that is less virulent than SQPV but can cause mortality when associated with other stress factors. Adenovirus has been reported in natural red squirrel populations that are free from grey squirrels with the disease persisting for many years (Martínez-Jiménez et al., 2011; Everest et al., 2013). Detailed investigations into the prevalence of Adenovirus in red populations is ongoing (Everest et al., 2013) but our modelling results suggest that the chronic nature of the disease may allow it to spread and persist should it be introduced into a naive population - such as the red population on Arran.

The results of our study highlight how wildlife management strategies should carefully consider the risk of disease outbreaks. Management strategies that increase population connectivity or increase population density (e.g. through supplementary feeding or changes to forest composition) may increase the risk of disease spread and so scale and location of such measures should be considered carefully. Our study suggests that a stochastic model frameworks that includes a realistic representation of habitat are useful tools for understanding the risk from EIDs and for developing conservation contingency plans for preventing disease spread.

Chapter 5

The impact of seasonality on species colonisation and persistence on complex landscapes

5.1 Introduction

Maintaining a diverse range of species is essential to the sustainability of agriculture, forests, and natural ecosystems (Pimentel et al., 1997). Despite this Pimm et al. (1995) estimates that the current rate of species extinction is $100 - 1000$ times their pre-human levels. Many acknowledge that the growing pressure on our environment is sourced from human activity (Deem et al., 2001; Pimm et al., 1995; Pimentel et al., 1997) with factors such as climate change (Van der Putten et al., 2010), emerging infectious diseases (Daszak, 2000) and habitat alteration (Dale et al., 2000) all contributing to the decline. Conserving biodiversity, the variety of life on Earth, is key a global challenge (International Union for Conservation of Nature, 2014).

The history of biodiversity conservation stems as far back as the 19th century (Yellowstone, the first national park in the United States, was formed in 1872, National Parks Conservation Association (2014)); however it wasn't until the International Union for Conservation of Nature (IUCN) created the Species Survival Commission (SSC) in 1987 that efforts to conserve species received scientific attention. Since then there has been an increasing commitment to conservation research from fields such as ecology, biology, geography and more recently mathematics and statistics (as we shall see later) and this has resulted in the development of conservation strategies such as species recovery programmes, establishment of protected areas, restoration of ecosystems and control of invasive species (Congress, 2013). However it is recognised that the success of these programs is largely dependent on appropriate planning, management and monitoring (Congress, 2013; Gaston et al., 2002; Kleiman and Reading, 2000; Knight et al., 2008; Wallace et al., 2002).

A key factor underlying conservation strategies is the maintenance of ecosystems (Finlayson et al., 2008; Griffith et al., 1989; Gyllenberg and Hanski, 1997; Pimm and Raven, 2000). Preserving landscape features (vegetation, soils, water resources, etc) is fundamental (Godefroid et al., 2011) as such landscapes provide key habitats for food and shelter to support many wildlife species (Gyllenberg and Hanski, 1997; Pimm and Raven, 2000). For instance habitat loss has been shown to increase the risk of extinction in 82% of endangered bird species (Gyllenberg and Hanski, 1997). When conservation efforts to improve habitat are a success, there is often a positive impact on the native wildlife (Donald and Evans, 2006).

In some circumstances habitat restoration alone may not be sufficient to protect threatened species - for example when species densities have declined to small numbers - and supplementary methods are often needed (Clark and Westrum, 1989; Rout et al., 2007). One such conservation method is the translocation of a threatened species, defined by IUCN (2013) as 'the deliberate movement of organisms from one site for release in another'. Translocations are beneficial as they can be used to 're-stock' a species at low density, 're-introduce' a species to a native area from which it has been extirpated, or 'introduce' a species to non-native ranges (although this is only recommended when no native areas remain viable).

The transportation of plants and wildlife is not a new concept (it has evolved with human migration, (Seddon et al., 2007)) but originally was rarely used in pursuit of conservation goals and instead often had the side-effect of releasing invasive species and/or disease into native environments (Armstrong and Seddon, 2008; Clark and Westrum, 1989; Deem et al., 2001; IUCN, 1987; Manchester and Bullock, 2000; Seddon et al., 2007). Through-out the 1900s conservation translocations became increasingly popular but the lack of research, regulation and monitoring often resulted in failure (i.e. a self-sustaining population was not achieved). This is highlighted in a review by Griffith et al. (1989) who found that between 1973 and 1986 only 44% of conservation translocations to the wild were successful in native birds and mammals that were registered as threatened, endangered or sensitive. The SSC/IUCN recognised potential benefits - and the poor regulation - of translocations to endangered species and so formed the Reintroduction Specialist Group, RSG, (Armstrong and Seddon, 2008; IUCN, 1987) in 1988 who sought to engage a host of specialists to 'combat the ongoing and massive loss of biodiversity by using re-introductions as a responsible tool for the management and restoration of biodiversity'. As a result there was a large increase in multi-disciplinary research and an increase in the recorded number of successful conservation translocations (Seddon et al., 2007).

In the recent edition (2011) of the IUCN's 'Global Re-introduction Perspectives' - which assemble case studies in a standardised format independent of the outcome - there are 50 case studies in a range of taxa with all but one recorded as at least

'partially successful' (Soorae, 2011). One of the largest and most successful case studies in the UK is the re-introduction of the large blue butterfly (*Maculinea arion* L) following its extinction in 1979. Despite conservation efforts beginning in 1920s scientific research only identified key drivers (the large blue was dependent on the ant *Myrmica sabuleti* which was also in decline because of agricultural changes in the landscape) in the mid 1970s and by then efforts to save the UK population of large blue were unfortunately too late. However a combination of conservation techniques, such as restoring the landscape at a National Trust site in Dartmoor to allow the ant population to recover and the re-introduction of large blue's (from Scandinavia), led to a successful conservation programme. The UK is now home to some of the largest known populations of large blue's in the world which has enabled this species IUCNs status to be downgraded from 'Vulnerable' to 'Near Threatened'. This case study highlights the benefit regulated re-introductions has to the maintenance of biodiversity (Soorae, 2011).

Habitat evaluation along with planning and monitoring is now widely accepted as a critical part of a re-introduction success (Armstrong and Seddon, 2008; Rout et al., 2007; Sarrazin and Barbault, 1996; Seddon et al., 2007; IUCN, 1987). One tool which helps examine and identify suitable release sites is Geographical Information Systems, GIS, software (Seddon et al., 2007). GIS was developed in the 1960s by R. Tomlinson in a bid to computationally analyse cartography, but the lack of available data often restricted its use (Coppock and Rhind, 1991). Over the last two decades a vast improvement in environmental mapping has increased the availability of data (Rodríguez et al., 2007) allowing layers of landscape (for example vegetation, rivers, roads, villages, Li et al. (2002)), wildlife species and climate change (Rodríguez et al., 2007) to be complied and analysed. GIS is now a well-established tool for exploring biodiversity.

Parallel to the evolution of GIS has been the development of computational models. An increasing amount of conservation studies now incorporate some form of predictive modelling to explore the short and long term consequences of different management strategies, identify key vital rates and ultimately the viability of populations (Seddon et al., 2007). Population viability analysis (PVA) has been used to assess the probability of a species persisting at some time point in the future (Boyce, 1992; Brook et al., 2000; Seddon et al., 2007). Computer-based PVA packages are available (Wintle et al., 2005) and have been used in conservation studies (Boyce, 1992). For example Leaper et al. (1999) assessed the feasibility of introducing wild boar (*Sus scrofa*) to Scotland using GIS to identify areas of suitable habitat in the landscape and a PVA package, RAMAS/age, to estimate the release number of wild boar required to enable the population to establish (Leaper et al., 1999).

Using a combination of GIS and PVA packages as a tool to pre-assess re-introductions

is now prevalent among case studies (Seddon et al., 2007). However it is only in the past decade or so that including realistic representation of the landscape in spatial re-introduction modelling has evolved; more specifically South et al. (2000) proposes that they were the first to include a realistic highly fragmented landscape when modelling the re-introduction of the European beaver (*Castor fiber*) in Scotland. South et al. (2000) used two approaches to model the re-introduction. The first was a combination of GIS (which identified available, although fragmented, habitat for beavers) and a custom-built spatial, individual-based population model which explicitly simulated the demographic and dispersal rates of individuals between habitat patches. Their second approach used a PVA model, Vortex (Lacy, 1993), to simulate the system but here the approach was more limited as it can be difficult to include key life history properties into PVA packages. Overall both modelling approaches produced similar results concluding that the release of 20 beavers in a single patch should be sufficient to produce a self-sustaining population (South et al., 2000). Individual-based, spatially explicit model on realistic landscapes have also been used to assess the re-introduction of female Persian fallow deer (*Dama mesopotamica*) to Israel (Bar-David et al., 2005). This study highlighted factors that limited home range establishment and indentified key corridors between suitable habitat. It concluded that model systems are key conservation tools as they can provide projections of species abundance and be used to assess any landscape changes which may affect the population.

The combination of GIS and computational models is a powerful tool which allows re-introduction strategies to be tested which can help form management decisions (Rodríguez et al., 2007). In addition long term strategies can be implemented as the increase in monitoring and data gathering can be used to update parameters whilst the re-introduction program is initiated, and models can be continually simulated in order to address any future changes (i.e. test the impact of a change in the landscape) (Bar-David et al., 2005; South et al., 2000). Poor connectivity between habitat patches has been shown to decrease patch biodiversity (Kareiva and Wennergren, 1995) and reduce population growth (Travis, 2003). GIS and spatial models can be used to identify habitat corridors promoting dispersal of a species. However, habitat suitability and the viability of dispersal corridors can change from year to year - particularly in forest habitat where resources for wildlife may depend heavily on multi-year cycles in seed crops (Kelly et al., 2008). The impact of seasonality on landscape connectivity and the affect this may have on species introductions has not been the subject of previous GIS/modelling studies and yet the affect of a dynamic habitat is likely to be important (Osborne and Seddon, 2012; Parlato and Armstrong, 2013).

In this chapter we aim to investigate how including seasonality in a spatial, individual-based, stochastic model will impact on the success of species introductions and population persistence in realistic landscapes. To do this we use a case

study of the Eurasian red squirrels (*Sciurus vulgaris*) on two complex landscapes - the Isle of Arran and the Isle of Mull. In the UK, native red squirrels are under threat from disease-mediated invasion from the grey squirrel (*Sciurus carolinensis*) which was introduced from North America to mainland UK in 1900s. In response the UK biodiversity Action Plan designed several strongholds around the UK to help protect the reds; one of which is the Isle of Arran. In Chapter 4 we used a combination of GIS and a spatial, individual-based, stochastic disease model to investigate the impact of SQPV in the red population on Arran (there are no greys presently on Arran). Our model showed that SQPV was unlikely to persist in the red population due to the virulence and lack of greys (which are believed to act like a reservoir for the disease). In addition to SQPV we investigated a range of disease parameters and found that disease spread was highly dependent on the connectivity between patches; poor connectivity inhibited disease spread. Like the spread of disease, the success of an introduction of a species is heavily dependent on the quality of connectivity between patches for promoting dispersal and population growth (Travis, 2003). In this chapter we extend the model framework in Chapter 4 to include a better representation of red squirrel population dynamics.

Many wildlife species, like the red squirrel, are highly susceptible to large population fluctuations, which can be attributed to seasonality in demographic rates (such as seasonal breeding) and also the seasonal production of food from trees. In UK squirrel populations there is a distinct breeding season in which births peak. Moreover the death rate is likely to be a function of resource and habitat availability (and so density dependent) (Bosch and Lurz, 2012). Seed crops, which provide the majority of resource, vary throughout the year and most tree species have distinct periodic 'masting' events with periods of between 3 and 8 years that lead to an increase in resources (Lurz et al., 1995). Using GIS enables us to extract the woodland composition of our case study islands to a tree species level from forest maps available from the Forestry Commission Scotland website. As in Chapter 4 resource availability is used as a proxy for the red squirrel carrying capacity; areas of high quality resource are able to sustain more squirrels thus result in a large carrying capacity, conversely low quality areas produce small carrying capacities. Further, we now include dominant seasonal forces in the resource signal which creates a temporal change in the carrying capacity dependent on the tree species mixture in a local patch. The carrying capacity can be directly inputted into our spatial, individual-based stochastic model which includes the seasonal effects on host demography.

The aim of this chapter is to construct a spatial, individual-based, stochastic framework for two test landscapes, the Isle of Arran and the Isle of Mull, which will allow us to analyse the rate of re-colonisation when we include seasonal effects on host demographics and resource availability. Moreover this framework permits the

examination of red squirrel population dynamics (once colonisation has been achieved) on complex landscape habitats with seasonal resource availability.

5.2 Methods

In Chapter 4 a spatial, individual-based, stochastic susceptible-infected model was used to examine the threat of introduced disease on the complex landscape of Arran. One result indicated that following an epidemic the disease may fade out, allowing the host population to recover to pre-infection levels. However we noted that this population recovery after the infection typically took 10 years (see Figure 5.1) at a local site whereas observations suggest recovery could occur in approximately 3 years (observed following recovery from infection in the stronghold population at Formby, Merseyside, Parrott et al. (2009)).

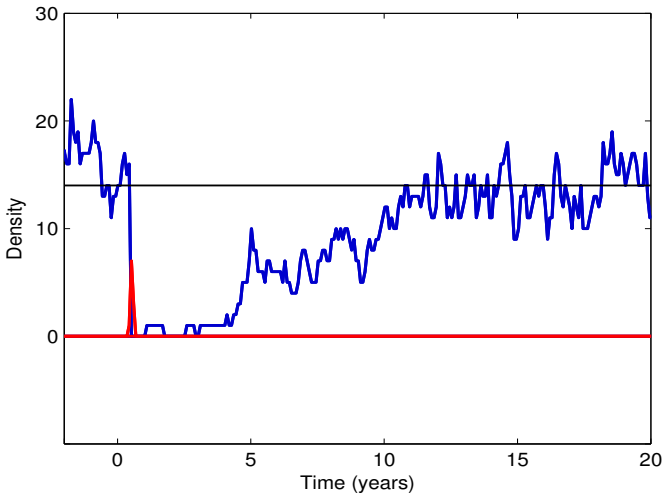

Figure 5.1: The susceptible (blue) and infected (red) host density for one cell on Arran against time. We use the spatial, individual-based, stochastic susceptible-infected model described in Chapter 4. Parameters are as given in Figure 4.3.

A possible explanation for the slower recovery in the disease framework (Figure 5.1) is that the host life history characteristics are simplified. We therefore use this as motivation to we examine some of the contributing seasonal effects on resource availability and host demographic rates which can impact the rate of recovery or colonisation of a population and use a spatial, individual-based, stochastic framework for two test landscapes, the Isle of Arran and the Isle of Mull (Section 5.2.2 and 5.2.3 respectively) to highlight important correlations.

5.2.1 The model including host seasonality

In order to produce a framework which better reflects red squirrel demographics we first examine the deterministic equation used in Chapter 4 to describe the host demographics. The total population H was represented by the following equation:

$$\frac{dH}{dt} = a\,(1 - qH)\,H - bH \tag{5.1}$$

Here the maximum, annual reproduction rate a is modified by subtracting a crowding term qH, with the crowding coefficient q being given by $q = (a - b)/(aK)$. The crowding term acts to limit the birth rate when the density is high relative to the carrying capacity, K. For fixed K this model has the solution that the population monotonically converges to the steady state where $H = K$ (provided $K > 0$) (Figure 5.2).

Initially we examine host seasonality in the case where the carrying capacity is constant, before also incorporating resource seasonality in Section 5.2.2. In order to incorporate host seasonality we first analyse the life history processes of red squirrels. Squirrels have a distinct breeding season during which a large increase in the population density occurs. Typically litters are born in May/June and September/October (yearlings, however, tend to only have one litter in their first year) (Bosch and Lurz, 2012). Following reproduction it is typical that the resource does not meet the demand of the total population forcing juveniles to either disperse and find new available habitat or die. In small mammals the mortality rate in juveniles is often higher than in adults (Kraus et al., 2004). From this we anticipate the squirrel density will experience large within year fluctuations peaking at densities above the carrying capacity at the end of the breeding season, followed by a sharp decline due to lack of available resource. This is unlike the solution of Equation (5.1) where the density evolves to stable a point equilibrium over time (see Figure 5.2). The complicated life history of red squirrels could be represented by an intricate model framework that, for example, included age structure where different cohorts could incur different demographic rates. However, in keeping with modelling philosophy of Chapter 4 we aim to construct a straightforward model framework that includes the key red squirrel life history characteristics and gives a clear understanding of the impact on the population dynamics. We therefore modify Equation (5.1) to include a distinct breeding season and density dependent death as follows:

$$\frac{dH}{dt} = \begin{cases} a_S\,(1 - q_S H)\,H - b\frac{H}{K}H & \text{when } 0 \leq t \leq 0.5, \\ -b\frac{H}{K}H & \text{when } 0.5 < t \leq 1. \end{cases} \tag{5.2}$$

Here we assume birth and death can occur during a 6 month breeding season ($0 \leq t < 0.5$) and only death can occur in the non-breeding season (also of 6 months

in duration). These dynamics repeat each year. The natural mortality rate, b, and the carrying capacity, K, are the same as in Equation (5.1). This implies that the total death rate across the population is equal to that in Equation (5.1) when the population is at the carrying capacity, with a reduced death rate when below the carrying capacity and an increased death rate when above it. The parameter a_S represents the maximum birth rate during the breeding season and we fix $a_S = 2a$, where a is the maximum birth rate over one year in Equation (5.1)) so that in absence of death and crowding, the density achieved over half a year from Equation (5.2) is consistent with the density produced over one year in Equation (5.1). The parameter q_S is fitted so that the long-term average density over one year is equal to the carrying capacity K (the equilibrium density in Equation (5.1)). To do this we use numerical approximations to integrate Equation (5.2) over one year and set the average density over one year equal to K. The resulting time series is shown in Figure 5.2 where the average density is the same for both Equations (5.1) and (5.2).

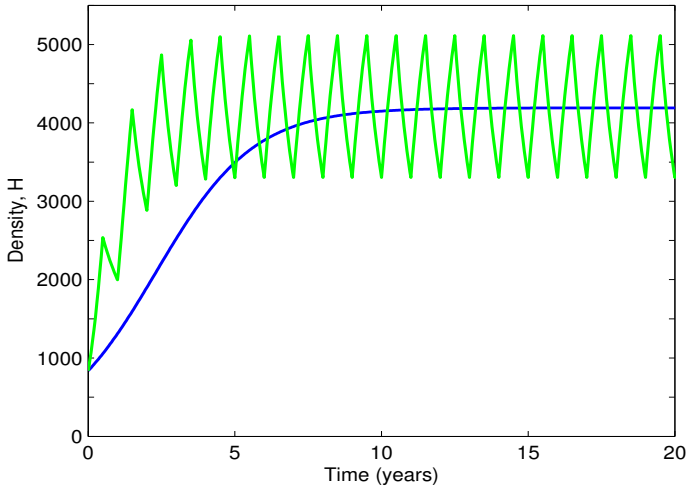

Figure 5.2: The host density against time is shown for Equation (5.1) in blue and Equation (5.2) in green. Parameter values used are $a = 1.5, a_S = 3, b = 0.9, K = 4192$ and $q_S = 9.294 \times 10^{-5}$. (Note that we have a fixed carrying capacity that represents the abundance of red squirrels on the whole of the Isle of Arran for a high carrying capacity estimate (see Section 5.2.2).)

Figure 5.2 makes it clear that the change in model formation to include a distinct breeding season and density dependent death has greatly increased the rate at which population recovery can occur. Peak populations reach carrying capacity levels in approximately 3 years in the seasonal model, compared to 10 years in the non-seasonal model. This compares well with observations in Parrott et al. (2009). The population

also shows a trend of peaking with densities greater than the carrying capacity at the end of the breeding season and then declining rapidly, which is also expected in natural populations (Bosch and Lurz, 2012). The modified model, Equation (5.2), therefore captures the fundamental trends observed in the red squirrel system.

Similar to Chapter 4 we develop a spatial, individual-based, stochastic version of the deterministic model represented by Equation (5.2) that allows us to describe the population dynamics on a complex heterogeneous habitat such as Arran and Mull. In Section 5.2.2 and 5.2.3 we divide the landscape into a 1km $\times$ 1km grid where each cell contains a proportion of the total carrying capacity (this is discussed in full later). To complete the model system we therefore need to include movement between neighbouring cells.

Long range dispersals, where an individual leaves the focal cell (i, j) and enters a neighbouring cell (i^*, j^*), are included by assuming saturation dispersal such that individuals are more likely to disperse as cell density increases (which is appropriate for dispersal in mammals (Poethke and Hovestadt, 2002)). The rate at which an individual leaves its focal cell is calculated independently of the available neighbouring cells, using the exponential function

$$D_{i,j} = d \exp\left(\frac{-(K_{i,j} - H_{i,j})}{0.5K_{i,j}}\right) \tag{5.3}$$

where d is the dispersal coefficient when the cell population is at its carrying capacity. There is no available data on the frequency of long range dispersals and so we make an assumption here that a squirrel will make approximately one long range dispersal in its lifetime, thus giving $d = b$ when the density is at carrying capacity. We plot Equation (5.3) against the relative cell density in Figure 5.3. Once an individual disperses from the focal cell it enters one of the eight neighbouring cells at random dependent on their cell density and location to the focal cell (with appropriate scaling between adjacent and corner cells, see Appendix B for more information).

We use the same methods described in Section 4.3.2 to simulate the events over time. The probabilities are given in Table 5.1 for the first and second half of the year separately (since births only occur in the first half of the year only). Repeating this process the spatial, individual-based, stochastic model enables tracking of the grid cell level abundance over spatial and temporal dimensions.

5.2.2 Resource seasonality of Arran

In Chapter 4 the disease framework used the red squirrel carrying capacity as a proxy for resource availability; areas of high quality resource are able to sustain more squirrels (high carrying capacity), conversely low quality areas have low carrying capacities. Forest habitats are in constant flux with factors such as species (resource quality and

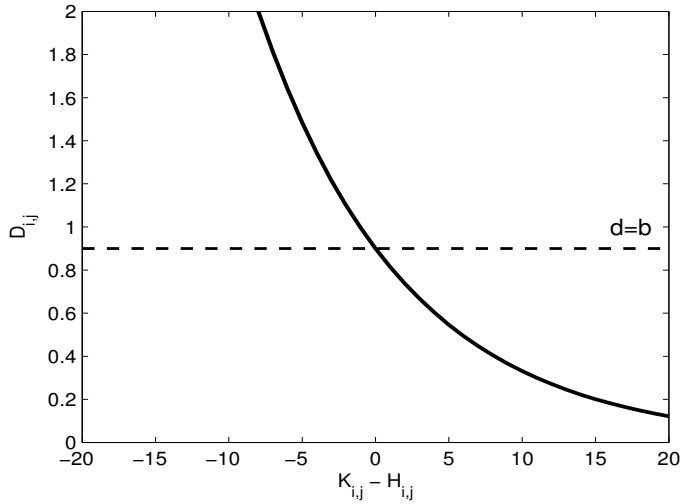

Figure 5.3: Individuals disperse from cell (i, j) at rate $D_{i,j}$ given in Equation (5.3). The dispersal rate is shown here against the relative density $K_{i,j} - H_{i,j}$ with $d = b$: individuals equally as likely to disperse or die when the cell is at carrying capacity.

Description	Outcome	Probability $0 \leq t \leq 0.5$	Probability $0.5 < t \leq 1$
Birth	$\Pr(H_{i,j} \to H_{i,j} + 1)$	: $[a_S (1 - q_S H) H]/R$	0
Natural death	$\Pr(H_{i,j} \to H_{i,j} - 1)$	: $[b\frac{H}{K}H]/R$	$[b\frac{H}{K}H]/R$
Dispersal	$\Pr(H_{i,j} \to H_{i,j} - 1)$ and		
	$\Pr(H_{i^*,j^*} \to H_{i^*,j^*} + 1)$	: $[DH]/R$	$[DH]/R$

Table 5.1: A list of all possible events in the spatial, individual-based, stochastic model described in Section 5.2.1. The outcome of each event in cell (i, j) is given in column 2 with the associated probability in column 3 and column 4 (for the breeding season and non-breeding season respectively), where the rate (within square brackets) is divided by the total sum of the rates $R = \Sigma\,[rates]$ across all the cells. The dispersal rate of an individual is given by $D = D_{i,j}$ which is defined in Equation (5.3).

quantity differs between species), age (trees must be mature before they produce seeds, with time to reach maturity varying between species), within year cycles (resource availability fluctuates during each year), mast seed crop cycles (in mast years a high quantity of resource is available), and pollution (Ashmore, 2005) attributing to their dynamics. Moreover it is believed that red squirrels may be able to anticipate the seed crop ahead of its production and alter their litter accordingly (White, 2007). Obtaining a precise framework for seed crop dynamics is clearly difficult due to the number of contributing factors; moreover if all the detail were included in a model framework the system may be difficult to interpret. We therefore include only the dominant seasonal forces attributing to changes in resource availability.

We first consider that the main food resource available to red squirrels is provided

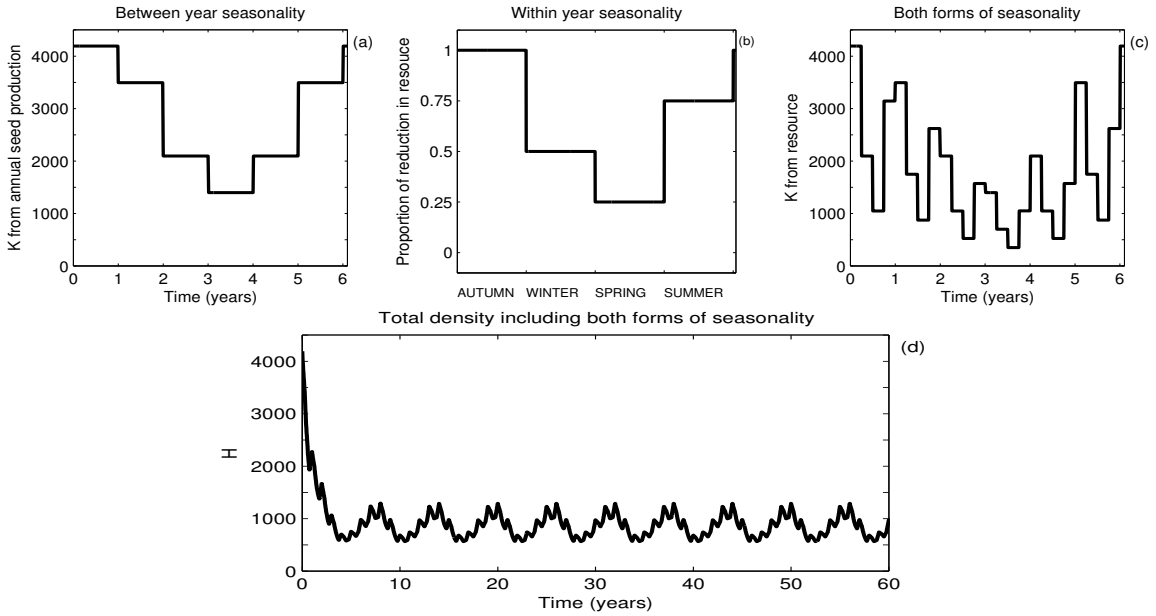

Figure 5.4: Red squirrel carrying capacity is directly correlated to resource production. Two seasonal effects impacting resource availability are highlighted in (a) the carrying capacity signal, K, of a seed crop cycle with a mast seed year every 6 years (cycle period and amplitude will vary between species) and (b) showing the within year resource availability. We combine both factors to produce the dynamic carrying capacity for red squirrels shown in (c). Using the carrying capacity from (c) we solve Equation (5.2) and show the host density over time in (d). Other parameter values used are $a_S = 3, b = 0.9, d = 0.9, q_S = (a_S - b)/(1.796 a_S K)$.

by the seed production from trees once a year. The magnitude of this seed crop fluctuates between years dependent on the tree species; for example Sitka spruce has a mast crop (high seed year) every 6 years with a 10 fold difference between high and poor seed years, whereas broadleaf trees exhibit only a 2 fold change in seed production between high and poor seed years and have a shorter 4 year crop cycle. Figure 5.4 (a) shows an example of a typical 6 year cycle, where the seed crop is updated annually, and the impact this has on red squirrel carrying capacity. However since the trees only produce seeds once a year in autumn there are also within year fluctuations in the resource availability: the seed crops are at a maximum in autumn (also coinciding with the end of the squirrel birthing season); while over winter the crop declines and is at a minimum in spring; by early summer squirrels feed on bulk foods such as buds and tree flowers, as well as invertebrates, and even occasionally bird eggs and chicks and in late summer fruits and berries, as well as green cones become available from trees (Bosch and Lurz, 2012; Moller, 1983) resulting in an increase in the resource (see Figure 5.4 (b)). We can combine both these seasonal effects by scaling the fixed seed crop in Figure 5.4 (a) by the within year availability shown in Figure 5.4 (b) which produces the carrying capacity shown Figure 5.4 (c). The impact of seasonal variation on squirrel density is found by solving Equation

(5.2) when including the carrying capacity signal from both forms of seasonality. The resulting plot of host density over time shown in Figure 5.4 (d). It is clear that year to year seed crop production is a dominant driver in the host density and we therefore neglect the within year cycle from our model for simplicity. Moreover data on mast seed crop cycles is more readily available than information on the within year dynamics of seed crops.

We now analyse the woodland composition of our case study island 'Arran' (and the Isle of 'Mull' in Section 5.2.3) using similar methods to Chapter 4. The forest estate map 2012 available from Forestry Commission Scotland (FCS) provides tree species level information for FCS controlled land. For other regions the forest inventory map (for 2012) (from FCS) provides information on combined woodland types which are classed as coniferous, broadleaf or shrub (i.e. no specific tree species). Extracting the data from both maps using GRASS Geographical Information System (GIS) (Westervelt et al., 1992) (using similar methods to Chapter 4, Rushton et al. (2000) and Lurz et al. (2003)) produces a list of the woodland species on Arran shown in Figure 5.5 (a) and also gives their total coverage. Combining this with published density ranges of red squirrels from Lurz (2012), we can estimate the maximum and minimum carrying capacities in different tree species on Arran (see Table 5.2). For each tree species the temporal oscillation in resource availability as a result of the seed crop cycle is represented by the following sinusoidal function

$$K(t) = \frac{1}{2}\left(K_{max} - K_{min}\right)\left(\sin\left(\frac{2\pi}{P}t + \frac{\pi}{2}\right)\right) + \frac{1}{2}\left(K_{max} + K_{min}\right) \tag{5.4}$$

where K_{max} and K_{min}, the maximum and minimum carrying capacity respectively, and the periodicity P are given in Table 5.2 for each species (Lurz et al., 1995; Wauters et al., 2008). Equation (5.4) creates a temporal carrying capacity for each tree species which is shown in Figure 5.5 (b); summing over the individual species creates the total carrying capacity in Figure 5.5 (c). A complete cycle of the total carrying capacity has a period of 24 years. Note that due to the low amplitude of Norway Spruce the 12 yearly cycle is almost equivalent. However there is no common poor seed year due to starting the phase of the cycles at a maximum. As discussed earlier we neglect within year fluctuations in the resource, therefore the carrying capacity is updated at the beginning of each year producing the step function shown in Figure 5.5 (d) describing the temporal changes to the total red squirrel carrying capacity on Arran. By determining the proportion of each species that is contained in each 1km by 1km grid square used in the stochastic model (Table 5.1) we can determine how carrying capacity changes at the grid square level. In Figure 5.6 we plot the spatial and temporal variation in the carrying capacity over 4 consecutive years (the variation in carry capacity has a period of 24 years see Figure 5.5 (c)). This figure also shows histograms of the number of grid patches at certain densities and the number

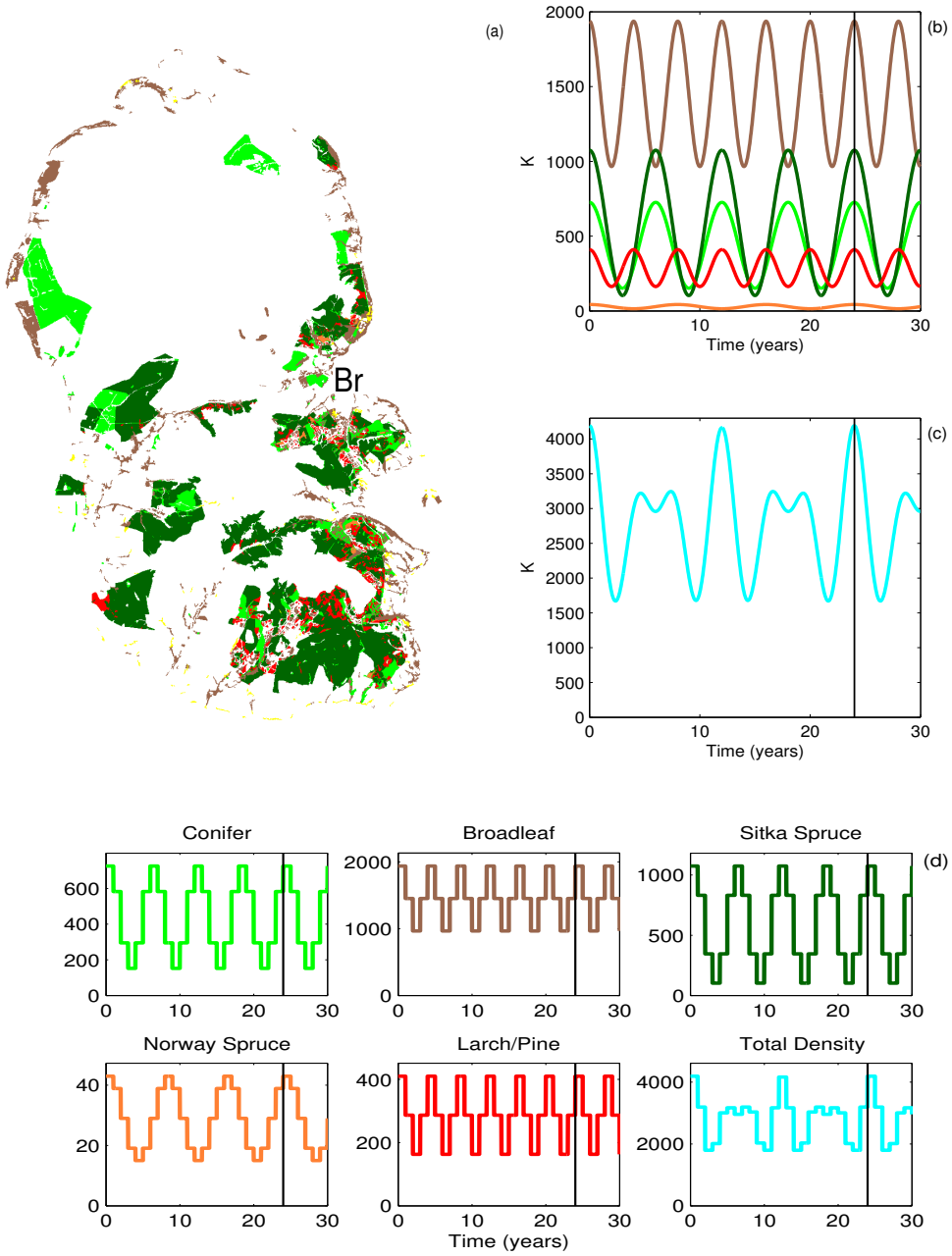

Figure 5.5: A map of the Isle of Arran is shown in (a) with the species data obtained from the databases of the Forestry Commission Scotland(see main text for further explanation). The tree species shown are coniferous (light green), broadleaf (brown), Sitka spruce (dark green), Norway spruce (orange), Larch and/or Pine (red) and shrub (yellow) and are kept consistent throughout the figure. 'Br' indicates Brodick which is the main port on Arran. Using Equation (5.4) and data in Table 5.2 a temporal carrying capacity is produced for (b) each species and (c) the total seed crop. Since we exclude within year resource seasonality, we fix the carrying capacity at the beginning of the year and annually update resulting in the step functions shown in (d). The black vertical line at $t = 24$ years indicates when all species experience a mast seed crop. (We neglect the shrub (yellow in (a)) from our species list as there is not enough of it to support squirrels on Arran.)

Species	Period	K_{min}	K_{max}
Conifer	6	152	726
Broadleaf	4	965	1937
Sitka Spruce	6	103	1075
Norway Spruce	8	15	43
Larch/Pine	4	163	410
Total		1398	4192

Table 5.2: Figure 5.5 (a) shows the tree species identified on Arran. Using GIS and the density ranges in different tree species from Lurz (2012), we produce the minimum and maximum carrying capacities for each species. Density ranges (min - max) are for Conifer $(0.08 - 0.36)$ per ha, Broadleaf $(0.5 - 1)$ per ha, Sitka Spruce $(0.02 - 0.2)$ per ha, Norway Spruce $(0.25 - 0.58)$ per ha and Larch/Pine $(0.22 - 0.55)$ per ha. Note that the minimum total carrying capacity is never achieved since a concurrent minimum seed year never occurs for all species.

of empty patches. The year by year variation in carrying capacity on Arran is used as an input in the spatial, individual-based, stochastic framework described in Section 5.2.1.

5.2.3 Resource seasonality of Mull

We use the same methods as described above for Arran to determine the spatial and temporal variation in red squirrel carrying capacity on the Isle of Mull (Table 5.3; Figure 5.7 and 5.8). Red squirrels are currently absent from Mull so this study offers insight into the outcome of any potential introduction of red squirrels to Mull. Whereas the woodland habitat on Arran is fairly mixed and forms a contiguous habitat (Figure 5.6) the woodland habitat on Mull forms several non-contiguous regions, some of which consist of a single tree species. Therefore Mull provides a contrasting landscape to Arran. Moreover due to the increasing pressure of the squirrelpox virus in the red population on mainland UK it would be advantageous to add to the list of strongholds and Shuttleworth (2005) proposes the Isle of Mull that may make a potential candidate.

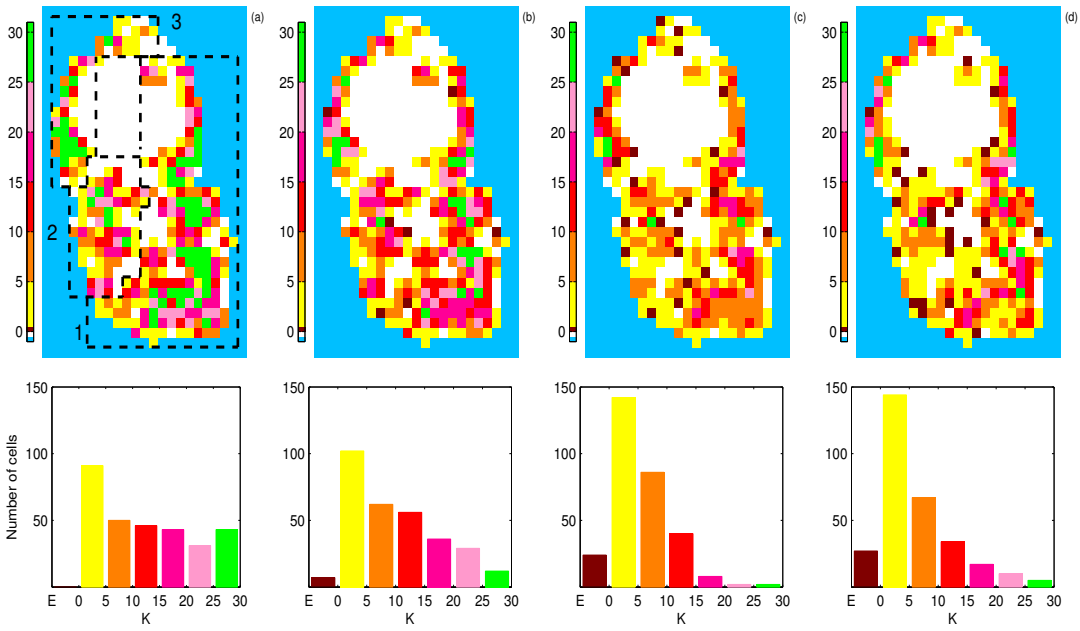

Figure 5.6: Table 5.2 shows the maximum and minimum carrying capacity for Arran. The resource, and carrying capacity, signal has a period of 24 years. We highlight the spatial distribution of the carrying capacity using maps of Arran for the first 4 years of the signal in (a)-(d). K_t denotes the carrying capacity at year t where (a) $t = 0$ (the maximum seed year, equivalent to K_{max} in Table 5.2), (b) $t = 1$, (c) $t = 2$ and (d) $t = 3$. Beneath each map a histogram shows the number of cells within the carrying capacity range shown along the x-axis. The colour on the histogram and maps are the same. For example, on the map, a yellow cell shows a carrying capacity between $0 - 5$, and on the histogram, the yellow bar shows the total number of cells on Arran with a carrying capacity between $0 - 5$. 'E' marks the number of cells that become extinct due to the resource signal (marked with the colour black).

Species	Period	Minimum K	Maximum K
Conifer	6	413	1946
Broadleaf	4	1250	2551
Sitka Spruce	6	66	726
Norway Spruce	8	7	18
Larch/Pine	4	371	483
Total		2109	5726

Table 5.3: Figure 5.7 (a) shows the tree species identified on Mull. Using GIS and the density ranges in different tree species from Lurz (2012), we produce the minimum and maximum carrying capacities for each species. Note that the minimum total carrying capacity is never achieved since all tree species never experience concurrent minimum seed year.

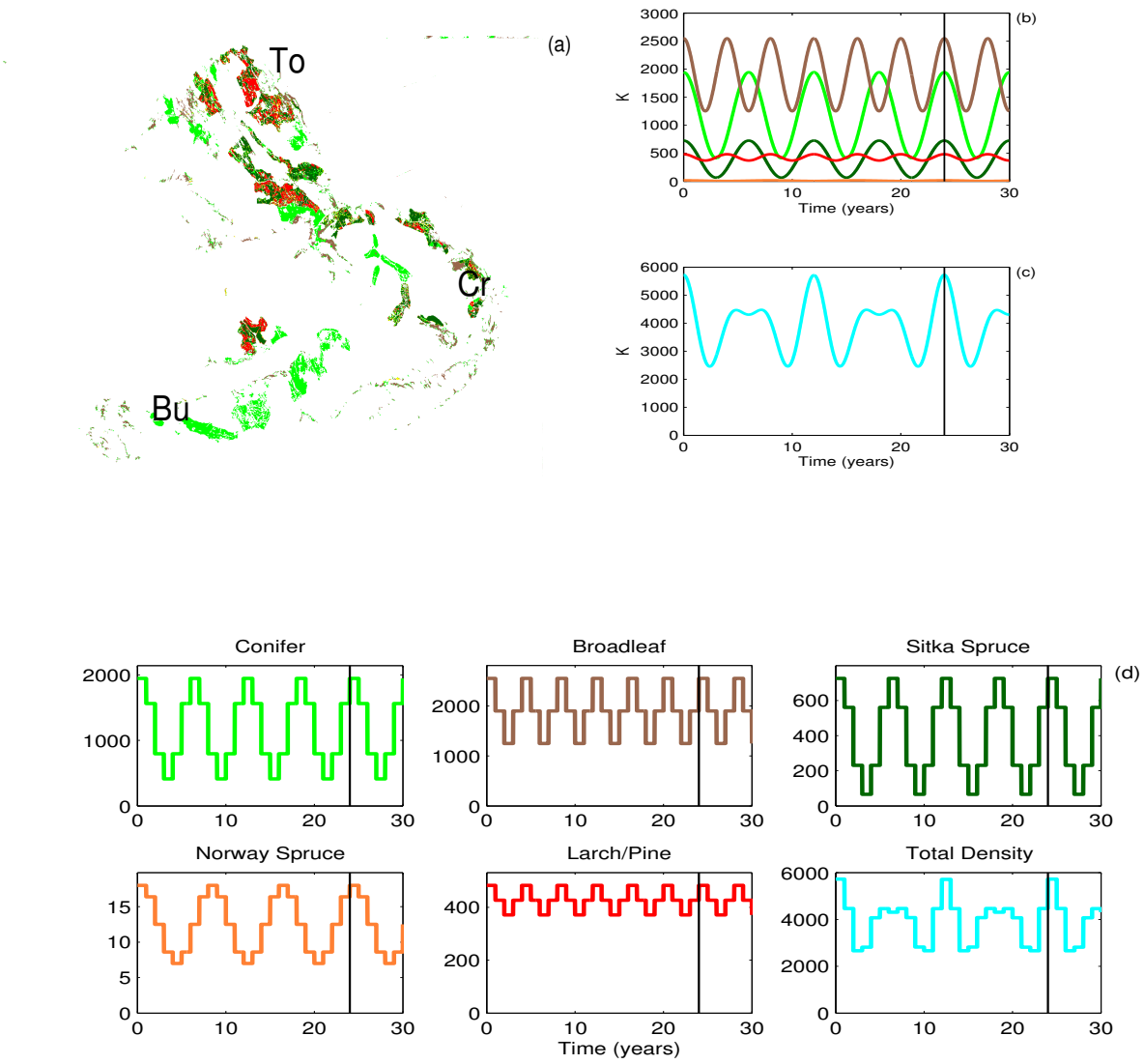

Figure 5.7: A map of the Isle of Mull is shown in (a) with the species data obtained from the databases of the Forestry Commission Scotland (see main text for further explanation). The tree species shown are coniferous (light green), broadleaf (brown), Sitka spruce (dark green), Norway spruce (orange), Larch and/or Pine (red) and shrub (yellow) and are kept consistent throughout the figure. We use the first two letters of a town for reference where 'To' is Tobermory, 'Cr' is Craignure and 'Bu' is Bunessan. Using Equation (5.4) and data in Table 5.3 a temporal carrying capacity is produced for (b) each species and (c) the total crop. Since we exclude within year resource seasonality we fix the carrying capacity at the beginning of the year and annually update, resulting in the step functions shown in (d). The black vertical line at $t = 24$ years indicates when all species experience a mast seed crop. We neglect the shrub (yellow in (a)) from our species list as there is not enough of it to support squirrels on Mull.

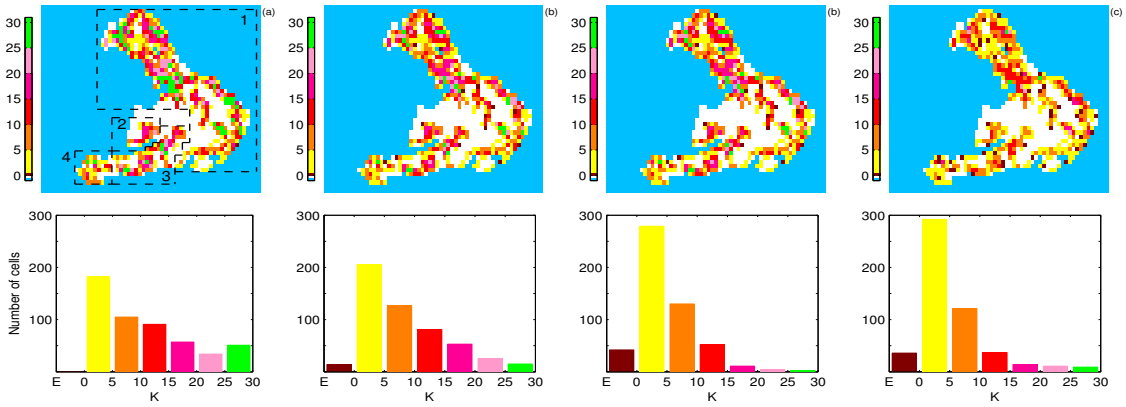

Figure 5.8: Table 5.3 shows the maximum and minimum carrying capacity for Mull. The resource, and carrying capacity, signal has a period of 24 years. We highlight the spatial distribution of the carrying capacity using maps of Mull for the first 4 years of the signal in (a)-(d). K_t denotes the carrying capacity at year t where (a) $t = 0$ (the maximum seed year, equivalent to K_{max} in Table 5.2), (b) $t = 1$, (c) $t = 2$ and (d) $t = 3$. Beneath each map a histogram shows the number of cells within the carrying capacity range shown along the x-axis. The colour on the histogram and maps are the same. For example, on the map, a yellow cell shows a carrying capacity between $0 - 5$, and on the histogram, the yellow bar shows the total number of cells on Arran with a carrying capacity between $0 - 5$. 'E' marks the number of cells that become extinct due to the resource signal (marked with the colour black).

5.3 Results

In this section we examine how either single point or multiple point introductions affect the colonisation dynamics for red squirrels on the Islands of Arran and Mull. We show how it is important to understand the habitat connectivity patterns for colonisation to be effective. In particular the woodland on Arran (Figure 5.5 and 5.6) is primarily mixed and forms a contiguous habitat around the outside of the island allowing potential island-wide re-population from only a single-point introduction. However Mull (Figure 5.7 and 5.8) consists of four separate woodland areas (each with different species composition) meaning a multiple-point introduction would have to be implemented for island-wide colonisation. Our two landscapes therefore allow us to compare single-point and multiple-point introductions on different complex landscapes.

We first analyse the impact of including host seasonality and multi-year seasonality in resources by comparing predictions of a single-point introduction on Arran using the three frameworks. In Section 5.3.2 we use a multiple-point introduction and compare the results to those attained from a single point introduction. Finally in Section 5.3.3 we examine both island wide and local introductions to the non-contiguous habitat on Mull. For both Arran and Mull we also compare how local tree species mixture impacts on population variability. This has an important implication for forest design in terms of its capacity to maintain populations of red squirrels.

5.3.1 Single point introduction on Arran

Since woodland on Arran is contiguous we explore colonisation techniques with the aim of achieving island-wide re-population. We first consider introducing red squirrels at a single point and use the carrying capacity maps established from the GIS data to find a high quality, well-connected cell in region 1 (Figure 5.6 (a)) where we introduce 12 squirrels. To examine the impact seasonality has on re-populating a complex spatial habitat such as Arran we compare three frameworks: a spatial, individual-based, stochastic version of the non-seasonal model, Equation (5.1), with a fixed resource as our baseline scenario (as used in Chapter 4 but without the disease component); and a spatial, individual-based, stochastic version of Equation (5.2) that includes host seasonality but with a fixed resource and lastly with host seasonality and a dynamic resource (defined in Section 5.2.2). (In the first two scenarios the carrying capacity is fixed at that of the maximum seed year, K_0, identified in Figure 5.6 (a).) The resulting simulations are shown in Figure 5.9 where each framework achieves island-wide re-population via a consistent dispersal route (around the outside of the island). There is a noticeable difference in the predicted colonisation times (note that we define the colonisation/re-population time as the time taken for all habitable cells to become

populated and the times are therefore taken from the spatial maps).

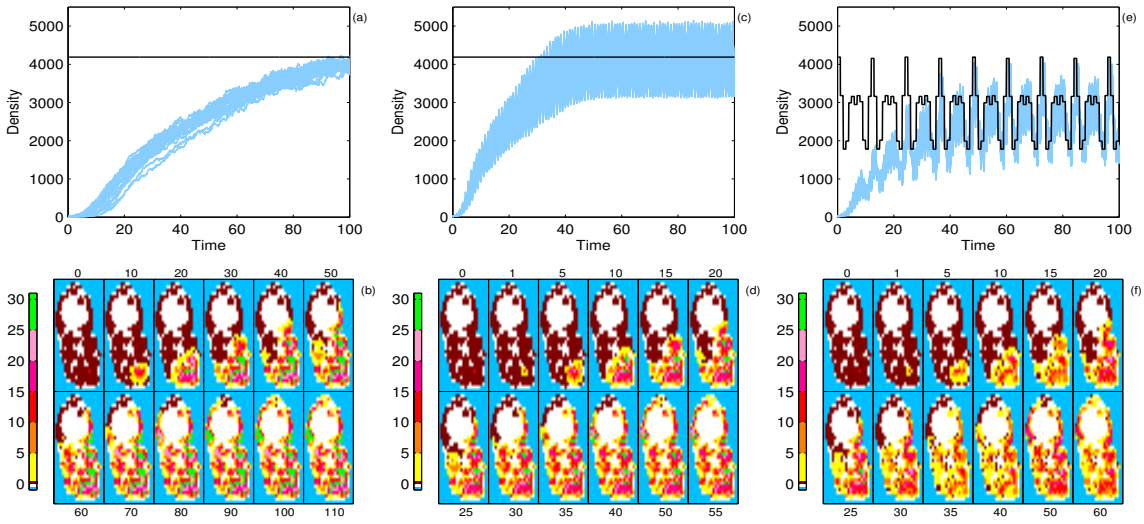

Figure 5.9: We introduce 12 squirrels to a cell in region 1 on Arran (Figure 5.6 (a)) and use the three model frameworks described in the text (a)-(b) Equation (5.1) with fixed the carrying capacity (K_0 in Figure 5.6 (a)), (c)-(d) Equation (5.2) with fixed the carrying capacity (K_0 in Figure 5.6 (a)) and (e)-(f) Equation (5.2) with a seasonal carrying capacity described in Section 5.2.2. (a), (c) and (e) show the total host population density (blue) against time for 25 model realisations with the carrying capacity highlighted in black. (b), (d) and (f) shows the host density on Arran at different number of years post introduction at different time frames. Parameter values are $a = 1.5, a_S = 3, b = 0.9, d = 0.9, q = 9.542 \times 10^{-5}$ and $q_S = 9.294 \times 10^{-5}$.

Figure 5.9 (a)-(b) show squirrels take 110 years to re-populate island-wide when the dynamics are described by a spatial, individual-based, stochastic version of Equation (5.1) in absence of seasonality. Once island-wide re-colonisation has been achieved, Figure 5.10 (a) reveals the host density tends to a quasi-steady state below the estimated carrying capacity. Henein and Merriam (1990) proposes poor connectivity can reduce the population density of these cells (since low quality, poorly connected patches may often become extinct) which may explain why the non-homogeneous habitat of Arran remains below the estimated carrying capacity (the histogram in Figure 5.6 (a) shows a high proportion of cells with low carrying capacity). Moreover hosts spread more slowly through poor quality patches which explains why colonisation of the North-West of Arran takes a relatively long time (Figure 5.6(a)).

Figure 5.9 (c)-(d) shows including host seasonality in our framework (a spatial, individual-based, stochastic version of Equation (5.2)) reduces the colonisation time to 55 years. This is due to host seasonality acting to increase patch density above the

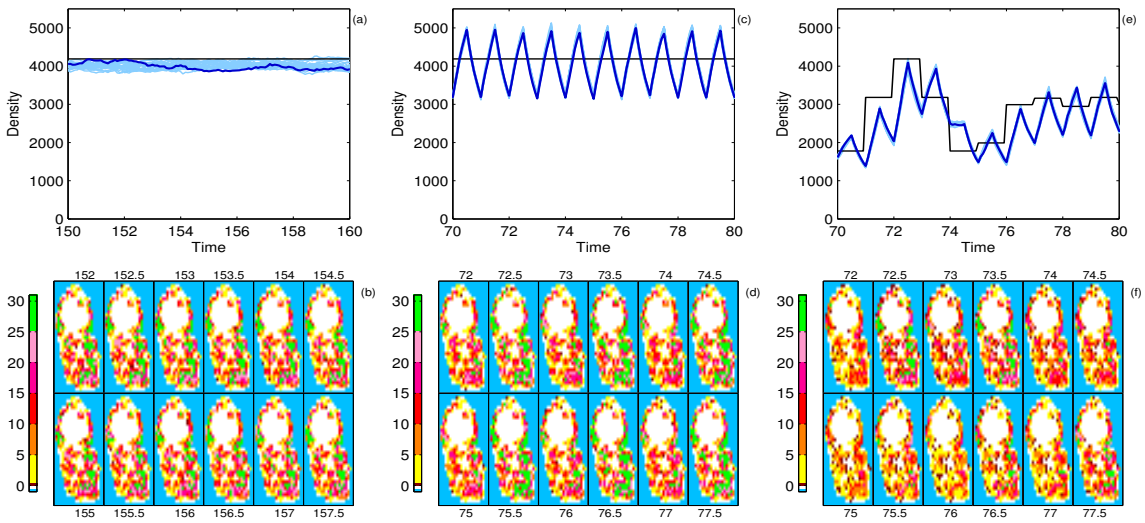

Figure 5.10: The total host population density is shown in blue over a period of 10 years for 25 model realisations in (a), (c) and (e) with the carrying capacity highlighted in black and one simulation highlighted in dark blue. (b), (d) and (f) show snap shots of the spatial distribution of the host density from the simulation highlighted in (a), (c) and (e) respectively at different time frames. Figure layout and parameters are consistent with Figure 5.9.

carrying capacity in the breeding season and thereby increases the rate of dispersal (see Figure 5.11). This is a feature of the natural squirrel system (Bosch and Lurz, 2012). Once the red squirrels have colonised Arran the squirrel density shows annual oscillations (Figure 5.10 (c)) where the density reaches a maximum after the birthing season. This oscillation can be seen at the spatial level (Figure 5.10 (d)) with cell density fluctuating between high and low levels due to host seasonality.

Finally the inclusion of host and resource seasonality in Figure 5.9 (e)-(f) shows island-wide re-colonisation within 60 years. Here, resource seasonality has the effect of lowering total and patch level density (compared to Figure 5.9 (c)-(d) where the carrying capacity is fixed at the maximum seed year) which reduces the dispersal rate. The population dynamics show an annual signal due to host seasonality and this signal tracks the varying carrying capacity resulting from resource seasonality (Figure 5.10 (e)-(f)). Both the annual and multi-year signal are clearly seen in the spatial dynamics, with densities peaking in year 72, which corresponds to the maximum carrying capacity and reach a minimum in year 76. The inclusion of a seasonal resource means that the host population only occasionally increases beyond the carrying capacity (compare Figure 5.10 (c) and (e)).

The impact of a seasonal resource can be understood by examining the number of birth, death and dispersal events that occur over time (Figure 5.11). Births only occur in the breeding season, show a high amplitude signal and also show an increase in years when the carrying capacity is high. In comparison, deaths oscillate with a

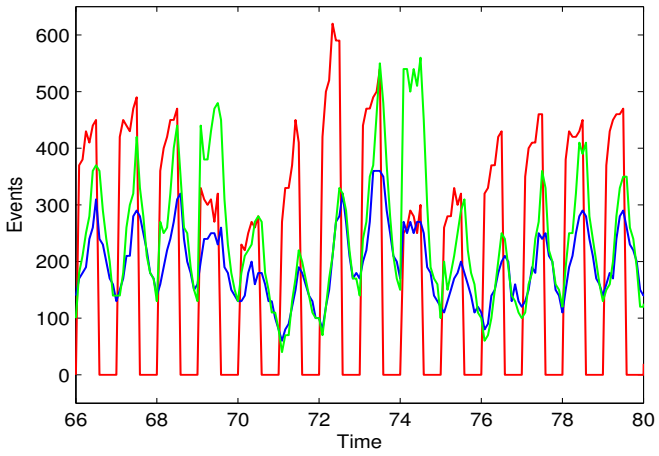

Figure 5.11: The number of birth (red), death (blue) and dispersal (green) events that occur in the realisation highlighted in Figure 5.10 (e) are plotted against time.

lower amplitude signal with a tendency to be low in years when resource availability is higher than the previous year (so that the population starts the year below carrying capacity) and higher when resource availability has decreased. High rates of dispersal occur when the host density exceeds the carrying capacity. There are two distinct mechanisms that drive dispersal. The first is the concentrated period of births that can push the density above carrying capacity and so increases dispersal due to local resource limitation. Second the variation in resources can cause a sudden decrease in the resource availability meaning the population density is in excess of the carrying capacity and a large number of individuals must disperse and/or die, for example in year 74 in Figure 5.11. This (broad) behaviour is also observed in the red squirrel system (Bosch and Lurz, 2012) and gives confidence that the extension to the model to include host and resource seasonality are able to capture the key population behaviour observed in nature.

In Figure 5.9 we show that including a more realistic representation of host life-history can reduce the time predicted for achieving island-wide colonisation compared to that for constant births throughout the year. We also represent multi-year seasonal oscillations in resource availability and show that once the host density reaches 'pseudo' equilibrium we observe density fluctuations similar to those seen in the field (Bosch and Lurz, 2012). Island wide colonisation on Arran is possible from a single point of introduction, however if a dynamical resource can alter the habitat connectivity as we suggest then it may be of advantage to introduce in multiple areas to speed up the colonisation process.

5.3.2 Multiple point introduction on Arran

We have shown that island-wide re-colonisation on Arran can be achieved from a single point, however Figure 5.9 highlights areas of poor connectivity may contribute to the delay in squirrels reaching isolated areas. It may therefore be an advantage to introduce red squirrels at multiple points on Arran so that the impact of poor connectivity can be reduced. We investigate this by using the same three frameworks as before (a stochastic, spatial, individual-based version of Equation (5.1), Equation (5.2) with a fixed resource and Equation (5.2) with a dynamic resource) and introduce 4 squirrels in each of the three regions identified in Figure 5.6 (a).

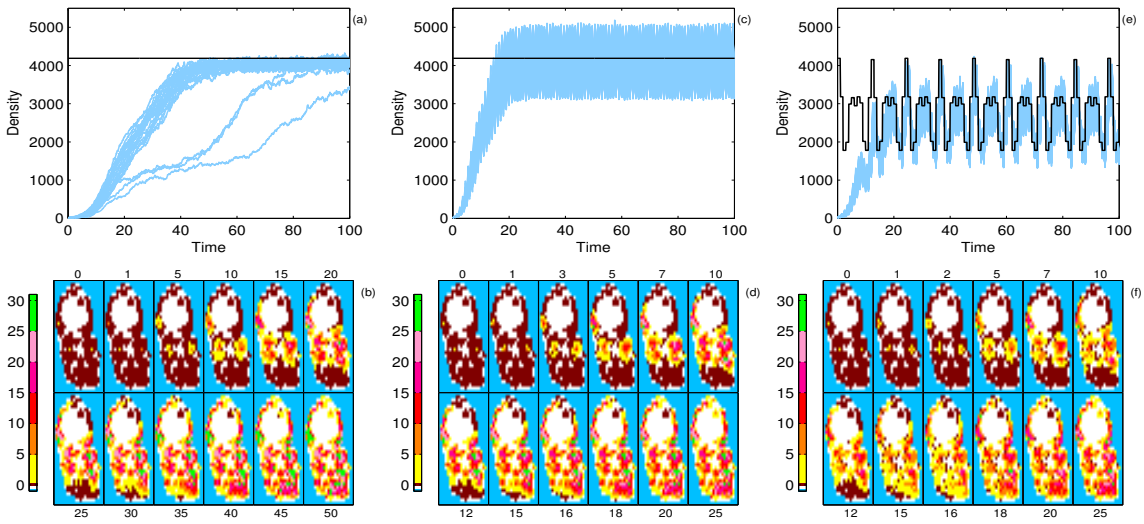

Figure 5.12: We introduce 4 squirrels to a cell in each region in Figure 5.6 (a), and use the three model frameworks described in the text (a)-(b) Equation (5.1) with fixed the carrying capacity, K_0, (c)-(d) Equation (5.2) with fixed the carrying capacity, K_0 and (e)-(f) Equation (5.2) with a seasonal carrying capacity described in Section 5.2.2. (a), (c) and (e) show the total host population density (blue) against time for 25 model realisations with the carrying capacity highlighted in black. (b), (d) and (f) shows the host density on Arran at different number of years post introduction. The layout and parameter values are consistent with Figure 5.9.

In Figure 5.12 we show that using multiple point introductions in the three regions on Arran reduces the time to colonise island-wide by over half in all frameworks. The model without any seasonality shows 22 simulations re-colonising the island in 50 years in Figure 5.12 (a)-(b); in 3 realisations the introduced squirrels in region 1 die-out thus showing a delay in re-populating the east coast from the west coast introductions. When we include host seasonality in Equation (5.2) both the fixed (Figure 5.12 (c)-

(d)) and dynamic resource (Figure 5.12 (e)-(f)) show a similar re-colonisation time scale: region 1 is re-colonised in 25 years with region 2 and 3 in 15 and 20 years respectively. In Section 5.3.1 we proposed that colonisation was delayed by areas of poor connectivity which were accentuated when we included a dynamic carrying capacity. This highlights two key results: first, when hoping to achieve large scale colonisation it is beneficial to use multiple point introductions as delays due to poor connectivity between regions can be bypassed; and second, assessing the landscape to identify areas of poor connectivity is essential to manage the introduction of a species. We argue that our model framework is a useful tool for determining how landscape connectivity would impact on the success and spread of an introduced species.

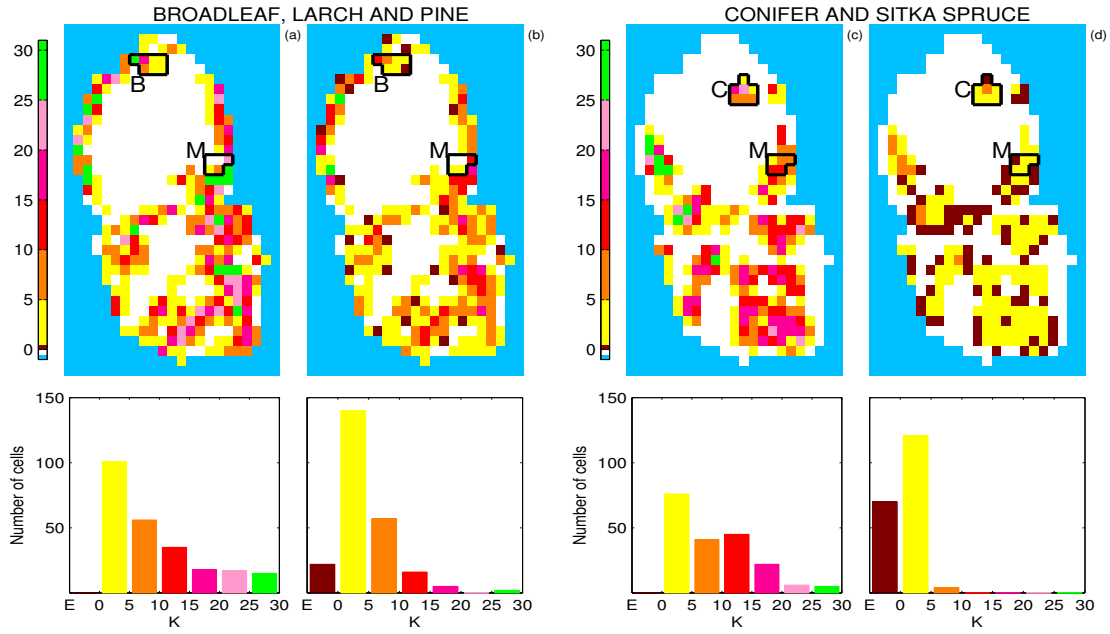

Figure 5.13: We split the tree species on Arran into two groups and display the carrying capacity maps for each group where (a)-(b) show the carrying capacity for cells containing broadleaf, larch and pine only and (c)-(d) show the carrying capacity for cells containing conifer and Sitka spruce only. We demonstrate the flux in the carrying capacity attributed to each species by showing the carrying capacity map for a high seed year K_0 in (a), (c) and a low seed year in (b) and (d). A histogram of the cell carrying capacities for each carrying capacity map, where 'E' now indicates the number of cells whose species carrying capacity has become extinct. We examine the three areas highlighted by boxes used in Figure 5.14 to show squirrel densities against time. 'B' indicates the cells are broadleaf only, 'C' is coniferous cells only, and 'M' mixed coniferous and broadleaf.

We have shown that a dynamic resource can contribute to the delay in reds dispersing across poorly connected areas. We now investigate the relationship between

red squirrel densities and tree species.

In Figure 5.6 we highlighted that despite the total population remaining at relatively high levels the total carrying capacity decreased by over half in two years and 8% of cells became uninhabitable due to the resource signal. Analysis of the underlying tree species on Arran shows that despite three quarters of the habitat being Sitka spruce or other coniferous species these only contribute 22% and 46% of the minimum and maximum carrying capacities respectively. The remainder of the carrying capacity is provided by broadleaf, larch and pine (Table 5.2)). Moreover, deciduous habitats in the UK tend to be mixed and are often protected for conservation purposes whereas conifers tend to be planted commercially (as monocultures or nursery-crop mixtures) with overall low species diversity, therefore deciduous woodlands tend to be more stable and dependable with respect to seed production for squirrels compared to conifer plantations (Wauters and Dhondt, 1992; Wauters et al., 1994). We therefore separate the species contribution of the total carrying capacity into two groups (the contribution from coniferous and Sitka spruce species and from broadleaf, larch and pine species) and show their maximum and minimum carrying capacity maps in Figure 5.13. From this it is clear that, independent of their seed year, broadleaf, larch and pine species persist in the majority of cells throughout Arran with only 9% of cells becoming extinct in a poor seed year. Sitka spruce and coniferous species are also found throughout Arran however they record a 5 fold difference in the carrying capacity and roughly a 30% of cells become extinct in a poor year. Such variation in the carrying capacity for regions dominated by a single species may explain the accentuated areas of poor connectivity and subsequent impact on colonisation. To highlight this effect, in Figure 5.14 we show density fluctuations for 'local' regions that consist of different mixtures of tree species types. For areas of either mixed or broadleaf woodland (Figures 5.14 (a) and (c) respectively) host density experience relatively low amplitude cycles whereas in a coniferous woodland large amplitude cycles that lead to low densities are observed (Figures 5.14 (b)). This suggests that plantations dominated with conifer may produce unstable habitat for red squirrels and in such regions the likelihood of local extinctions is increased. Therefore, increasing the diversity of tree species may help improve the resource for red squirrels and reduce the impact of seed crop fluctuations. Moreover we notice that the area connecting region 2 to region 1 and 3 are predominately composed of coniferous species (Figure 5.13). This explains why colonisation times increased when a dynamic resource was included in the model and emphasises the importance of analysing habitat distribution (i.e. landscape connectivity and forest area) as well habitat composition (such as tree species composition of woodlands) when planning the introduction of a species.

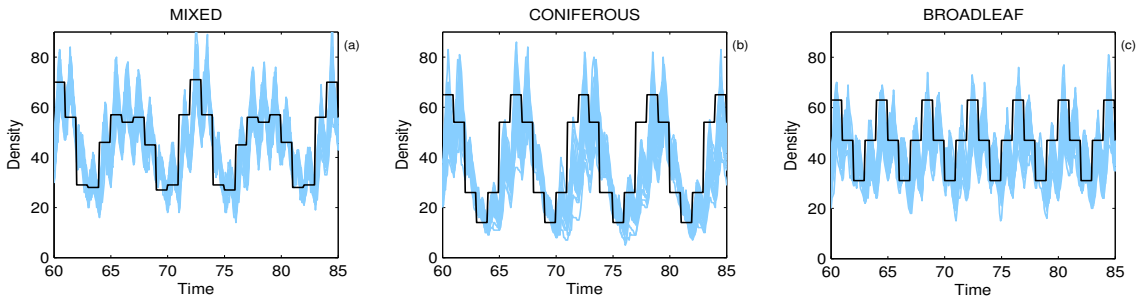

Figure 5.14: The red squirrel density (blue) is shown against time for 25 realisations once the density has reached equilibrium in Figure 5.12. We trace the density in the cells highlighted in Figure 5.13 where (a) is 'M', a mixture of tree species, (b) is 'C', coniferous species only and (c) is 'B', broadleaf only. The carrying capacity is shown for each region in black.

5.3.3 Multiple point introduction on Mull

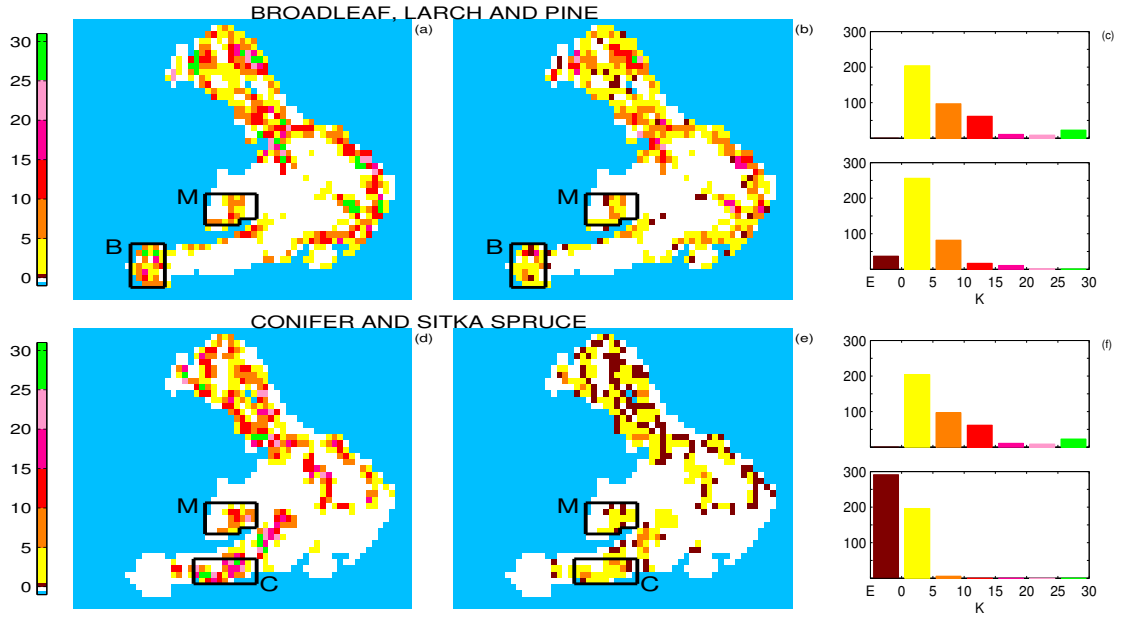

Figure 5.15: Maps of the tree species on Mull separated into two groups showing the carrying capacity for each where (a)-(b) show the cells containing broadleaf, larch and pine only and (d)-(e) show the cells containing conifer and Sitka spruce only. To demonstrate the range of the carrying capacity attributed to each species we show the carrying capacity map for a high seed year K_0 in (a), (d) and a low seed year in (b) and (e). We examine the three areas highlighted by black boxes where 'B' indicates the cells are broadleaf only, 'C' is coniferous cells only, and 'M' mixed coniferous and broadleaf. We show a histogram of the cell carrying capacities for a maximum (top) and minimum (bottom) seed year for each species in (c) and (f) , where 'E' indicates the number of cells where the carrying capacity has gone to zero for the respective species.

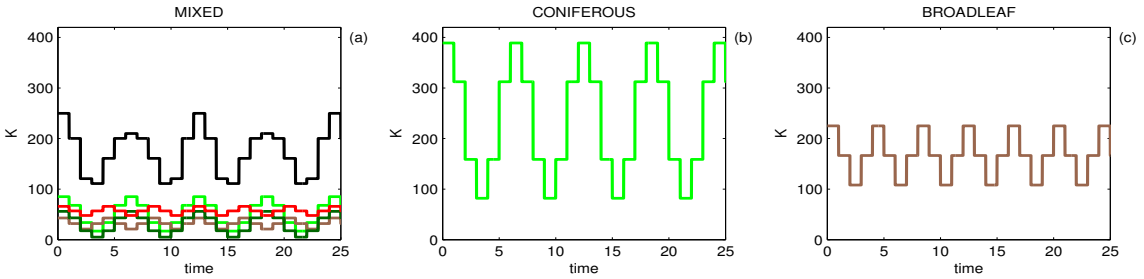

Figure 5.16: The carrying capacity for each block of cells highlighted in Figure 5.15 is shown against time where (a) shows a mixture of species 'M' in region 2, (b) is coniferous only cells 'C' in region 3, and (c) is broadleaf only cells 'B' in region 4. The colours correspond to the tree species where coniferous (light green), broadleaf (brown), Sitka spruce (dark green), Norway spruce (orange), Larch and/or Pine (red) and the total carrying capacity (black).

In this section we simulate red squirrel colonisation on the Isle of Mull (Figure 5.8) using the spatial, individual-based, stochastic framework of Equation (5.2) to describe the seasonal demographics of red squirrels and include a seasonal resource by means of a dynamic carrying capacity defined in Section 5.2.3. Pre-assessment of the habitat reveals that, unlike Arran, introduction at a single point would be insufficient to colonise Mull as the habitat forms four unconnected woodland regions. Mull therefore provides an ideal framework in which to compare the red squirrel introduction and population dynamics at both an island wide and local scale.

Previous sections have highlighted the importance of analysing the habitat distribution at a species level. Using GIS we identify the main tree species in each region on Mull (Figure 5.7) and show the carrying capacity for groups of broadleaf, larch and pine in Figure 5.15(a)-(c) and conifer and Sitka spruce in Figure 5.15(d)-(f). In Section 5.3.2 we saw that red squirrel population density follows the carrying capacity signal meaning that regions of broadleaf and mixed woodlands experience relatively stable population dynamics in comparison to the large amplitude oscillations in density in coniferous woodland. This is stressed in Figure 5.15(f) where roughly half the cells consisting of conifer and Sitka spruce become extinct in a poor seed year whilst Figure 5.15(c) shows cells containing broadleaf, larch and pine show a much smaller variation in seed year.

We now consider island wide colonisation in Figure 5.17 by introducing 6 squirrels at a single point in each of the four regions on Mull shown in Figure 5.8. Region 1 contains 86% of the island carrying capacity and takes 40 years to populate with the poorly connected areas in the south-east taking the longest for hosts to inhabit. Despite region 1 on Mull appearing more disconnected than the whole of Arran (although they share a similar maximum total carrying capacity), the colonisation time for region 1 on Mull is reduced by 20 years compared to the colonisation of Arran

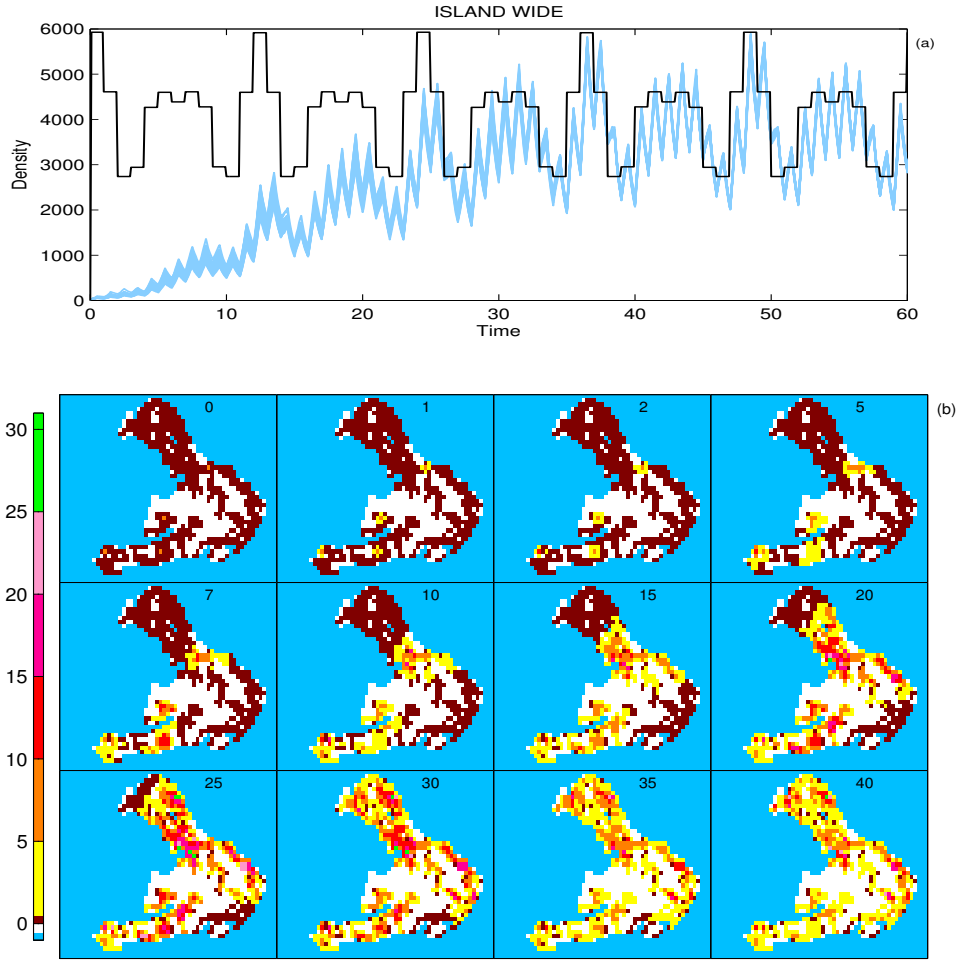

Figure 5.17: We introduce 6 squirrels in one cell in each of the four regions marked in Figure 5.8 and use the spatial, individual-based, stochastic framework of Equation (5.2) with a dynamic carrying capacity described in Section 5.2.3 to examine the island wide colonisation on Mull. (a) shows the total host population density (blue) against time for 25 model realisations and (b) shows snap shots of the average host density at different time frames on Mull. The parameter values are consistent with Figure 5.9.

(Figure 5.9). The tree species maps in Figure 5.15 indicate that region 1 on Mull is dominated by broadleaf, larch and pine which provides a more stable and good quality resource and therefore improves connectivity. Region 3 which represents only 6% of the total island carrying capacity takes 20 years to colonise with the colonisation speed hindered due to the habitat consisting primarily of poorly connected coniferous woodland (Figure 5.15). The remaining component of the total carrying capacity is split between region 2, a mixed woodland, and region 4, a broadleaf woodland, and colonisation in these regions occurs in half the time of region 3. This shows that island-wide colonisation is possible for Mull, however this requires species introduction to each of the four distinct regions.

Section 5.3.2 highlighted multiple points of introduction at a large scale can achieve

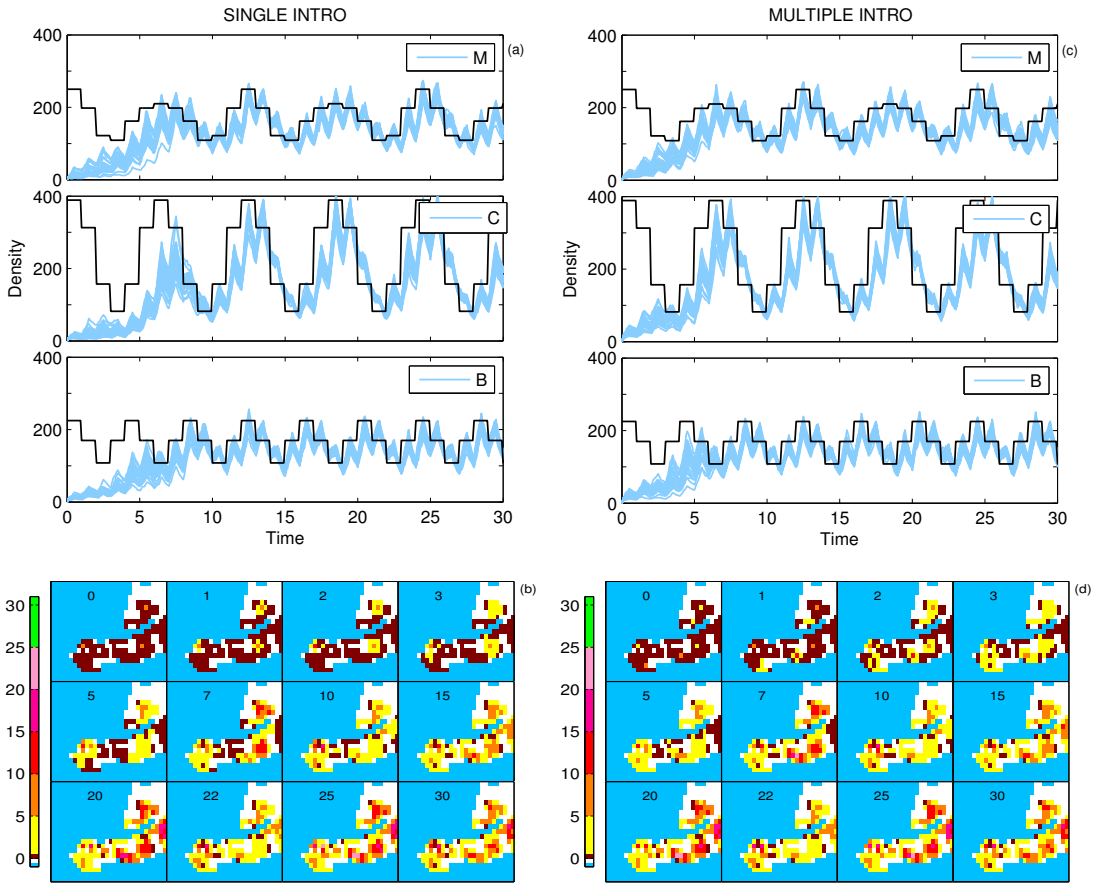

Figure 5.18: We introduce 6 squirrels in one cell (left-hand column) and 3 squirrels in two cells (right-hand column) to regions $2-4$ in Figure 5.8 and use the spatial, individual-based, stochastic framework of Equation (5.2) with a dynamic carrying capacity described in Section 5.2.3 to examine colonisation on Mull at a local scale. The host population density (blue) is plotted against time for 25 model realisations in (a) and (c) for each of the boxes highlighted in Figure 5.15 with 'M' a mixture of species (top), 'C' coniferous only species (middle) and 'B' broadleaf only species (bottom). The carrying capacity for each area is in black. (b)-(d) show snap shots of the average host density at different time frames in region $2-4$ on Mull. The parameter values are consistent with Figure 5.9.

island-wide colonisation more quickly than a single point of introduction. We examine this effect at a regional scale on Mull in equal sized areas, highlighted by boxes in Figure 5.15, for different tree species. The carrying capacities for each of these areas are shown at a species level in Figure 5.16 where box 'M' in region 2 consists of mixed species (conifer, Sitka spruce, broadleaf, larch and pine), box 'C' in region 3 is coniferous, and box 'B' in region 4 is broadleaf.

For a multiple point introduction we introduce 3 squirrels to two cells in each region and compare this with results for a single point introduction (6 squirrels to one cell in each region). Figure 5.18 shows that each region is colonised in 10 years for one point of introduction and 5 years for two points of introduction. Therefore, at the regional scale multiple introductions can reduce the colonisation time.

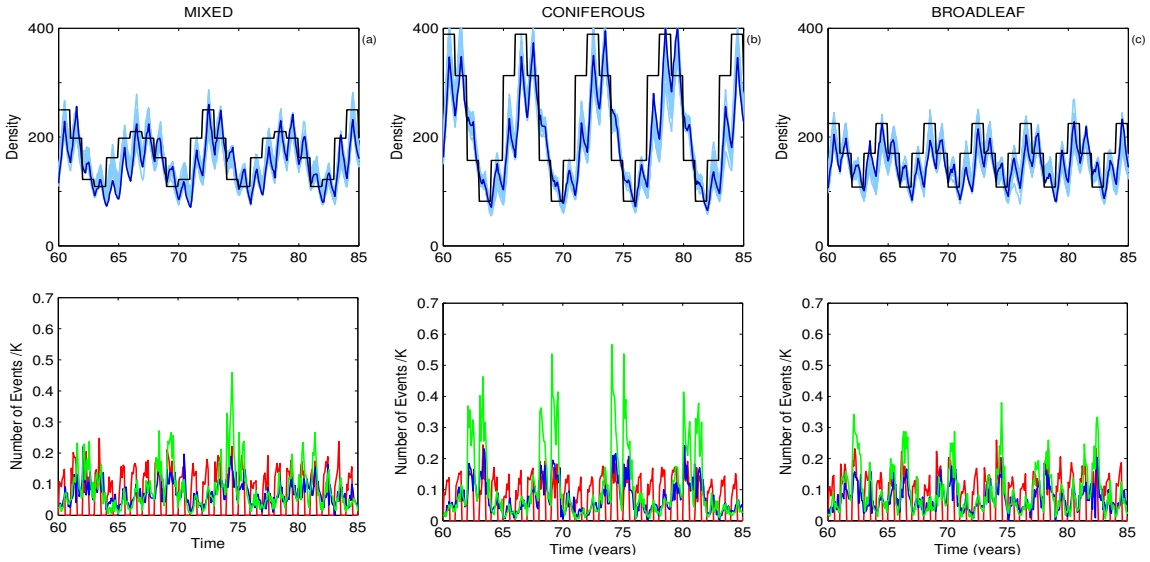

Figure 5.19: Once the host density has reached equilibrium in Figure 5.18 we trace the total density (in blue, top row) over 16 years and show the carrying capacity in black for each region (a) box 'M' in region 2, (b) box 'C' in region 3 and (c) box 'B' in region 4. A realisation is highlighted in the top row and the number of birth (red), death (blue) and dispersal (green) events are divided by the carrying capacity and shown below the corresponding plot.

Following colonisation we trace the density and the number of birth, death and dispersal events against time for each of the boxed areas in Figure 5.19. The density closely follows the pattern of the resource seasonality with the amplitude of the population oscillations greatest in the coniferous woodland. This further emphasises that mixed or broadleaf woodlands provide a more stable resource for red squirrels. By plotting the number of events over time (Figure 5.19) it is clear that high levels of dispersal and increases in the death rate are triggered by reductions in resource availability. This is most clearly observed in the coniferous habitat where reductions in carrying capacity are most pronounced. Both dispersal and mortality drop to low levels during the increasing phase of the resource cycle - again this is most pronounced for the coniferous region. Conservation practice aims to maintain relatively stable population levels. The regional assessment of population dynamics presented here indicates that in regions dominated by coniferous species population variability is high with repeated periods of high dispersal and mortality. Therefore, regions containing a mixture of species would present a better habitat for the long-term viability of this introduced species.

5.4 Discussion

Maintaining biodiversity has become a global challenge. Over the last two decades many conservation techniques have been developed to help conserve endangered taxa;

one of which is the re-introduction of a species (IUCN, 1987). The success rate of conservation translocations is increasing mainly due to appropriate pre-assessment, planning and monitoring in addition to the increase of research efforts from inter-disciplinary fields (Soorae, 2011). An emerging method which complements the construction of a re-introduction program is the combined use of geographical information systems (GIS) and computational models (Rodríguez et al., 2007; Seddon et al., 2007). In this study we used a custom-built spatial, individual-based, stochastic model to analyse the re-introduction and persistence of red squirrels on two real-life landscapes of Arran and Mull.

Our model included two forms of seasonality. The first considered the seasonal demographic processes of squirrels. In Chapter 4 we used a disease version of Equation (5.1) to analyse disease spread in red squirrels on the complex landscape of Arran. We noted that after disease fade-out it took longer than expected for the population to recover to their pre-infection densities; we proposed this was due to the simplification of squirrel demographics and updated our framework to include a seasonal birth and density dependent death terms (Equation (5.2)). The inclusion of more realistic representation of host life-history led to a more rapid increase in population numbers and simulations showed that the colonisation of Arran could be achieved in half the time compared to Equation (5.1) in Figure 5.9. The decrease in colonisation time is due to the pulse of births during the breeding season which accelerates growth and allows the population to increase above the carrying capacity leading to increased levels of dispersal.

We also included multi-year seasonality of resources to reflect the periodic nature of seed crops at a tree species level. Careful analysis of the habitat is critical when one introduces a species (Armstrong and Seddon, 2008; Rout et al., 2007; Sarrazin and Barbault, 1996; Seddon et al., 2007; IUCN, 1987), especially when the landscape is composed of fragmented woodlands and movement between habitat patches is restricted by the quality of connectivity (Gardner and Gustafson, 2004). Both Arran and Mull have complex landscapes; the habitat on Arran forms a contiguous route around the island and the tree species are predominately mixed, whereas Mull forms four unconnected woodland blocks some of which are predominantly consisting of a single tree species. We argue that identifying the habitat at a tree species level is beneficial since red squirrels persist at different abundances dependent on the tree species and seed year (broadleaf, larch and pine produce a relatively constant supply of seeds whereas species with irregular seed production patterns such as Norway and Sitka spruce experience large fluctuations). Whilst previous studies have assessed the importance of habitat connectivity on the success of species introductions very few have included the seasonal effects of resource availability in their predictive models. This could critically affect the success of re-introduction schemes for species where

resource levels fluctuate naturally. The results demonstrates that re-introduction projects should include a pre-assessment phase that considers the impact of changes in resource levels on the colonisation and long-term persistence of regional and local populations in complex landscapes. Moreover results of local colonisation simulations may have implications for the conservation of red squirrels in managed forest systems which are subject to large scale forestry. Commercial forestry operations fell and replant large areas of woodland which do not provide a resource for squirrels until the woodland has matured (which takes approximately 25 years). These areas would therefore act similar to small scale re-introductions.

The seasonal host and resource framework model decreased regional colonisation times on Arran when compared to the original framework in absence of seasonality. However comparing to the full seasonal model to the model which included seasonal host demographics in a fixed habitat the colonisation time was increased slightly (Figure 5.9). We propose the delay is due to the poor connectivity when the habitat quality is low; more specifically the area of low connectivity between region 1 and 2 is predominately coniferous so in a poor year the carrying capacity would be very low reducing the probability of dispersal (Figure 5.13). This highlights that seasonality can affect the quality of corridors between habitat patches and inhibit the movement of individuals.

In all scenarios tested in this chapter the colonisation speed was increased when multiple release sites were used. On Arran the colonisation time was halved when three release sites were used and similarly on Mull when two release sites per woodland region were used. An advantage of using multiple release sites is that areas of low connectivity can be bypassed (as seen on Arran in Figure 5.12). Pre-assessment of the habitat composition can be combined with modelling approaches to identify isolated regions of poor connectivity and provide vital information to determine optimum number and locations of release sites.

A species introduction is defined as a success if the release species becomes self-sustaining (Rout et al., 2007) we therefore evaluated the population persistence once colonisation was achieved, in different tree species. When we include both host and resource seasonality in the framework red squirrels exhibit density fluctuations similar to those experienced in the field (Figure 5.10). Within year variation in the host density fluctuates around the carrying capacity and this can be attributed to the seasonal breeding pattern. The within year variation is relatively small compared to the density fluctuations driven by multi-year variation in the resource and these fluctuations could affect the persistence of red squirrels. When assessing the local squirrel density in areas of mixed, coniferous and broadleaf species on Arran and Mull, we observed that squirrel population dynamics were dominated by the multi-year signal of the resource. Specifically the dynamics in coniferous woodlands show large

amplitude population cycles compared with reduced amplitude cycles in broadleaf and mixed species (Figure 5.14 and 5.19 for Arran and Mull respectively).

As discussed in Chapter 4 the distribution of the red squirrels in the UK is currently confined to red squirrel strongholds or to the Highlands of Scotland. Here the habitat is dominated by coniferous species. This has the advantage of deterring grey squirrels (which prefer broadleaf or mixed forest) but the disadvantage is that it exposes red squirrels to large amplitude population oscillations. Our results would suggest red squirrel persistence may be improved by increasing tree species diversity, by including broadleaf tree species where appropriate. In stronghold populations that neighbour grey squirrel population this would be problematic as it would increase the risk of competitive replacement (Gurnell et al., 2004). However, the Isle of Arran is an isolated stronghold and so forest management could include the planting of a mixture of tree species to reduce the variability in resource quality. Our work here supports the current conservation strategy on Arran which has recommended increasing the diversity of tree species in managed areas (Lurz, 2012).

In summary, using GIS and custom-built models can benefit the success of species introductions by exploring the short and long term consequences of different management strategies (Seddon et al., 2007). Analysing the landscape is critical (Armstrong and Seddon, 2008) as it can identify suitable release sites; this is especially important when the landscape is composed of a network of habitat patches (Gardner and Gustafson, 2004; Lookingbill et al., 2010; Schadt et al., 2002). We have highlighted how including species specific information and representing the multi-year variability in resource is critical to understand population colonisation and persistence in a complex environment.

Chapter 6

Discussion

Mathematical models make a substantial addition to the theoretical toolkit used to understand and manage ecological systems. In this thesis we have shown how mathematical frameworks can be developed and analysed to answer specific ecological questions. Each chapter contains a detailed discussion of the specific findings and therefore in this chapter we will highlight only the key findings. We will also explain how our work could be extended to answer further ecological questions.

In Chapter 2 we adapted the host-pathogen framework of Anderson and May (1981) to measure the impact that a maternal effect acting on disease resistance may have on the population dynamics. Previous research linking maternal effects to population growth traits revealed that the maternal effect may increase the propensity for population cycles (Beckerman et al., 2002; Inchausti and Ginzburg, 2009). Recent empirical studies have shown that disease resistance traits in invertebrates may also be dependent on the maternal environment (Boots and Roberts, 2012; Mitchell and Read, 2005) and this motivated us to examine the impact this may have on host-pathogen dynamics. We considered a maternal effect linked to the maternal environment through either host density or through resource density. In a harsh maternal environment (high density and/or low resource) there was an increase in inherited offspring resistance. Our main results highlighted that a maternal effect acting to increase the resistance of offspring in a poor environment, reduces the propensity for population cycles. This is a key result and shows that maternal effects may stabilise population dynamics. The result can be interpreted biologically. In the absence of a maternal effect disease epidemics are triggered as the population increases in density (past a threshold). This epidemic rapidly reduces population density back below the disease threshold. The density recovers and increases over time causing the cycle to repeat (Anderson and May, 1981; Bowers et al., 1993; White et al., 1996). However, the inclusion of maternal effects acts to increase the resistance when the density is high. This decreases disease transmission opportunities at high density and reduces the severity of an epidemic. This acts to reduce the propensity for population cycles.

In our study we considered the maternal effect by splitting the host into two cohorts (high and low disease resistance) and partitioning host births into each cohort dependent on the maternal environment. This straightforward approach captures the key features observed in the experimental system (Boots and Roberts, 2012; Mitchell and Read, 2005) and permitted analysis of the dynamic host-pathogen behaviour using bifurcation software. In reality there are likely to be more than two levels of disease resistance. It would be possible to consider many distinct resistance classes with the offspring allocated to a particular class dependent on the maternal environment. As a first step towards this process we considered the two cohort system with a steep (but smooth) transition function to represent the switch between cohorts. We used the following function to represent the proportion of births allocated to the different cohorts:

$$E_1 = \frac{1}{2}\left(1 - \frac{\tanh\frac{\delta(H-H_{crit})}{H_{crit}}}{\tanh\delta}\right) \tag{6.1a}$$

$$E_2 = 1 - E_1 \tag{6.1b}$$

where δ controls the slope and H_{crit} is the host density at which both cohorts are allocated an equal proportion of births (see Figure 6.1 (a)). Preliminary results using this function are shown in Figure 6.1 (b). When H_{crit} is large all hosts are born with lower resistance, when H_{crit} is small the maternal effect acts to increase the number of hosts born with higher resistance. Figure 6.1 (b) shows the maternal effect acts to reduce the propensity to cycle although the non-linearity of this function makes tracing the hopf-bifurcation curve more difficult. Figure 6.1 (c) extends the set-up by partitioning host births in to three cohorts (further extension could include more cohorts). This represents a potential avenue of further work but under this set-up it would be difficult to determine the stability boundaries of the system (although some progress could be made through simulation). It would be of interest to examine whether the multi-cohort set-up produces similar findings to that of the two cohort set-up outlined in Chapter 2.

It is clear that short term time-lags may be created since the inherited phenotype may not be expressed until the offspring is exposed to the pathogen (which may happen when they are mature) (Grindstaff et al., 2003). As mentioned in Section 2.3.1 our assumption of the instantaneous transfer of maternal disease resistance is rather crude, but due to the additional complexity in the system we omitted this examination. There appears to a lack of maternal effects on disease resistance models in the literature, and it may be interesting to include a time-lag in the model, and in particular whether the host dynamics are altered by the length of the lag.

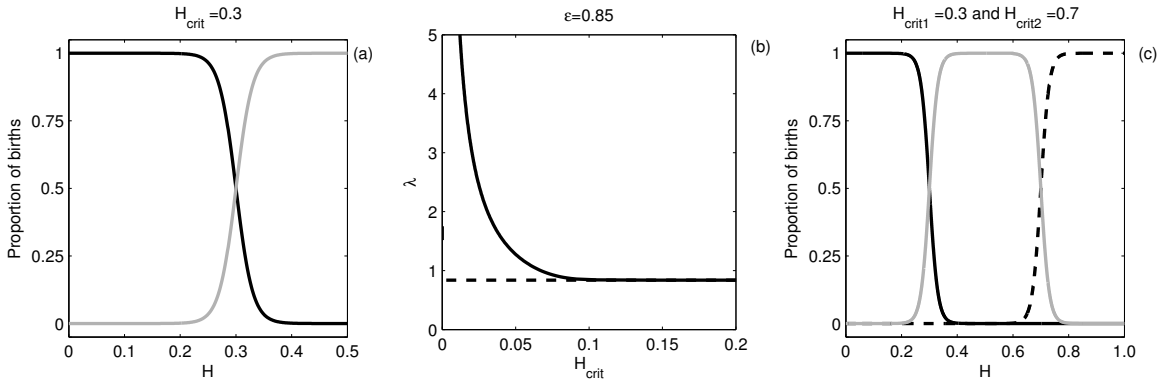

Figure 6.1: A smooth function given by Equations (6.1) shows E_1 (black) and E_2 (grey) in (a) where $H_{crit} = 0.3$ and $\delta = 10$. Hopf-bifurcation curve (black solid) of Equations (2.7) with $\eta = 0.9$ and costs $\epsilon = 0.85$ are plotted in $\lambda - H_{crit}$ parameter space using Equations (6.1) to allocate the proportion of births to H_1 and H_2 in (b). The dashed line represents the hopf-bifurcation curve for the original system Equations (2.3) with lower resistance (β_1) with other parameter values the same as Figure 2.5. Three host cohorts with the proportion of births to cohort H_1 (black), H_2 (grey) and H_3 (dashed black) are considered in (c). The switch between cohorts are controlled by $H_{crit1} = 0.3$ and $H_{crit2} = 0.8$ and $\delta = 10$.

Alternatively, further work may also consider the evolution of maternal effects on disease resistance. Studies that consider the evolutionary impacts of the maternal effect (Grindstaff et al., 2003; Mousseau, 1998; Räsänen and Kruuk, 2007; Wade, 1998) suggest that evolutionary consequences of variable phenotypes attributed to maternal effects can arise in response to natural selection or increased levels of phenotypic plasticity corresponding to fluctuating environments. The model developed here could be used to examine how the strength of the maternal effect on resistance (our parameter p) would evolve. Adaptive dynamics techniques have been applied to systems which exhibit population cycles (White et al., 2006) and are appropriate for examining the evolution of disease resistance (Boots et al., 2009). This technique could be used to examine how the parameter p would evolve, in particular whether a large enough maternal effect would develop to quench population cycles.

In Chapter 3 we considered the effect of infection dependent capture rates on Capture-Mark-Recapture (CMR) techniques and used statistical programs to produce estimates of the population size. In this case study deterministic and stochastic frameworks were used to simulate the trapping and infection process at a population and an individual level respectively. We showed that the statistical program, Capture, was able to handle different levels of heterogeneity in the data sets and generally we found that the appropriate models responded well to the data with infection dependent capture rates. However selecting the correct estimator is dependent on identifying the heterogeneity.

The stochastic modelling approaches developed in Chapter 3 were applied to two

case studies of populations in the presence of disease, in Chapters 4 and 5. In Chapter 4 we analysed the impact of disease spread in a red squirrel population on the Isle of Arran and in Chapter 5 we examined re-introduction techniques and population persistence in the same species, including seasonal fluctuations in heterogeneous (realistic) landscapes (Isle of Arran and Isle of Mull). In both cases the use of GIS techniques to build landscape maps of species specific habitat allowed a spatial aspect to be included in the mathematical framework. This enabled us to consider local interaction and identify dispersal corridors connecting patches of habitat which may influence disease spread (in Chapter 4) or re-colonisation (in Chapter 5). The techniques in these chapters were developed in collaboration with expert squirrel ecologists and with the Forestry Commission Scotland. Therefore the results have informed red squirrel conservation practices.

In Chapter 4 a mathematical model was used to investigate the spread of infection in the red squirrel population on Arran for different disease characteristics. A key result indicated that if SQPV was introduced to Arran (currently Arran is free from SQPV) its spread would be limited to a short term, local outbreak at the point of introduction. This has important implications for red squirrel strongholds in mainland UK. Namely that in isolation (i.e. absence of grey squirrels) SQPV may be able to cause localised outbreaks but is unable to persist in the long-term. Thus our theoretical study confirms the ideas based on field studies (Gurnell et al. (2006) and Duff et al. (2010)). Moreover, in the stronghold population at Formby in Merseyside there have been several outbreaks of SQPV, which has reduced red squirrel abundance. However, here the disease fade-outs and the red populations return to their pre-infection levels (Parrott et al., 2009). This observation supports our model results.

The study of the spread of disease on Arran also revealed the intrinsic relationship between habitat connectivity and disease spread; more specifically an acute disease can spread rapidly through well connected areas (since the squirrel density is generally high), whereas poorly connected regions reduce or prevent disease spread. Often when populations become small and isolated, improving habitat connectivity will promote the movement between patches and hence stabilise the population (Fahrig and Merriam, 1985; Henein and Merriam, 1990; Schumaker, 1996; Dobson et al., 1999; Lookingbill et al., 2010; Andel and Aronson, 2012). Our results, and others (Hess, 1994; Bienen, 2002; Real and Biek, 2007) would suggest that analysis of disease threats should be conducted prior to alterations of habitat which may affect connectivity and promote the spread of infectious disease and thereby threaten sub-populations which may have otherwise been at low infection risk. Our results have been used to devise a contingency plan to prevent disease spread in red squirrels on Arran and in particular it is proposed that any improvements in habitat should also take account of the potential risk of disease spread. The Arran project also highlighted the

importance of using local expert knowledge when designing mathematical models. In particular, communication with the local foresters allowed dispersal routes used by red squirrels on Arran to be clarified (ground-truthing) which had a marked difference in the predicted route of disease spread (Figure 4.3). The two-way collaborative process with conservation practitioners from the outset also has the benefit that model results are more readily accepted and understood.

In Chapter 5 we included seasonality in red squirrel births in a spatial, individual-based, stochastic model to analyse the relationship between specific tree species and red squirrel introduction and persistence. The results indicated that seasonal patterns in the resource quality of different tree species can have a dramatic affect on squirrel population density. For instance Sitka spruce, which dominates large parts of the landscape on the Isle of Arran and Mull, can lead to high amplitude fluctuations in squirrel density and in particular squirrel densities may reach low levels. Our work indicted that these fluctuations are less extreme in regions where there are a mixture of tree species types. This supports conservation practice on the Isle of Arran that advocates planting tree types that will provide a more reliable food supply adjacent to large Sitka spruce plantations (Lurz, 2012). With red squirrels still in decline in the UK the Isle of Mull has previously been proposed as a potential red squirrel stronghold (Shuttleworth, 2005). Our work indicates that the Isle of Mull, which is composed of four isolated woodland regions (Figure 5.17), may provide a suitable habitat for red squirrels. The proposal to introduce red squirrels to Mull by Shuttleworth (2005) was previously declined due to a lack of evidence to support red persistence on the island. Should red squirrel survival in other parts of the UK deteriorate then our work supports the option of a stronghold being created on Mull and highlights dispersal routes and regions of low connectivity.

In Chapter 4 we discussed the pressure on red squirrels from the invasive grey squirrel and SQPV on mainland UK. Red squirrels are declining due to the competition and infection of SQPV which is carried by grey squirrels (Tompkins et al., 2002). The current interface between the distribution of red and grey populations in the UK occurs in Highland Scotland and has been relatively stable for 40 years. However recent disease surveys have indicated that SQPV is spreading northwards through the grey population in the South of Scotland and the risk of spreading into the red population at this interface is evident (Scottish Wildlife Trust, 2013). Should SQPV reach the interface between red and grey squirrels it may have consequences for the persistence of the red populations. Our work on the Isle of Arran has indicated that although we may not expect the disease to spread through the red only populations it is likely that there will be disease outbreaks in the red population if introduced by greys. These outbreaks will reduce red density and allow the greys to extend into regions where they were previously not present. This has been shown to be possible in

a deterministic model of the red/grey/SQPV system on a simplified landscape (Bell et al., 2008). To test this possibility more rigorously future work could combine the interaction of red and grey squirrels with the disease model used on Arran (Chapter 4) and with the model that includes a realistic representation of tree species type and squirrel life history (Chapter 5) to assess the impact of SQPV on the survival of red population in Highland Scotland. This may highlight regions in which red squirrels are particularly vulnerable and grey control measures could be tested to prevent red squirrel extinction. This work could be developed in collaboration with conservation bodies who are responsible for protecting the remaining red populations in UK.

In this thesis we have developed mathematical models to explore four ecological case studies designed using a combination of previously published studies and inter-disciplinary collaboration. The techniques have been shown to be useful in answering specific ecological questions and highlight the flexibility and power of mathematical techniques to understand complex ecological systems.

Bibliography

J. V. Andel and J. Aronson. *Restoration ecology: the new frontier*. Blackwell, 2012. ISBN 063205834X. URL http://books.google.com/books?hl=en\&lr=\&id=s39Pu01h_vwC\&oi=fnd\&pg=PR7\&dq=Restoration+Ecology+The+new+Frontier\&ots=8nEXqIwLsT\&sig=JrPuap4GdeOIi0ha7VtNHhlDSio.

R. Anderson and R. May. Population biology of infectious diseases: Part I. *Nature*, 1979. URL http://bio.research.ucsc.edu/people/kilpatrick/READINGSDE10/Readings/Anderson\%26May1979Nature.pdf.

R. Anderson and R. May. Infectious diseases and population cycles of forest insects. *Science*, 210(4470):658–661, 1980. URL http://www.sciencemag.org/content/210/4470/658.short.

R. Anderson and R. May. The population dynamics of microparasites and their invertebrate hosts. *Philosophical Transactions of the Royal Society*, 291(1054), 1981. URL http://www.jstor.org/stable/10.2307/2395437.

R. M. Anderson, R. M. May, and B. Anderson. *Infectious diseases of humans: dynamics and control*, volume 28. Wiley Online Library, 1992.

D. P. Armstrong and P. J. Seddon. Directions in reintroduction biology. *Trends in ecology & evolution*, 23(1):20–5, Jan. 2008. ISSN 0169-5347. doi: 10.1016/j.tree.2007.10.003. URL http://www.ncbi.nlm.nih.gov/pubmed/18160175.

M. R. Ashmore. Assessing the future global impacts of ozone on vegetation. *Plant, Cell and Environment*, 28(8):949–964, Aug. 2005. ISSN 0140-7791. doi: 10.1111/j.1365-3040.2005.01341.x. URL http://www.blackwell-synergy.com/doi/abs/10.1111/j.1365-3040.2005.01341.x.

A. Bahar and X. Mao. Stochastic delay LotkaVolterra model. *Journal of Mathematical Analysis and Applications*, 292(2):364–380, Apr. 2004. ISSN 0022247X. doi: 10.1016/j.jmaa.2003.12.004. URL http://linkinghub.elsevier.com/retrieve/pii/S0022247X03009089.

S. Bar-David, D. Saltz, and T. Dayan. Predicting the spatial dynamics of a reintroduced population: the Persian fallow deer. *Ecological Applications*, 15(5):1833–1846, 2005. URL http://www.esajournals.org/doi/abs/10.1890/04-0798.

F. S. Barkalow, H. R. B, and S. R. F. The Vital Statistics of an Unexploited Gray Squirrel Population. *The Journal of Wildlife Management*, 34(3):489–500, July 1970.

A. Barnes and M. Siva-Jothy. Density-dependent prophylaxis in the mealworm beetle Tenebrio molitor L. (Coleoptera: Tenebrionidae): cuticular melanization is an indicator of investment in immunity. *Proceedings. Biological sciences / The Royal Society*, 267(1439):177–82, Jan. 2000. ISSN 0962-8452. doi: 10.1098/rspb.2000.0984. URL http://www.pubmedcentral.nih.gov/articlerender.fcgi?artid=1690519\&tool=pmcentrez\&rendertype=abstract.

G. Beck and G. S. Habicht. Immunity and the invertebrates. *Scientific American*, 275 (5):60–3, 66, Nov. 1996. ISSN 0036-8733. URL http://www.ncbi.nlm.nih.gov/pubmed/8875808.

A. Beckerman, T. G. Benton, E. Ranta, V. Kaitala, and P. Lundberg. Population dynamic consequences of delayed life-history effects. *Trends in Ecology & Evolution*, 17(6):263–269, 2002.

P. Beier and R. Noss. Do habitat corridors provide connectivity? *Conservation Biology*, 12(6):1241–1252, 1998. URL http://onlinelibrary.wiley.com/doi/10.1111/j.1523-1739.1998.98036.x/full.

S. S. Bell, A. White, J. a. Sherratt, and M. Boots. Invading with biological weapons: the role of shared disease in ecological invasion. *Theoretical Ecology*, 2(1):53–66, Dec. 2008. ISSN 1874-1738. doi: 10.1007/s12080-008-0029-x. URL http://link.springer.com/10.1007/s12080-008-0029-x.

T. G. Benton, E. Ranta, V. Kaitala, and A. P. Beckerman. Maternal effects and the stability of population dynamics in noisy environments. *Journal of Animal Ecology*, 70(4):590–599, Dec. 2001. ISSN 00218790. doi: 10.1046/j.1365-2656.2001.00527.x. URL http://doi.wiley.com/10.1046/j.1365-2656.2001.00527.x.

J. Bernardo. The particular maternal effect of propagule size, especially egg size: patterns, models, quality of evidence and interpretations. *American zoologist*, 236(December 1993):216–236, 1996. URL http://icb.oxfordjournals.org/content/36/2/216.short.

A. A. Berryman. Population cycles: causes and analysis. *Population Cycles: The Case for Trophic Interactions: The Case for Trophic Interactions*, page 1, 2002.

L. Bienen. Informed Decisions: Conservation Corridors and the spread of infectious disease. *Conservation in Practice*, 3(2):10–17, 2002.

A. J. Black and A. J. McKane. Stochastic formulation of ecological models and their applications. *Trends in ecology & evolution*, 27(6):337–45, June 2012. ISSN 0169-5347. doi: 10.1016/j.tree.2012.01.014. URL `http://www.ncbi.nlm.nih.gov/pubmed/22406194`.

M. Boots and M. Begon. Trade-offs with resistance to a granulosis virus in the Indian meal moth, examined by a laboratory evolution experiment. *Functional Ecology*, 7 (5):528–534, 1993. URL `http://www.jstor.org/stable/10.2307/2390128`.

M. Boots and K. E. Roberts. Maternal effects in disease resistance: poor maternal environment increases offspring resistance to an insect virus. *Proceedings of the Royal Society B: Biological Sciences*, 279(1744):4009–4014, 2012.

M. Boots, A. Best, M. R. Miller, and A. White. The role of ecological feedbacks in the evolution of host defence: what does theory tell us? *Philosophical Transactions of the Royal Society B: Biological Sciences*, 364(1513):27–36, 2009.

S. Bosch and P. Lurz. *The Eurasian Red Squirrel*. Wolf, Verlagskg, 1st edition, June 2012.

R. Bowers, M. Begon, and D. Hodgkinson. Host-pathogen population cycles in forest insects? Lessons from simple models reconsidered. *Oikos*, 67(3):529–538, 1993. URL `http://www.jstor.org/stable/10.2307/3545365`.

M. Boyce. Population viability analysis. *Annual review of Ecology and Systematics*, pages 481–506, 1992. URL `http://www.jstor.org/stable/2097297`.

D. Briske, R. Washington-Allen, C. Johnson, J. Lockwood, D. Lockwood, T. Stringham, and H. Shugart. Catastrophic Thresholds: A Synthesis of Concepts, Perspectives, and Applications. *Ecology and society*, 15(3):37, 2010. URL `http://ecite.utas.edu.au/65930`.

B. W. Brook, J. J. O'Grady, a. P. Chapman, M. a. Burgman, H. R. Akçakaya, and R. Frankham. Predictive accuracy of population viability analysis in conservation biology. *Nature*, 404(6776):385–7, Mar. 2000. ISSN 0028-0836. doi: 10.1038/35006050. URL `http://www.ncbi.nlm.nih.gov/pubmed/10746724`.

K. Burnham and W. Overton. Estimation of the size of a closed population when capture probabilities vary among animals. *Biometrika*, pages 625–633, 1978. URL `http://biomet.oxfordjournals.org/content/65/3/625.short`.

R. Chesser and N. Ryman. Inbreeding as a strategy in subdivided populations. *Evolution*, 40(3):616–624, 1986.

T. Clark and R. Westrum. High-performance teams in wildlife conservation: a species reintroduction and recovery example. *Environmental Management*, 1989. URL `http://link.springer.com/article/10.1007/BF01868305`.

J. C. Coltherd, C. Morgan, J. Judge, L. A. Smith, and M. R. Hutchings. The effects of parasitism on recapture rates of wood mice (Apodemus sylvaticus). *Wildlife Research*, 37:413–417, 2010.

C. Congress. The IUCN Programme 20132016, 2013.

J. T. Coppock and D. W. Rhind. The history of gis. *Geographical information systems: Principles and applications*, 1(1):21–43, 1991.

A. Cornish-Bowden. *Fundamentals of enzyme kinetics*. John Wiley & Sons, 2013.

J. Cushing. Periodic solutions of two species interaction models with lags. *Mathematical Biosciences*, 1976. URL `http://www.sciencedirect.com/science/article/pii/0025556476900468`.

V. H. Dale, S. Brown, R. Haeuber, N. Hobbs, N. Huntly, R. Naiman, W. Riebsame, M. Turner, and T. Valone. Ecological principles and guidelines for managing the use of land 1. *Ecological applications*, 10(3):639–670, 2000.

P. Daszak. Emerging Infectious Diseases of Wildlife– Threats to Biodiversity and Human Health. *Science*, 287(5452):443–449, Jan. 2000. ISSN 00368075. doi: 10.1126/science.287.5452.443. URL `http://www.sciencemag.org/cgi/doi/10.1126/science.287.5452.443`.

P. Daszak, a. a. Cunningham, and a. D. Hyatt. Anthropogenic environmental change and the emergence of infectious diseases in wildlife. *Acta tropica*, 78(2):103–16, Feb. 2001. ISSN 0001-706X. URL `http://www.ncbi.nlm.nih.gov/pubmed/11230820`.

S. L. Deem, W. B. Karesh, and W. Weisman. Putting Theory into Practice: Wildlife Health in Conservation. *Conservation Biology*, 15(5):1224–1233, Oct. 2001. ISSN 0888-8892. doi: 10.1046/j.1523-1739.2001.00336.x. URL `http://doi.wiley.com/10.1046/j.1523-1739.2001.00336.x`.

O. Diekmann, J. Heesterbeek, and J. Metz. The legacy of kermack and mckendrick. *Epidemic Models: Their Structure and Relation to Data (D. Mollison, ed.)*, pages 95–115, 1995.

A. Dobson, K. Ralls, and M. Foster. *Corridors: reconnecting fragmented landscapes*. Island Press, 1999. URL `http://books.google.com/books?hl=en\&lr=\&id=9fEWaQHM6cYC\&oi=fnd\&pg=PA129\&dq=Corridors+reconnecting+fragmented+landscapes\&ots=UuWX3h65wk\&sig=-LlfaXS1cNgQALPuzH5iJbzp67M`.

E. Doedel. AUTO: A program for the automatic bifurcation analysis of autonomous systems. *Congr. Numer*, pages 265–384, 1981. URL `http://cmvl.cs.concordia.ca/publications/CongNum30.pdf`.

E. Doedel and B. Oldeman. *AUTO-07P: continuation and bifurcation software for ordinary differential equations*, 1981.

P. F. Donald and A. D. Evans. Habitat connectivity and matrix restoration: the wider implications of agri-environment schemes. *Journal of Applied Ecology*, 43(2): 209–218, Mar. 2006. ISSN 00218901. doi: 10.1111/j.1365-2664.2006.01146.x. URL `http://doi.wiley.com/10.1111/j.1365-2664.2006.01146.x`.

J. Duff, J. Holmes, and A. Barlow. Surveillance turns to wildlife. *Veterinary Record*, 167:154–156, 2010.

G. Dwyer. Density dependence and spatial structure in the dynamics of insect pathogens. *The American Naturalist*, 143(4):533–562, 1994.

L. Edelstein-Keshet. *Mathematical models in biology*, volume 46. Siam, 1988.

D. J. Everest, H. Butler, T. Blackett, V. R. Simpson, and C. M. Shuttleworth. Adenovirus infection in red squirrels in areas free from grey squirrels. *The Veterinary record*, 173(8):199–200, Aug. 2013. ISSN 2042-7670. doi: 10.1136/vr.f5304. URL `http://www.ncbi.nlm.nih.gov/pubmed/23997167`.

L. Fahrig and G. Merriam. Habitat patch connectivity and population survival. *Ecology*, 66(6):1762–1768, 1985. URL `http://www.jstor.org/stable/10.2307/2937372`.

W. G. Feero, A. E. Guttmacher, and K. L. Hudson. Genomics, health care, and society. *New England Journal of Medicine*, 365(11):1033–1041, 2011.

G. R. Finlayson, E. M. Vieira, D. Priddel, R. Wheeler, J. Bentley, and C. R. Dickman. Multi-scale patterns of habitat use by re-introduced mammals: A case study using medium-sized marsupials. *Biological Conservation*, 141(1):320–331, Jan. 2008. ISSN 00063207. doi: 10.1016/j.biocon.2007.10.008. URL `http://linkinghub.elsevier.com/retrieve/pii/S0006320707004119`.

Forestry Commission Scotland. Chalara dieback of ash (Chalara fraxinea), December 2013. URL http://www.forestry.gov.uk/chalara).

J. M. Fryxell, D. J. T. Hussell, A. B. Lambert, and P. C. Smith. Time Lags and Population Fluctuations in White-Tailed Deer. *The Journal of Wildlife Management*, 55(3):377–385, 1991. URL http://www.jstor.org/discover/10.2307/3808963?uid=25955&uid=3738032&uid=2&uid=3&uid=5910784&uid=67&uid=25953&uid=62&sid=21102426630171.

R. H. Gardner and E. J. Gustafson. Simulating dispersal of reintroduced species within heterogeneous landscapes. *Ecological Modelling*, 171(4):339–358, Feb. 2004. ISSN 03043800. doi: 10.1016/j.ecolmodel.2003.08.008. URL http://linkinghub.elsevier.com/retrieve/pii/S0304380003003387.

K. J. Gaston, R. L. Pressey, and C. R. Margules. Persistence and vulnerability: retaining biodiversity in the landscape and in protected areas. *Journal of biosciences*, 27(4 Suppl 2):361–84, July 2002. ISSN 0250-5991. URL http://www.ncbi.nlm.nih.gov/pubmed/12177535.

F. Gheranrdi. Crayfish invading Europe: the case study of Procambarus clarkii. *Marine and Freshwater Behaviour and Physiology*, 39(3):175–191, 2006.

D. Gillespie. Exact stochastic simulation of coupled chemical reactions. *The journal of physical chemistry*, 93555(1):2340–2361, 1977. URL http://pubs.acs.org/doi/pdf/10.1021/j100540a008.

L. Ginzburg and D. Taneyhill. Population cycles of forest Lepidoptera: a maternal effect hypothesis. *Journal of Animal Ecology*, 63(1):79–92, 1994. URL http://www.jstor.org/stable/10.2307/5585.

S. Godefroid, C. Piazza, G. Rossi, S. Buord, A.-D. Stevens, R. Aguraiuja, C. Cowell, C. W. Weekley, G. Vogg, J. M. Iriondo, I. Johnson, B. Dixon, D. Gordon, S. Magnanon, B. Valentin, K. Bjureke, R. Koopman, M. Vicens, M. Virevaire, and T. Vanderborght. How successful are plant species reintroductions? *Biological Conservation*, 144(2):672–682, Feb. 2011. ISSN 00063207. doi: 10.1016/j.biocon.2010.10.003. URL http://linkinghub.elsevier.com/retrieve/pii/S0006320710004362.

B. Griffith, J. Scott, J. Carpenter, and C. Reed. Translocation as a species conservation tool: status and strategy. *Science(Washington)*, 1989. URL http://lynx.uio.no/lynx/ibelynxco/04_library/4_3_publications/G/Griffith_et_al_1989_Translocation_as_a_species_conservation_tool.pdf.

V. Grimm. Ten years of individual-based modelling in ecology: what have we learned and what could we learn in the future? *Ecological Modelling*, 115(2-3):129–148,

Feb. 1999. ISSN 03043800. doi: 10.1016/S0304-3800(98)00188-4. URL http://linkinghub.elsevier.com/retrieve/pii/S0304380098001884.

J. L. Grindstaff, E. D. Brodie, and E. D. Ketterson. Immune function across generations: integrating mechanism and evolutionary process in maternal antibody transmission. *Proceedings. Biological sciences / The Royal Society*, 270(1531):2309–19, Nov. 2003. ISSN 0962-8452. doi: 10.1098/rspb.2003.2485. URL http://www.pubmedcentral.nih.gov/articlerender.fcgi?artid=1691520\&tool=pmcentrez\&rendertype=abstract.

J. Gurnell, L. a. Wauters, P. W. W. Lurz, and G. Tosi. Alien species and interspecific competition: effects of introduced eastern grey squirrels on red squirrel population dynamics. *Journal of Animal Ecology*, 73(1):26–35, Jan. 2004. ISSN 00218790. doi: 10.1111/j.1365-2656.2004.00791.x. URL http://doi.wiley.com/10.1111/j.1365-2656.2004.00791.x.

J. Gurnell, S. Rushton, P. Lurz, A. Sainsbury, P. Nettleton, M. Shirley, C. Bruemmer, and N. Geddes. Squirrel poxvirus: Landscape scale strategies for managing disease threat. *Biological Conservation*, 131(2):287–295, 2006.

Y. Gutterman. Maternal effects on seeds during development. *Seed: the ecology of regeneration in plant*, 2000. URL http://books.google.com/books?hl=en\&lr=\&id=wu5JLxbYZJMC\&oi=fnd\&pg=PA59\&dq=Maternal+Effects+on+Seeds+During+Development\&ots=y6goYh8XkD\&sig=4zdsiPg-r2jHXiEIH4VZBDK_8Bs.

M. Gyllenberg and I. Hanski. Habitat Deterioration, Habitat Destruction, and Metapopulation Persistence in a Heterogenous Landscape. *Theoretical population biology*, 52(3):198–215, Dec. 1997. ISSN 1096-0325. URL http://www.ncbi.nlm.nih.gov/pubmed/9466961.

I. Hanski. Metapopulation dynamics: brief history and conceptual domain. *Biological Journal of the Linnean Society*, 42:3–16, 1991.

I. Hanski. Metapopulation dynamics. *Nature*, 396:41–49, 1998. URL http://www.nature.com/nature/journal/v396/n6706/abs/396041a0.html.

K. Henein and G. Merriam. The elements of connectivity where corridor quality is variable. *Landscape Ecology*, 4(2-3):157–170, July 1990. ISSN 0921-2973. doi: 10.1007/BF00132858. URL http://link.springer.com/10.1007/BF00132858.

G. Hess. Conservation corridors and contagious disease: a cautionary note. *Conservation Biology*, 8(1):256–262, 1994. URL http://onlinelibrary.wiley.com/doi/10.1046/j.1523-1739.1994.08010256.x/full.

H. W. Hethcote. The mathematics of infectious diseases. *SIAM review*, 42(4):599–653, 2000.

C. S. Holling. The functional response of invertebrate predators to prey density. *Memoirs of the Entomological Society of Canada*, 98(S48):5–86, 1966.

P. Inchausti and L. R. Ginzburg. Small mammals cycles in northern Europe: patterns and evidence for a maternal effect hypothesis. *Journal of Animal Ecology*, 67(2): 180–194, Mar. 1998. ISSN 00218790. doi: 10.1046/j.1365-2656.1998.00189.x. URL http://doi.wiley.com/10.1046/j.1365-2656.1998.00189.x.

P. Inchausti and L. R. Ginzburg. Maternal effects mechanism of population cycling: a formidable competitor to the traditional predator-prey view. *Philosophical transactions of the Royal Society of London. Series B, Biological sciences*, 364(1520):1117–24, Apr. 2009. ISSN 1471-2970. doi: 10.1098/rstb.2008.0292. URL http://www.pubmedcentral.nih.gov/articlerender.fcgi?artid=2666685\&tool=pmcentrez\&rendertype=abstract.

International Union for Conservation of Nature, 2014. URL http://www.iucn.org/.

IUCN. Guidelines for Reintroductions and Other Conservation Translocations, 2013.

S. IUCN. IUCN Position Statement on the Translocation of Living Organisms. *Introductions, Reintroductions and Re-Stocking*, 1987. URL http://scholar.google.com/scholar?hl=en\&btnG=Search\&q=intitle:IUCN+Position+Statement+on+Translocation+of+Living+Organisms\#1.

Joint Nature Conservation Committee. Uk biodiversity action plan, 2012. URL http://jncc.defra.gov.uk/page-5155.

O. P. Judson. The rise of the individual-based model in ecology. *Trends in ecology & evolution*, 9(1):9–14, 1994.

J. Jungck. Ten equations that changed biology: mathematics in problem-solving biology curricula. *Bioscene*, 1997. URL http://academic.evergreen.edu/curricular/ins/0708/fall/presentations/Ten_Equations_of_Biology.pdf.

P. Kareiva and U. Wennergren. Connecting landscape patterns to ecosystem and population processes. *Nature*, 373:299–302, 1995.

T. Kawecki and S. Stearns. The evolution of life histories in spatially heterogeneous environments: optimal reaction norms revisited. *Evolutionary Ecology*, 7:155–174, 1993. URL http://www.springerlink.com/index/G677868668T06462.pdf.

M. Keeling. The effects of local spatial structure on epidemiological invasions. *Proceedings. Biological sciences / The Royal Society*, 266(1421):859–67, 1999.

M. Keeling and P. Rohani. *Modeling Infectious Disease in humans and animals*. Princeton University Press, 2008.

D. Kelly, W. D. Koenig, and A. M. Liebhold. An intercontinental comparison of the dynamic behavior of mast seeding communities. *Population Ecology*, 50(4): 329–342, Oct. 2008. ISSN 1438-3896. doi: 10.1007/s10144-008-0114-4. URL `http://link.springer.com/10.1007/s10144-008-0114-4`.

W. Kermack and A. McKendrick. Contributions to the mathematical theory of epidemicsiii. further studies of the problem of endemicity. *Bulletin of mathematical biology*, 53(1):89–118, 1991.

D. Kleiman and R. Reading. Improving the evaluation of conservation programs. *Conservation ...*, 2000. URL `http://onlinelibrary.wiley.com/doi/10.1046/j.1523-1739.2000.98553.x/full`.

A. T. Knight, R. M. Cowling, M. Rouget, A. Balmford, A. T. Lombard, and B. M. Campbell. Knowing but not doing: selecting priority conservation areas and the research–implementation gap. *Conservation Biology*, 22(3):610–617, 2008.

E. Korpimäki and C. Krebs. Predation and population cycles of small mammals. *BioScience*, 46(10):754–764, Nov. 1996. ISSN 00063568. doi: 10.2307/1312851. URL `http://bioscience.oxfordjournals.org/cgi/doi/10.2307/1312851http://www.jstor.org/stable/1312851`.

C. Kraus, D. L. Thomson, J. Künkele, and F. Trillmich. Living slow and dying young? Life-history strategy and age-specific survival rates in a precocial small mammal. *Journal of Animal Ecology*, 74(1):171–180, Dec. 2004. ISSN 00218790. doi: 10.1111/j.1365-2656.2004.00910.x. URL `http://doi.wiley.com/10.1111/j.1365-2656.2004.00910.x`.

R. Lacy. VORTEX: a computer simulation model for population viability analysis. *Wildlife Research*, 1993. URL `http://www.publish.csiro.au/paper/WR9930045`.

R. Leaper, G. Massei, M. Gorman, and R. Aspinall. The feasibility of reintroducing Wild Boar (Sus scrofa) to Scotland. *Mammal Review*, 29(4):239–259, 1999. URL `http://onlinelibrary.wiley.com/doi/10.1046/j.1365-2907.1999.2940239.x/abstract`.

M. A. Leibold, M. Holyoak, N. Mouquet, P. Amarasekare, J. Chase, M. Hoopes, R. Holt, J. Shurin, R. Law, D. Tilman, et al. The metacommunity concept: a framework for multi-scale community ecology. *Ecology letters*, 7(7):601–613, 2004.

X. Li, D. Li, Y. Li, Z. Ma, and T. Zhai. Habitat evaluation for crested ibis: A gis-based approach. *Ecological Research*, 17(5):565–573, 2002.

T. Little, B. O'Connor, N. Colegrave, K. Watt, and A. Read. Maternal transfer of strain-specific immunity in an invertebrate. *Current Biology*, 13(Figure 1):489–492, 2003. doi: 10.1016/S. URL `http://www.sciencedirect.com/science/article/pii/S0960982203001635`.

T. R. Lookingbill, R. H. Gardner, J. R. Ferrari, and C. E. Keller. Combining a dispersal model with network theory to assess habitat connectivity. *Ecological applications: a publication of the Ecological Society of America*, 20(2):427–41, Mar. 2010. ISSN 1051-0761. URL `http://www.ncbi.nlm.nih.gov/pubmed/20405797`.

A. J. Lotka. Contribution to the theory of periodic reactions. *The Journal of Physical Chemistry*, 14(3):271–274, 1910.

G. M. Lovett, C. D. Canham, M. a. Arthur, K. C. Weathers, and R. D. Fitzhugh. Forest Ecosystem Responses to Exotic Pests and Pathogens in Eastern North America. *BioScience*, 56(5):395, 2006. ISSN 0006-3568. doi: 10.1641/0006-3568(2006)056[0395:FERTEP]2.0.CO;2. URL `http://bioscience.oxfordjournals.org/cgi/doi/10.1641/0006-3568(2006)056[0395:FERTEP]2.0.CO;2`.

P. Lurz. Arran Red Squirrel Assessment, 2012.

P. Lurz, P. Garson, and S. Rushton. The ecology of squirrels in spruce dominated plantations: implications for forest management. *Forest Ecology and Management*, 79(1-2):79–90, Nov. 1995. ISSN 03781127. doi: 10.1016/0378-1127(95)03617-2. URL `http://linkinghub.elsevier.com/retrieve/pii/0378112795036172`.

P. Lurz, N. Geddes, A. Lloyd, M. Shirley, S. Rushton, and B. Burlton. Planning a red squirrel conservation area: using a spatially explicit population dynamics model to predict the impact of felling and forest design plans. *Forestry*, 76(1):93–106, 2003. URL `http://forestry.oxfordjournals.org/content/76/1/95.short`.

M. Macpherson, R. Davidson, D. Duncan, A. White, P. Lurz, and A. Jarrett. Assessing the impact of the squirelpox virus on Eurasian Red squirrel. Technical report, 2013.

S. Manchester and J. Bullock. The impacts of non-native species on UK biodiversity and the effectiveness of control. *Journal of Applied Ecology*, 37:845–864, 2000. URL `http://onlinelibrary.wiley.com/doi/10.1046/j.1365-2664.2000.00538.x/full`.

G. Marten. A regression method for mark-recapture estimation of population size with unequal catchability. *Ecology*, 51(2):291–295, 1970. URL `http://gerrymarten.com/publicatons/pdfs/GM\_Mark-Recapture-Estimation.pdf`.

D. Martínez-Jiménez, D. Graham, D. Couper, M. Benkö, S. Schöniger, J. Gurnell, and A. W. Sainsbury. Epizootiology and pathologic findings associated with a newly described adenovirus in the red squirrel, Sciurus vulgaris. *Journal of wildlife diseases*, 47(2):442–54, Apr. 2011. ISSN 1943-3700. doi: 10.7589/0090-3558-47.2.442. URL `http://www.ncbi.nlm.nih.gov/pubmed/21441198`.

R. May and R. Anderson. Population biology of infectious diseases: Part II. *Nature*, 1979. URL `http://www.math.unm.edu/~sulsky/mathcamp/AndersonMay1979a.pdf`.

M. McCormick. Behaviorally induced maternal stress in a fish influences progeny quality by a hormonal mechanism. *Ecology*, 79(6):1873–1883, 1998. URL `http://www.esajournals.org/doi/abs/10.1890/0012-9658(1998)079\%5B1873:BIMSIA\%5D2.0.CO\%3B2`.

S. E. Mitchell and A. F. Read. Poor maternal environment enhances offspring disease resistance in an invertebrate. *Proceedings. Biological sciences / The Royal Society*, 272(1581):2601–7, Dec. 2005. ISSN 1471-2954. doi: 10.1098/rspb.2005.3253. URL `http://www.pubmedcentral.nih.gov/articlerender.fcgi?artid=1559984\&tool=pmcentrez\&rendertype=abstract`.

H. Moller. Foods and foraging behaviour of red (sciurus vulgaris) and grey (sciurus carolinensis) squirrels. *Mammal Review*, 13(2-4):81–98, 1983.

D. Morens, G. Folkers, and A. Fauci. The challenge of emerging and re-emerging infectious diseases. *Nature*, 430(6996):242–9, 2004.

S. S. Morse. Factors in the emergence of infectious diseases. *Emerging infectious diseases*, 1(1):7–15, 1995. ISSN 1080-6040. doi: 10.3201/eid0101.950102. URL `http://www.ncbi.nlm.nih.gov/pubmed/15577934`.

T. Mousseau. The adaptive significance of maternal effects. *Trends in Ecology & Evolution*, 13(10):403–407, 1998. URL `http://www.sciencedirect.com/science/article/pii/S0169534798014724`.

J. Murray. *Mathematical Biology*, volume 19. Springer-Verlag, third edition, 2002.

National Parks Conservation Association. Yellowstone National Park, 2014. URL `http://www.npca.org/parks/yellowstone-national-park.html`.

E. P. Odum, H. T. Odum, and J. Andrews. *Fundamentals of ecology*, volume 3. Saunders Philadelphia, 1971.

P. Opdam and D. Wascher. Climate change meets habitat fragmentation: linking landscape and biogeographical scale levels in research and conservation. *Biological Conservation*, 117(3):285–297, May 2004. ISSN 00063207. doi: 10.1016/j.biocon.2003.12.008. URL `http://linkinghub.elsevier.com/retrieve/pii/S0006320703004890`.

P. E. Osborne and P. J. Seddon. Selecting suitable habitats for reintroductions: variation, change and the role of species distribution modelling. *Reintroduction biology: integrating science and management*, pages 73–104, 2012.

R. Ostfeld, G. Glass, and F. Keesing. Spatial epidemiology: an emerging (or re-emerging) discipline. *Trends in ecology and evolution*, 20(6):328–336, 2005.

E. H. Parlato and D. P. Armstrong. Predicting post-release establishment using data from multiple reintroductions. *Biological Conservation*, 160:97–104, Apr. 2013. ISSN 00063207. doi: 10.1016/j.biocon.2013.01.013. URL `http://linkinghub.elsevier.com/retrieve/pii/S0006320713000232`.

D. Parrott, R. Quy, K. Van Driel, P. LURZ, S. Rushton, J. Gurnell, N. Aebischer, and J. Reynolds. Review of red squirrel conservation activity in northern england. *Natural England Commissioned Report NECR019*, 2009.

L. Parvulescu, A. Schrimpf, E. Kozubikova, S. Cabanillas Resino, T. Vralstad, A. Petrusek, and R. Schulz. Invasive crayfish and crayfish plague on the move: first detection of the plague agent Aphanomyces astaci in the Romanian Danube. *Diseases of aquatic organisms*, 98(1):85–94, 2012.

J. Patz, P. Daszak, G. Tabor, A. Aguirre, M. Pearl, J. Epstein, N. Wolfe, A. Kilpatrick, J. Foufopoulos, D. Molyneux, and D. Bradley. Unhealthy Landscapes: Policy Recommendations on Land Use Change and Infectious Disease Emergence. *Environmental Health Perspectives*, 112(10):1092–1098, 2004.

D. Pimentel, C. Wilson, C. McCullum, R. Huang, P. Dwen, J. Flack, Q. Tran, T. Saltman, and B. Cliff. Economic and Environmental Benefits of Biodiversity. *BioScience*, 47(11):747–757, Dec. 1997. ISSN 00063568. doi: 10.2307/1313097. URL `http://www.jstor.org/stable/info/10.2307/1313097`.

S. L. Pimm and P. Raven. Extinction by numbers. *Nature*, 403:843–845, 2000.

S. L. Pimm, G. J. Russell, J. L. Gittleman, and T. M. Brooks. The future of biodiversity. *Science (New York, N.Y.)*, 269(5222):347–50, July 1995. ISSN 0036-8075. doi: 10.1126/science.269.5222.347. URL `http://www.ncbi.nlm.nih.gov/pubmed/17841251`.

H. J. Poethke and T. Hovestadt. Evolution of density- and patch-size-dependent dispersal rates. *Proceedings. Biological sciences / The Royal Society*, 269(1491):637–45, Mar. 2002. ISSN 0962-8452. doi: 10.1098/rspb.2001.1936. URL `http://www.pubmedcentral.nih.gov/articlerender.fcgi?artid=1690934\&tool=pmcentrez\&rendertype=abstract`.

K. Pollock. The use of auxiliary variables in capture-recapture modelling: an overview. *Journal of Applied Statistics*, 29:85–102, 2002. URL `http://www.tandfonline.com/doi/abs/10.1080/02664760120108430`.

K. H. Pollock. A capture-recapture design robust to unequal probability of capture. *The Journal of Wildlife Management*, pages 752–757, 1982.

K. H. Pollock. Statistical inference for capture-recapture experiments. *Wildl Monogr*, 107:1–97, 1990.

J. Prenter, C. Macneil, J. T. Dick, and A. M. Dunn. Roles of parasites in animal invasions. *Trends in ecology & evolution*, 19(7):385–90, July 2004. ISSN 0169-5347. doi: 10.1016/j.tree.2004.05.002. URL `http://www.ncbi.nlm.nih.gov/pubmed/16701290`.

K. Räsänen and L. E. B. Kruuk. Maternal effects and evolution at ecological time-scales. *Functional Ecology*, 21(3):408–421, June 2007. ISSN 0269-8463. doi: 10.1111/j.1365-2435.2007.01246.x. URL `http://doi.wiley.com/10.1111/j.1365-2435.2007.01246.x`.

L. Real and R. Biek. Spatial dynamics and genetics of infectious dieases on heterogeneous landscapes. *Journal of Royal Society, Interface*, 4(16):935–948, 2007.

J. R. Reilly and A. E. Hajek. Density-dependent resistance of the gypsy moth Lymantria dispar to its nucleopolyhedrovirus, and the consequences for population dynamics. *Oecologia*, 154(4):691–701, Jan. 2008. ISSN 0029-8549. doi: 10.1007/s00442-007-0871-3. URL `http://www.ncbi.nlm.nih.gov/pubmed/17968593`.

E. Renshaw. *Modelling Biological Populations in Space and Time.* Cambridge University Press, 1991.

E. Renshaw. *Modelling biological populations in space and time*, volume 11. Cambridge University Press, 1993.

E. Rexstad and K. P. Burnham. *User's guide for interactive program CAPTURE.* Color. Cooperative Fish and Wildlife Research Unit, 1991.

J. J. H. Reynolds, A. White, J. A. Sherratt, and M. Boots. The population dynamical consequences of density-dependent prophylaxis. *Journal of theoretical biology*, 288: 1–8, Nov. 2011. ISSN 1095-8541. doi: 10.1016/j.jtbi.2011.07.029. URL `http://www.ncbi.nlm.nih.gov/pubmed/21835185`.

S. Riley. Large-scale spatial-transmission models of infectious disease. *Science (New York, N.Y.)*, 316(5829):1298–301, June 2007. ISSN 1095-9203. doi: 10.1126/science.1134695. URL `http://www.ncbi.nlm.nih.gov/pubmed/17540894`.

D. Roach. Maternal effects in plants. *Annual Review of Ecology and Systematics*, 18 (1987):209–235, 1987. URL `http://www.jstor.org/stable/10.2307/2097131`.

J. P. Rodríguez, L. Brotons, J. Bustamante, and J. Seoane. The application of predictive modelling of species distribution to biodiversity conservation. *Diversity and Distributions*, 13(3):243–251, May 2007. ISSN 13669516. doi: 10.1111/j.1472-4642.2007.00356.x. URL `http://doi.wiley.com/10.1111/j.1472-4642.2007.00356.x`.

M. Rossiter. Environmentally-based maternal effects: a hidden force in insect population dynamics? *Oecologia*, 87(2):288–294, 1991. URL `http://www.springerlink.com/index/X240273K31N7J2NT.pdf`.

T. Rout, C. Hauser, and H. Possingham. Minimise long-term loss or maximise short-term gain? *Ecological Modelling*, 201(1):67–74, Feb. 2007. ISSN 03043800. doi: 10.1016/j.ecolmodel.2006.07.022. URL `http://linkinghub.elsevier.com/retrieve/pii/S0304380006003565`.

S. Rushton, P. Lurz, J. Gurnell, and R. Fuller. Modelling the spatial dynamics of parapoxvirus disease in red and grey squirrels: a possible cause of the decline in the red squirrel in the UK? *Journal of Applied Ecology*, 37(6):997–1012, 2000.

F. Sarrazin and R. Barbault. Reintroduction: challenges and lessons for basic ecology. *Trends in Ecology & Evolution*, 5347(96):474–478, 1996. URL `http://www.sciencedirect.com/science/article/pii/0169534796200928`.

S. Schadt, F. Knauer, and P. Kaczensky. Rule-based assessment of suitable habitat and patch connectivity for the Eurasian lynx. *Ecological ...*, 12(5):1469–1483, 2002. URL `http://www.esajournals.org/doi/abs/10.1890/1051-0761(2002)012\%5B1469:RBAOSH\%5D2.0.CO\%3B2`.

N. Schumaker. Using landscape indices to predict habitat connectivity. *Ecology*, 77 (4):1210–1225, 1996. URL `http://www.jstor.org/stable/10.2307/2265590`.

C. J. Schwarz and G. A. Seber. Estimating animal abundance: review iii. *Statistical Science*, pages 427–456, 1999.

Scottish Wildlife Trust. Annual Report and Financial Statements for the year ended 31st March 2013, 2013.

G. Seber. The estimation of animal abundance and related parameters, 1982. *Griffin, London*, 1982. URL `http://scholar.google.com/scholar?hl=en\&btnG=Search\&q=intitle:THE+ESTIMATION+OF+ANIMAL+ABUNDANCE+and+related+parameters\#2`.

P. J. Seddon, D. P. Armstrong, and R. F. Maloney. Developing the science of reintroduction biology. *Conservation biology : the journal of the Society for Conservation Biology*, 21(2):303–12, Apr. 2007. ISSN 0888-8892. doi: 10.1111/j.1523-1739.2006.00627.x. URL `http://www.ncbi.nlm.nih.gov/pubmed/17391180`.

K. Shanker. Small mammal trapping in tropical montane forests of the upper nilgiris, southern india: an evaluation of capture-recapture models in estimating abundance. *Journal of biosciences*, 25(1):99–111, 2000.

C. Shuttleworth. An assessment of the suitability of the woodland habitat on mull for the red squirrel. *European Squirrel Initiative. Suffolk, United Kingdom*, 2005.

K. Smith, D. Sax, and K. Lafferty. Evidence for the role of infectious disease in species extinction and endangerment. *Conservation biology: the journal of the Society for Conservation Biology*, 20(5):1349–57, 2006.

K. Soderhall and L. Cerenius. Role of the prophenoloxidase-activating system in invertebrate immunity. *Current opinion in immunology*, pages 23–28, 1998. URL `http://www.sciencedirect.com/science/article/pii/S0952791598800265`.

P. Soorae. Global re-introduction perspectives: 2011. *...from around the globe.: IUCN/SSC Re-introduction ...*, 2011. URL `http://scholar.google.com/scholar?hl=en\&btnG=Search\&q=intitle:Global+Re-introduction+Presepectives+2011\#0`.

A. South, S. Rushton, and D. Macdonald. Simulating the proposed reintroduction of the European beaver (Castor fiber) to Scotland. *Biological Conservation*, 93: 103–116, 2000. URL `http://www.sciencedirect.com/science/article/pii/S0006320799000725`.

A. Strauss, A. White, and M. Boots. Invading with biological weapons: the importance of disease-mediated invasions. *Functional Ecology*, 26(6):1249–1261, 2012.

D. Tompkins, A. White, and M. Boots. Ecological replacement of native red squirrels by invasive greys driven by disease. *Ecology Letters*, 6(3):189–196, 2003. URL `http://doi.wiley.com/10.1046/j.1461-0248.2003.00417.x`.

D. M. Tompkins, A. W. Sainsbury, P. Nettleton, D. Buxton, and J. Gurnell. Parapoxvirus causes a deleterious disease in red squirrels associated with uk population declines. *Proceedings of the Royal Society of London. Series B: Biological Sciences*, 269(1490):529–533, 2002.

J. M. J. Travis. Climate change and habitat destruction: a deadly anthropogenic cocktail. *Proceedings. Biological sciences / The Royal Society*, 270(1514):467–73, Mar. 2003. ISSN 0962-8452. doi: 10.1098/rspb.2002.2246. URL `http://www.pubmedcentral.nih.gov/articlerender.fcgi?artid=1691268\&tool=pmcentrez\&rendertype=abstract`.

W. H. Van der Putten, M. Macel, and M. E. Visser. Predicting species distribution and abundance responses to climate change: why it is essential to include biotic interactions across trophic levels. *Philosophical transactions of the Royal Society of London. Series B, Biological sciences*, 365 (1549):2025–34, July 2010. ISSN 1471-2970. doi: 10.1098/rstb.2010.0037. URL `http://www.pubmedcentral.nih.gov/articlerender.fcgi?artid=2880132\&tool=pmcentrez\&rendertype=abstract`.

M. J. Wade. The evolutionary genetics of maternal effects. *Maternal effects as adaptations*, pages 5–21, 1998.

R. L. Wallace, T. W. Clark, and R. P. Reading. An Interdisciplinary Approach to Endangered Species Recovery: Concepts Applications Cases Special Issue. *Endangered Species UPDATE*, 19(4):65–204, 2002.

L. Wauters and A. A. Dhondt. Spacing behaviour of red squirrels, *Sciurus vulgaris*: variation between habitats and the sexes. *Animal Behaviour*, 43(2):297–311, 1992.

L. Wauters, P. Casale, and A. A. Dhondt. Space use and dispersal of red squirrels in fragmented habitats. *Oikos*, pages 140–146, 1994.

L. A. Wauters, M. Githiru, S. Bertolino, A. Molinari, G. Tosi, and L. Lens. Demography of alpine red squirrel populations in relation to fluctuations in seed crop size. *Ecography*, 31(1):104–114, Feb. 2008. ISSN 09067590. doi: 10.1111/j.2007.0906-7590.05251.x. URL `http://doi.wiley.com/10.1111/j.2007.0906-7590.05251.x`.

J. D. Westervelt, M. Shapiro, W. D. Goran, and D. P. Gerdes. *Geographic Resources Analysis Support System (GRASS) Version 4.0 User's Reference Manual*. US Army Corps of Engineers, Construction Engineering Research laboratory, 1992.

A. White and P. W. W. Lurz. A modelling assessment of control strategies to prevent/reduce Squirrelpox spread. Technical report, Scottish Natural Heritage Report., 2013.

A. White, R. Bowers, and M. Begon. Host-pathogen cycles in self-regulated forest insect systems: resolving conflicting predictions. *The American Naturalist*, 148(1): 220–225, 1996. URL `http://www.jstor.org/stable/10.2307/2463081`.

A. White, J. Greenman, T. Benton, and M. Boots. Evolutionary behaviour in ecological systems with trade-offs and non-equilibrium population dynamics. *Evolutionary Ecology Research*, 8(3):387–398, 2006.

G. C. White and K. P. Burnham. Program mark: survival estimation from populations of marked animals. *Bird study*, 46(S1):S120–S139, 1999.

K. A. White and K. Wilson. Modelling density-dependent resistance in insect-pathogen interactions. *Theoretical population biology*, 56(2):163–81, Oct. 1999. ISSN 0040-5809. doi: 10.1006/tpbi.1999.1425. URL `http://www.ncbi.nlm.nih.gov/pubmed/10544067`.

T. C. R. White. Mast seeding and mammal breeding: Can a bonanza food supply be anticipated? *New Zealand Journal of Zoology*, 34(3):179–183, Jan. 2007. ISSN 0301-4223. doi: 10.1080/03014220709510076. URL `http://www.tandfonline.com/doi/abs/10.1080/03014220709510076`.

B. A. Wintle, J. Elith, and J. M. Potts. Fauna habitat modelling and mapping: A review and case study in the Lower Hunter Central Coast region of NSW. *Austral Ecology*, 30(7):719–738, Nov. 2005. ISSN 1442-9985. doi: 10.1111/j.1442-9993.2005.01514.x. URL `http://doi.wiley.com/10.1111/j.1442-9993.2005.01514.x`.

J. Xu. Microbial ecology in the age of genomics and metagenomics: concepts, tools, and recent advances. *Molecular ecology*, 15(7):1713–31, June 2006. ISSN 0962-1083. doi: 10.1111/j.1365-294X.2006.02882.x. URL `http://www.ncbi.nlm.nih.gov/pubmed/16689892`.

Appendix A

Parameterisation of the host-pathogen model with a dynamic resource in Chapter 2.5

In Section 2.5.1 we revised the framework presented by Anderson and May (1981) to explicitly include a dynamic resource in a Susceptible-Infected model given by Equations (2.11). We parameterise this model by comparing the coexistence equilibrium densities of Equations (2.11) and the model without resource in Equations (2.3). Setting the left-hand side of Equations (2.11) to zero we achieve

$$R_C = \kappa_R \left(1 - \frac{c}{\rho}(X_C + Y_C)\right) \tag{A.1a}$$

$$X_C = \frac{\mu(b+\alpha)}{\beta\lambda} \tag{A.1b}$$

$$V_C = \frac{\lambda}{\mu} Y_C \tag{A.1c}$$

$$0 = \left((\frac{a_R c^2 \kappa_R}{\rho}\right) Y_C^2 + \left((\frac{\beta\lambda}{\mu} + \frac{2a_R c^2 \kappa_R}{\rho})X_C - a_R c \kappa_R\right) Y_C + \left(a_R c \kappa_R (\frac{c}{\rho} X_C - 1) + b\right) \tag{A.1d}$$

The coexistence equilibrium of Equations (2.3) is given in Equations (2.4). We see that the term for X_C is identical and V_C is the same when both Y_C values are similar. By equating coefficients for Equation (A.1d) to Equation (2.4c) we achieve

$$a = a_R c \kappa_R \tag{A.2a}$$

$$q = \frac{c}{\rho} \tag{A.2b}$$

Therefore parameter values $a_R = 1, c = 4.3, \kappa_R = 1$ and $\rho = 1$ in Equations (2.11) produce similar host population densities to Equations (2.3) without resource.

Appendix B

Parameterisation of models in Chapter 4 and 5

A derivation of the parameters used in the spatial, individual-based, stochastic SI model in Section 4.3.2 and the spatial, individual-based, stochastic model in Section 5.2.1 are given here.

B.1 Demographic parameters

The average yearly mortality of squirrels is estimated in Barkalow et al. (1970) to be 60%. Therefore the death rate parameter b can be found by solving $dH/dt = -bH$ and assuming host density decreases to 0.4 of its initial value after one year, giving $b = 0.9\text{yr}^{-1}$. This is used in combination with the growth rate $r = 0.6\text{yr}^{-1}$ from Tompkins et al. (2003) to establish the maximum birth rate $a = r + b = 1.5\text{yr}^{-1}$.

B.2 Disease transmission and the reproductive number, R_0

The framework defined by Section 4.3.2 decribes infection occurring through susceptible-infected contact within a focal cell (i, j) and neighbouring cells. The interaction between neighbouring cells is shown in Figure B.1 (a) where a buffer of $\alpha/2$ km is placed around focal cell (i, j) highlighting the region from which a susceptible in the focal cell can become infected (where α is the average diameter of core range activity for an individual squirrel). The density of infected individuals from each neighbouring buffering areas must be calculated and weighted depending on their position to the focal cell. Figure B.1 (b)-(c) shows the infected and susceptible densities of a horizontal cross-section of the buffering area in Figure B.1 (a). (Note the curves in the buffer region in Figure B.1 (b) could increase or decrease and depend on the density

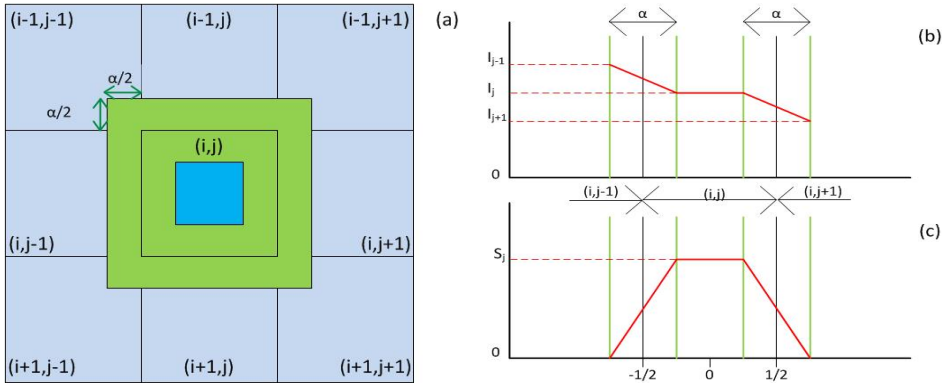

Figure B.1: A grid of 9 cells (in blue) is shown in (a) with focal cell (i, j) highlighted in dark blue. A green buffer around the focal cell highlights the maximum red squirrel core range movement (with diameter α km) from neighbouring cells to the focal cell and vice versa. A horizontal cross-section across cells $(i, j-1 : j+1)$ in (a) shows the possible density of (b) infected and (c) susceptible hosts. The area under these curves show the total number of infected hosts interacting with the susceptible hosts from the focal cell.

of infecteds in neighbouring cells.) The total number of infected and susceptible hosts across the cross-section is therefore the area under the respective curves

$$S^{tot} = S_{i,j} \tag{B.1a}$$

$$I^{tot} = I_{i,j} + \frac{\alpha}{2}(I_{i,j-1} + I_{i,j+1}) \tag{B.1b}$$

By direct analogy we can find the densities for a vertical cross-section of Figure B.1 (a) and following the same method we can determine the contribution from neighbouring corner cells. Disease transmission for the focal cell (i, j) can then be calculated by

$$\beta S_{i,j}\left(I_{i,j} + \frac{\alpha}{2}\Sigma I_a + \frac{\alpha^2}{4}\Sigma I_c\right) \tag{B.2a}$$

where β is the transmission coefficient and ΣI_c and ΣI_a are the sum of the infected hosts in the corner and adjacent cells to (i, j) respectively.

There is no available data from which to determine the disease transmission coefficient β between red squirrels. We therefore use White and Lurz (2013) who derive $\beta = 0.6\text{km}^2\text{yr}^{-1}$ from field observations where grey squirrels test seropositive to SQPV and trapping data in the South of Scotland. Infected hosts are subjected to additional mortality due to infection at rate $\sigma = 26\text{yr}^{-1}$ from Tompkins et al. (2003).

The range of infection parameter values are given in Table 4.2. We fix $\beta = 0.6$ as the low transmission coefficient, and multiply this by 20 for a high transmission case. $\sigma = 26$ denotes the acute (high virulence) parameter scenarios and we use the basic

	Acute (high virulence)		Chronic (low virulence)	
R_0	(SQPV) Low transmission	High transmission	Low transmission	High transmission
High density estimate	0.20	4.01	4.01	80.30
Low density estimate	0.09	1.78	1.78	35.69

Table B.1: The value of R_0 from Equation B.3 the parameters give in Table 4.2 and the median carrying capacity $K = 9$ and $K = 4$ for high and low density estimates respectively.

reproductive ratio, R_0, to find the σ for the chronic (low virulence) parameters. R_0 can be defined for each grid cell with a carrying capacity $K_{i,j}$ using the Equations (4.1) to produce

$$R_0 = \frac{\beta K_{i,j}}{\sigma + b} \tag{B.3}$$

We fix R_0 at the same level for the acute, high transmission scenario and the chronic, low transmission scenario to find σ for chronic case (see Table 4.2). Representative values of R_0 in the high and low density scenarios are shown in Table B.1.

B.3 Derivation of the dispersal term

We assumed saturation dispersal in Equation (4.4), i.e. individuals are more likely to disperse as cell density increases (Poethke and Hovestadt, 2002), for the long distance dispersal rate given by

$$D_{i,j} = d \exp\left(\frac{-(K_{i,j} - H_{i,j})}{0.5K_{i,j}}\right) \tag{B.4}$$

where $H_{i,j} = S_{i,j} + I_{i,j}$. Once an individual disperses from the focal cell (i, j) it enters a neighbouring cell (i^*, j^*) dependent on the cell density and location to the focal cell. We assume individuals preferentially disperse to cells that have lower relative densities (compared to the carrying capacity of the cell) and therefore the probability of entering a neighbouring cell (i^*, j^*) is determined by the following function

$$D^*_{i^*,j^*} = \omega \exp\left(\frac{(K_{i^*,j^*} - H_{i^*,j^*})}{0.5K_{i^*,j^*}}\right) \tag{B.5}$$

where $\omega = (\alpha^2)/4$ for corner cells, $\omega = \alpha/2$ for the adjacent cells, and $H_{i^*,j^*} = S_{i^*,j^*} + I_{i^*,j^*}$.

Appendix C

Further simulations for Chapter 4

C.1 Red squirrel carrying capacity in a poor seed year

In Chapter 4 we use the upper range of published density estimates of red squirrel abundance in different tree species (Figure C.1 (a)). To understand the impact of species density on disease spread we also consider the lower range of the density estimates, representative of a poor seed year in Figure C.1 (b).

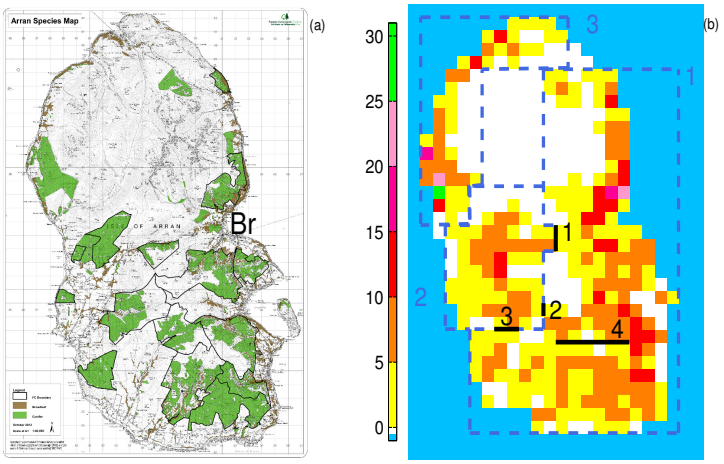

Figure C.1: The Isle of Arran is shown in (a) (with permission from FCS) with the coniferous (green) and broadleaf (brown) woodland highlighted and 'Br' represents the main port Brodick. The carrying capacity of red squirrels (per km^2) is shown in (b) using estimates of 0.08/ha in coniferous and 0.5/ha in broadleaf representative of for a poor seed year. Cells which are well connected are grouped together by the dashed coloured blocks (labelled $1-3$); there is poor connectivity between the blocks. In addition, ground-truthing in collaboration with Forestry Commission Scotland, has identified routes which do not permit movement, identified by thick black lines.

C.2 Simulations in absence of disease

Simulations of the stochastic model described in Chapter 4 were undertaken in the absence of the disease using the two connectivity scenarios (GIS data and ground-truthing and GIS data only). Figure C.2 shows the population densities reach a quasi-stable state for both the high and low seed year scenarios suggesting the habitat structure on Arran is favourable to red squirrels. Whilst there is little difference between the connectivity scenarios it is evident that the squirrel population remains roughly 5% below their potential densities that would be attained if each cell was at its carrying capacity. This reduction in density is arises as grid cells that have low carrying capacity and that are poorly connected often become extinct and rely on rare dispersal events for repopulation.

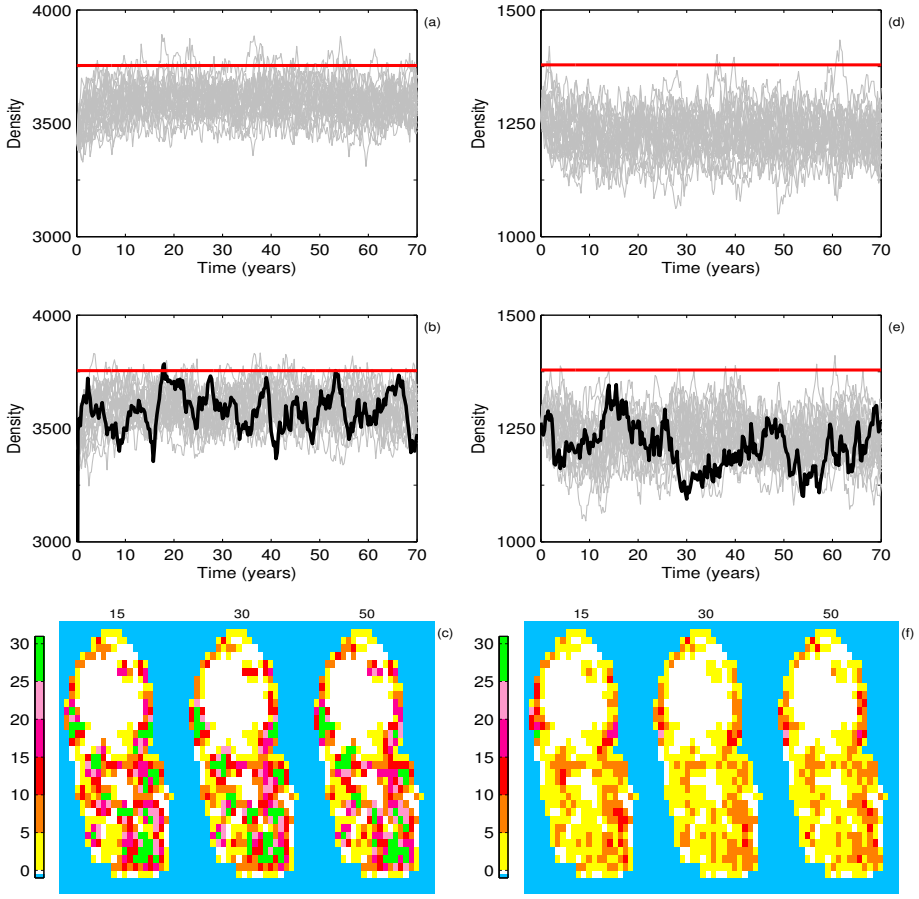

Figure C.2: The spatial, individual-based, stochastic SI model in absence of disease for a (a)-(c) high and (d)-(f) low seed year. The top four figures show the total population density (grey) against time for 25 model realisations with connectivity established from GIS information only in (a) and (d) and GIS information and ground-truthing in (b) and (e). The carrying capacity is shown in red. (c) and (f) show the cell densities on Arran at three time frames for the realisation highlighted in (b) and (e) respectively. Parameters are given in Table B.1.

C.3 Further disease simulations

C.3.1 Acute infection with high transmissibility in a poor seed year

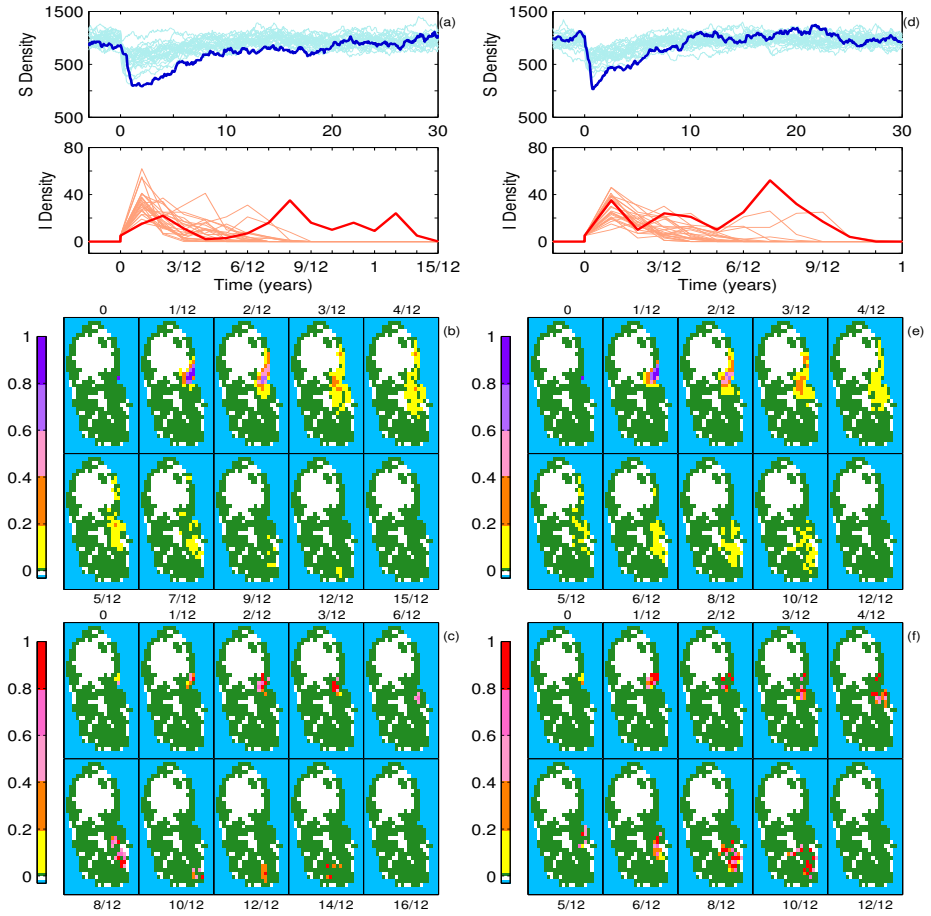

Figure C.3: The spatial, individual-based, stochastic SI model with acute, high transmission parameters (Table 4.2) in a poor seed year where in (a)-(c) connectivity includes GIS information and ground-truthing and in (d)-(f) GIS information only. The initial condition and descriptions are consistent with Figure 4.2 for both the left and right hand columns.

In a high seed year the acute, high transmission scenario revealed extensive disease spread throughout region 1 when imposing restrictions of both GIS and ground-truthing, and throughout both region 1 and 2 when using GIS information only (see Figure 4.3). When we undertake the analysis for the low density estimates the extent and severity of disease spread is reduced (Figure C.3) and the disease remain contained in region 1. The reduction in disease spread is associated with the lower value

of R_0 due to reduced densities (see Table B.1). As in the high density scenarios there are local outbreaks of the disease followed by disease fade-out.

C.3.2 Chronic infection with low transmissibility in a poor seed year

In Chapter 4 we showed that a chronic infection with low transmission was able to persist endemically (see Figure 4.4) in region 1 and 2 and in most realisations infection reached and persisted in region 3. In Figure C.4 we undertake this analysis in the low density scenario. When we include dispersal information from GIS and ground-truthing Figure C.4 (a)-(c) disease persists endemically in region 1 only. When we include dispersal from GIS only Figure C.4 (d)-(f) the disease can persist endemically in regions 1 and 2. The reduction in R_0 associated with the lower cell densities (see Table B.1) therefore reduces the extent of disease spread but the chronic infection can still persist over an extensive region at endemic levels.

C.3.3 Chronic infection with high transmissibility in a high seed year

In Chapter 4 we detail parameters for a chronic disease with high transmission (with the effect of these parameters on R_0 shown in see Table B.1). In Figure C.5 we show the results from simulations using these parameters for the high density scenario (results for the low density scenario follow the same pattern). Figure C.5 shows that the disease spreads rapidly across the whole landscape and that the total population abundance is reduced dramatically with most individuals becoming infected. This leads to the local extinction of populations. In the long term there are two possible outcomes. Either the entire population becomes extinct or the disease becomes extinct and the population recovers to pre-infection levels

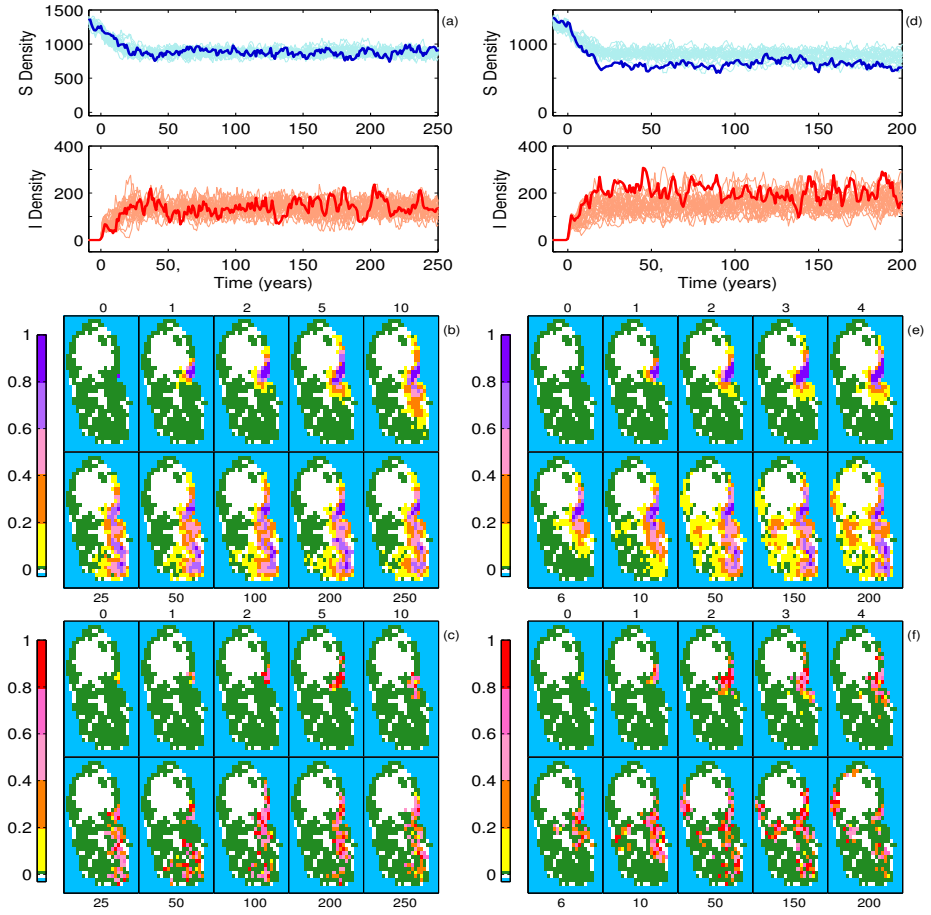

Figure C.4: The spatial, individual-based, stochastic SI model with chronic, low transmission parameters (Table 4.2) in a poor seed year where in (a)-(c) connectivity includes GIS information and ground-truthing and in (d)-(f) GIS information only. The initial condition and descriptions are consistent with Figure 4.2 for both the left and right hand columns.

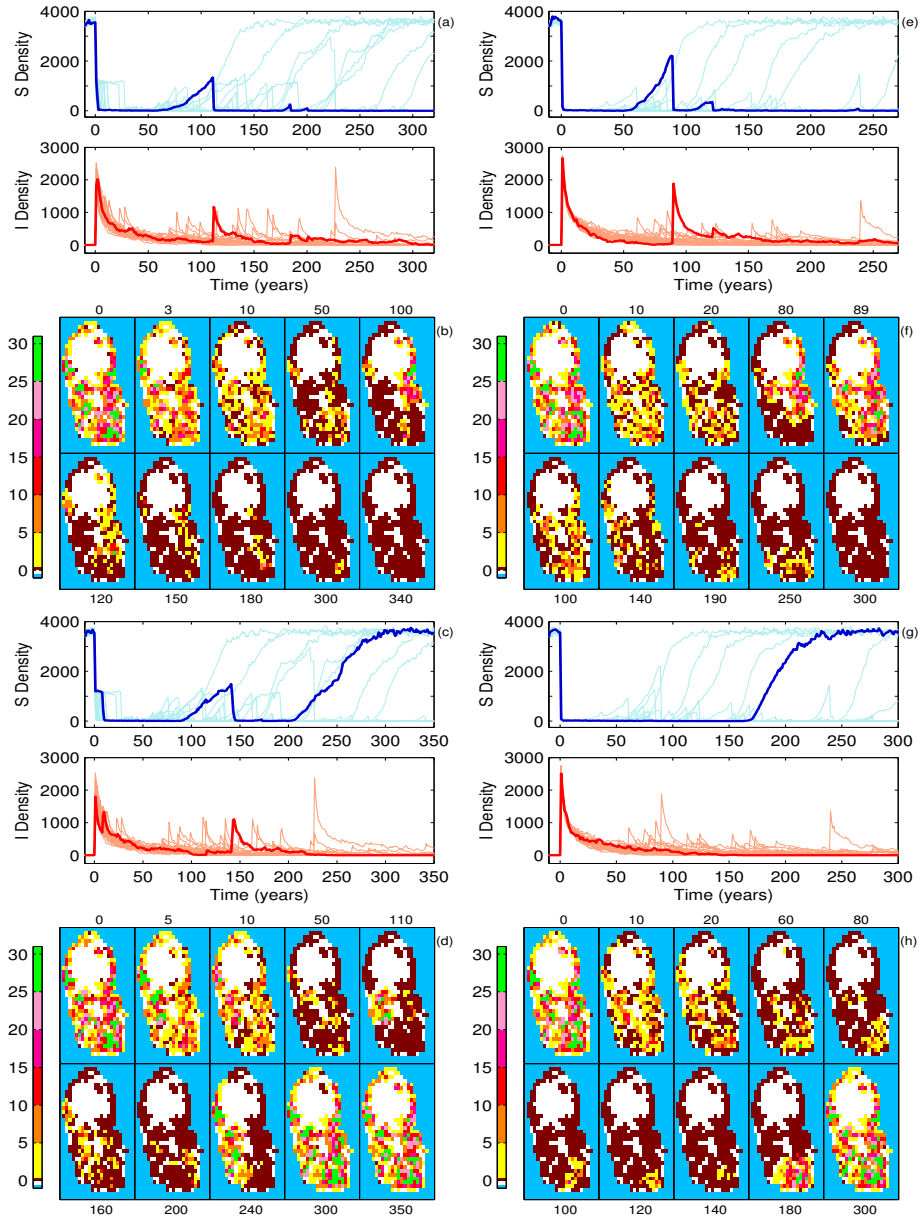

Figure C.5: The spatial, individual-based, stochastic SI model with chronic, high transmission parameters (Table 4.2) in a high seed year where in (a)-(c) connectivity includes GIS information and ground-truthing and in (d)-(f) GIS information only. Once the total population has achieved quasi-steady state, 5 infected red squirrels are introduced at Brodick (Figure 4.1 (a)) at time 0. In (a), (c), (e) and (g) the total susceptible (blue) and infected (red) population densities are shown against time for 25 model realisations with a single realisation highlighted. In (b), (d), (f) and (h) the cell density maps are shown for the realisations highlighted in (a), (c), (e) and (g) respectively.